POLITECNICO DI MILANO

Dipartimento di Elettronica, Informazione e Bioingegneria
Master of Science in Telecommunication Engineering

An application of transformation acoustics to model propagation of guided acoustic waves in deformed pipelines

Supervisor:
Prof. **Gian Guido Gentili**

Thesis work by:
Martina Pammelati
Student ID: 900101

Academic year 2019/2020

Alla mia famiglia
e ai miei amici

"Audantes fortuna iuvat"

Abstract

In this thesis work we consider the problem related to the monitoring of deformations in pipes. These deformations can be caused by external agents such as, for example, the pressure of the sea, in the case of underwater pipelines, and geological settling phenomena. It is therefore necessary to develop a procedure that allows us to evaluate these deformations in a short time and continuously monitor the state of the pipes. For this purpose, the case of two-dimensional geometries is considered first and the Finite Element Method (FEM) is used, for which an appropriate general description is provided and, subsequently, we extend the case to the specific acoustic problem. Given the need for a faster response from the pipes, we evaluate a new calculation method, the Hierarchical Model Reduction (HiMod) which allows to obtain the same results by improving computational time without compromising accuracy. This method is applied here for the first time to the linear acoustic wave equation in 2D and 3D. The application is the computation of the multimode scattering matrix for guided wave propagation in pipelines.

Sommario

In questo lavoro di tesi consideriamo il problema relativo al monitoraggio di deformazioni in tubi. Queste deformazioni possono essere causate da agenti esterni quali, ad esempio, la pressione del mare, nel caso di condutture sottomarine, e fenomeni di assestamento geologico. Si rivela quindi necessario lo sviluppo di una procedura che ci permette di valutare queste deformazioni in tempi brevi e tenere continuamente sotto controllo lo stato delle condutture. A tale scopo, si considera dapprima il caso di geometrie bidimensionali e si adopera il Metodo degli Elementi Finiti (FEM), del quale si fornisce un'opportuna descrizione generale e, a seguire, estendiamo il caso al problema acustico specifico. Data la necessità di una risposta più veloce da parte delle condutture, valutiamo un nuovo metodo di calcolo, la Riduzione Gerarchica di Modello (HiMod) che permette di ottenere gli stessi risultati migliorando il tempo computazionale senza compromettere l'accuratezza. Questo metodo viene applicato qui per la prima volta all'equazione lineare dell'onda acustica in 2D e in 3D. L'applicazione è il calcolo della matrice di scattering multimodale per la propagazione d'onda guidata nei tubi.

List of Figures

V

VI

Contents

VIII

Chapter 1

Acoustic Transformation

Our study is aimed at identifying and evaluating any deformations in pipes. These deformations are due to external agents and a multimodal acoustic analysis is used to achieve our goal. In particular, it is necessary to measure the sound pressure at each point of the structure. We start directly from the examination of the deformed geometry and, by adopting a coordinate transformation, we perform the mapping of the structure to the reference geometry, which would be the structure without any deformation. To better clarify the procedure, which lies at the basis of the general problem, we start from the definition of acoustic wave by providing the related equation [1]. For the original geometry, where the coordinates system is defined by $\mathbf{r}'$, we have that, given the pressure field $p'(\mathbf{r}')$ in the frequency domain:

$$\nabla' p' = -j\omega\rho_0 \mathbf{v}' \tag{1.1}$$

$$j\omega p' = -B_0 \nabla' \cdot \mathbf{v}' \tag{1.2}$$

where $\mathbf{v}' = \mathbf{v}'(\mathbf{r}')$ is the velocity field, ρ_0 is the average density and B_0 is the average compression modulus which is defined as the density increase caused by a compression. Eq. (1.1) is the linear Euler equation, whereas eq. (1.2) represents continuity in the linear regime, connecting the motion of fluid with its contraction and expansion. What we have to do now is the following: we first define a coordinate transformation that converts the original geometry to a uniform pipeline, then we introduce an anisotropic material such that the wave equation in the transformed coordinate frame is equivalent to that in the original frame. Finally we use an efficient method

to solve the wave equation. We start with the transformation $\mathbf{r}' \to \mathbf{r}(\mathbf{r}')$ with Jacobian:

$$\mathbf{J} = \begin{bmatrix} \frac{\partial x}{\partial x'} & \frac{\partial x}{\partial y'} & \frac{\partial x}{\partial z'} \\ \frac{\partial y}{\partial x'} & \frac{\partial y}{\partial y'} & \frac{\partial y}{\partial z'} \\ \frac{\partial z}{\partial x'} & \frac{\partial z}{\partial y'} & \frac{\partial z}{\partial z'} \end{bmatrix} \tag{1.3}$$

It can be shown that the solution $p[\mathbf{r}(\mathbf{r}')]$, which is the pressure field of the reference geometry, does not change, i.e. it is equivalent to $p'(\mathbf{r}')$, using the following anisotropic material in the transformed domain:

$$B = B_0 \det \mathbf{J} \tag{1.4}$$

$$\overline{\boldsymbol{\rho}}^{-1} = \rho_0^{-1} \frac{\mathbf{J}\mathbf{J}^T}{\det \mathbf{J}} = \rho_0^{-1} \overline{\boldsymbol{\rho}_r}^{-1} = \rho_0^{-1} \overline{\mathbf{T}} \tag{1.5}$$

Knowing that the equations related to the reference structure defined by $\mathbf{r}$ are:

$$\nabla p = -j\omega \rho_0 \mathbf{v} \tag{1.6}$$

$$j\omega p = -B_0 \nabla \cdot \mathbf{v} \tag{1.7}$$

these can be rewritten by replacing (1.4) and (1.5) in the following way:

$$\overline{\boldsymbol{\rho}_r}^{-1} \cdot \nabla p = -j\omega \rho_0 \mathbf{v} \tag{1.8}$$

$$j\omega p = -B_0 \det \mathbf{J} \nabla \cdot \mathbf{v} \tag{1.9}$$

Considering the divergence and placing $v_0 = \sqrt{\frac{B_0}{\rho_0}}$:

$$\nabla \cdot \overline{\mathbf{T}} \cdot \nabla p + \frac{\omega^2}{v_0^2 \det \mathbf{J}} p = 0 \tag{1.10}$$

2

Subsequently, we rewrite it as:

$$\nabla \cdot \overline{\mathbf{T}} \cdot \nabla p + k^2 p = 0 \qquad (1.11)$$

where:

$$k^2 = k^2(\mathbf{r}) = \frac{\omega^2}{v_0^2 \det \mathbf{J}} = \frac{k_0^2}{\det \mathbf{J}} \qquad (1.12)$$

$$\overline{\mathbf{T}} = \frac{\mathbf{J}\mathbf{J}^T}{\det \mathbf{J}} \qquad (1.13)$$

It can be demonstrated that the pressure field associated with the transformed geometry is equal to the pressure field of the deformed one and the material used to make this equivalence is given by the transformation matrix $\overline{\mathbf{T}}$ which takes into account the Jacobian matrix. At this point, our problem is to solve the wave equation in an undeformed pipeline filled with an anisotropic material and a method that is very suitable for this type of problems is the Finite Element Method (FEM).

In the next chapter, we describe the FEM starting initially from two-dimensional geometries and from a general description of the procedure. Next, we will see the specific acoustic case of our interest by specifying in more details the equations seen previously in this chapter. Finally, we introduce the HiMod method, which is a straightforward modification of FEM that is particularly suitable to study wave propagation in waveguides with smooth deformations, since it boosts the efficiency of FEM.

Chapter 2

The Finite Element Method

The Finite Element Method is a numerical technique used for solving the most common problems of engineering. It is a very important method because it gives us the approximate solutions to boundary-value problems for partial differential equations.

The first development of the FEM dates back to 1941 and 1943 thanks to the studied conducted by A. Hrennikoff [2] and R. Courant [3]. Although these pioneers used different point of views in their approaches, they identified the most important point: mesh discretization of a geometrical continuous domain into different subdomains. These subdomains are called **finite elements**, in which the unknown function is represented by a series of interpolation functions with unknown coefficients.

Other important studies regarding the FEM were done in the 70s and these can be found in the book "An Analysis of the Finite Element Method" written by G. Strang and G. Fix, published in 1973 [4]. In general, many books have been written on the method [5−8] and thanks to the experiments done, FEM is now one of the most used method for modeling physical systems that are part of everyday reality.

The Finite Element Method is divided into different steps:

1. Mesh discretization of the domain
2. Choice of the interpolation function
3. Formulation of the system of equations
4. Solution of the system of equation

The discretization phase is the most important step because the way into which the domain is divided is going to influence the computational time and the accuracy of the results. The domain Ω is divided into smaller

subdomains called Ω^e where the superscript indicates the e-th element of the domain subdivision. Naturally, the discretization can be done for 1D, 2D and 3D dimensional domain. In the 1D domain, the elements are short segments which together create a line. In the 2D domain, the elements are usually triangles. In 3D domain, the elements are tetrahedra, triangular prisms or rectangular bricks. The basic 1D, 2D and 3D elements for modeling curved lines or surfaces are line segments, triangles and tetrahedra respectively.
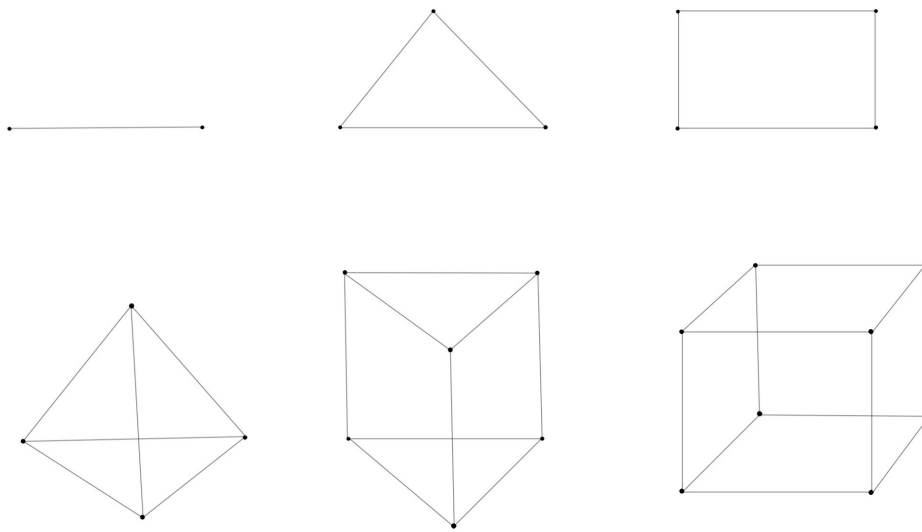
Figure 2.1: One-dimensional, two-dimensional and three-dimensional basic finite elements

The problem can be solved by describing the unknown function u at nodes associated with each element. To describe a node it is necessary to know its coordinate values, the local number and the global number. The local number indicates the position of the node in the element while the global number gives its position in the system.

The second phase consists in the consideration of an interpolation function to approximate the solution within each element. The interpolation function is a polynomial. After the selection of the interpolation function, the unknown solution in each element is obtained.

The selection of the interpolation function is related to the accuracy of the method. If an higher accuracy is required, it is necessary to choose an higher-order interpolation function, so higher-order elements. We can improve the

accuracy also by using smaller elements in the mesh so, considering a higher mesh density.

The third and fourth step consist in the formulation and resolution of the system of equations. There are two different procedures: the Ritz method and the Galerkin method. In electromagnetics, these systems are usually associated with scattering, radiation and also wave propagation in waveguides and resonances in cavities.

Once we have solved the system of equations, we can then compute the desired parameters such as capacitance, inductance, input impedance and scattering or radiation patterns and display the result in form of curves [8].

In this chapter we will focus on the description of the Finite Element Method in two-dimensional domains mainly considering linear triangular elements: we will start from the definition of the boundary-value problem and then get to the detailed analysis of the different steps of the method and the characterization of more sophisticated higher-order and isoparametric elements. After that, we will go into the specific case of the Finite Element Method for measuring the sound pressure in the two-dimensional world: in particular we will study a planar case that uses Cartesian coordinates and a radial case that instead considers a system of polar coordinates. Finally, we will discuss transformation acoustics also considering the case related to quadrilaterals. All these procedures will lead us to the evaluation of sound pressure values in the two-dimensional geometry and to the analysis of modal behavior as a function of a certain frequency range. In particular, the values of the S parameters will be extrapolated, the nature and properties of which will be described in more details in the next chapter, for different geometries and we will see what happens to these graphs by modifying for example the type of elements used and the density of the mesh. The most important thing will be to compare the graph of the S parameters related to a deformed two-dimensional geometry with the same graph associated with the regular geometry of the pipe, obtained after the transformation.

2.1 Two-Dimensional Finite Element Method

2.1.1 The Boundary-Value Problem and the Variational Formulation

Boundary-value problems refer to the modeling of physical systems and their solution is fundamental for understanding the functioning of systems from a mathematical point of view. In general, a boundary-value problem is identified by a differential equation of this type:

$$\mathcal{L}u = f \tag{2.1}$$

where we have to deal with the boundary conditions on the domain contour Γ. In the equation, $\mathcal{L}$ is a differential operator, f is the continuous function and u is the unknown quantity.

Of course, the differential equation can be presented in different forms based on the problem we are analyzing, while the boundary conditions range from the Dirichlet and Neumann conditions to even more complicated conditions. It is preferable to solve boundary-value problems analytically. However this way is possible only for very few cases such as wave propagation in rectangular and circular waveguides or cavity resonance within rectangular and cylindrical cavities. Most practical problems do not present any analytical method and that is why approximations have been adopted [8]. Among these, we meet the Ritz and Galerkin methods which have been mentioned previously.

The Finite Element Method has been widely used in the two-dimensional case. To describe the FEM, it is necessary to define the boundary-value problem, expressed by a second-order differential equation. From now on, we will refer to [8] for the description of the FEM, adopting a similar formulation. In this case, the second-order differential equation is given by:

$$-\frac{\partial}{\partial x}\left(a_x\frac{\partial u}{\partial x}\right) - \frac{\partial}{\partial y}\left(a_y\frac{\partial u}{\partial y}\right) + bu = f \qquad in \quad \Omega \tag{2.2}$$

where u is the unknown function, a_x, a_y and b are known parameters associated with the physical properties of the domain and f is the source or excitation function.

The boundary conditions are given by:

$$u = u_0 \quad on \quad \Gamma_1 \tag{2.3}$$

$$\left(a_x \frac{\partial u}{\partial x} \widehat{x} + a_y \frac{\partial u}{\partial y} \widehat{y} \right) \cdot \widehat{n} + \gamma u = t_0 \quad on \quad \Gamma_2 \tag{2.4}$$

where $\Gamma = \Gamma_1 + \Gamma_2$ is the boundary enclosing the area Ω, $\widehat{n}$ is the normal vector and γ, u_0 and t_0 are known parameters associated with the physical properties of the boundary. The first boundary condition must be enforced explicitly while the second is known as natural boundary condition which is satisfied implicitly. When it turns out $\gamma = 0$, the second condition becomes the Neumann boundary condition.

If there are discontinuities, the unknown function u has to satisfy the **continuity conditions**:

$$u^+ = u^- \quad on \quad \Gamma_d \tag{2.5}$$

$$\left(a_x^+ \frac{\partial u^+}{\partial x} \widehat{x} + a_y^+ \frac{\partial u^+}{\partial y} \widehat{y} \right) \cdot \widehat{n} = \left(a_x^- \frac{\partial u^-}{\partial x} \widehat{x} + a_y^- \frac{\partial u^-}{\partial y} \widehat{y} \right) \cdot \widehat{n} \quad on \quad \Gamma_d \tag{2.6}$$

where Γ_d represents the discontinuity interface: the superscript "+" denotes that the observation point approaches Γ_d from the "+" side, the superscript "−" denotes that the observation point approaches Γ_d from the "−" side.
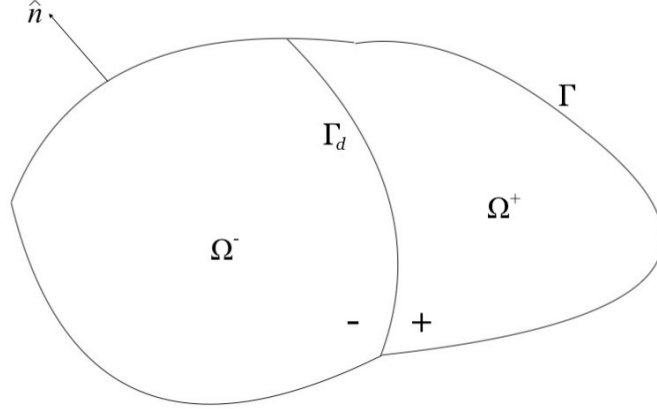
Figure 2.2: Two-dimensional domain with a discontinuity interface denoted by Γ_d

The boundary-value problem presents an equivalent problem known as **variational problem** [9]. It is represented by the following system of equations:

$$
\begin{cases}
\delta F\left(u\right) = 0 \\
u = u_0 \quad on \quad \Gamma_1
\end{cases}
\tag{2.7}
$$

where:

$$
\begin{aligned}
F\left(u\right) \;=\; & \frac{1}{2} \iint_{\Omega} \left[a_x \left(\frac{\partial u}{\partial x}\right)^2 + a_y \left(\frac{\partial u}{\partial y}\right)^2 + bu^2 \right] d\Omega \\
& + \int_{\Gamma_2} \left(\frac{\gamma}{2}u^2 - t_0 u\right) d\Gamma - \iint_{\Omega} f u \, d\Omega
\end{aligned}
\tag{2.8}
$$

If there are any discontinuities, it is necessary to add the continuity conditions to the system considered above.

9

2.1.2   Two-Dimensional Finite Element Method Calculation

After the definition of the boundary-value problem and the variational problem, we can analyze the basic steps of the FEM listed before for the two-dimensional case. For simplicity, we consider linear triangular elements. As it is already known, the first step is to divide the area domain Ω into a number of two-dimensional elements, for example triangular elements. It is important to underline that these elements should not overlap among each other. All the elements are connected together via their vertices.
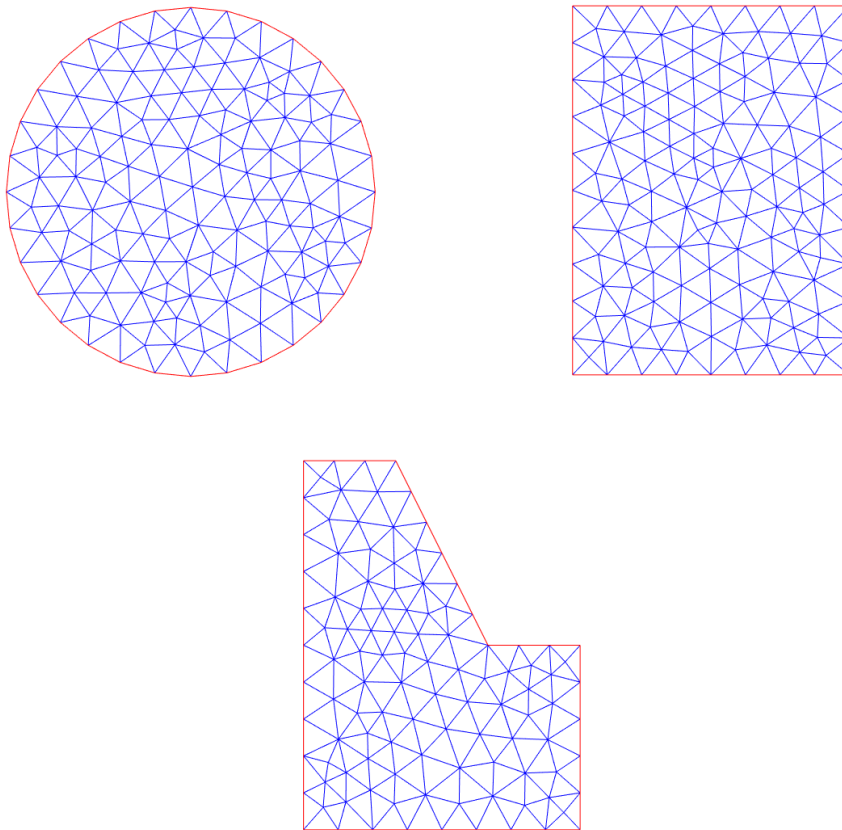
Figure 2.3:   Subdivision of a circular, rectangular and irregular two-dimensional domain into Finite Elements

If we choose smaller elements, the results will be more accurate but there will be also a growth in the memory demand and computing time. The compromise would be to use smaller elements where the solution presents a drastic variation and larger elements where the variation is less evident.

The elements and nodes can be labeled with integers for their recognition inside the domain. In the case of linear triangular elements, each element is associated with three nodes and each node has a local number that identifies its position with respect to the element and a global number related to the whole system. The global and local numbers, together with the number of the element, will be linked thanks to an array. This array includes all information concerning the elements and nodes. In addition to this array, it is necessary to consider another one which relates the segments coincident with Γ_2 with their nodes. This array will be used to facilitate the incorporation of the second boundary condition (2.4). Then, to impose the Dirichlet boundary condition (2.3), we consider another vector that stores the global numbers of the nodes that are located on Γ_1. In addition to these data, others are needed such as the coordinates values of the nodes in the domain, the values of a_x, a_y, b and f for each element, the value of u_0 for the nodes placed on Γ_1 and the values of γ and t_0 for each segment with nodes on Γ_2.
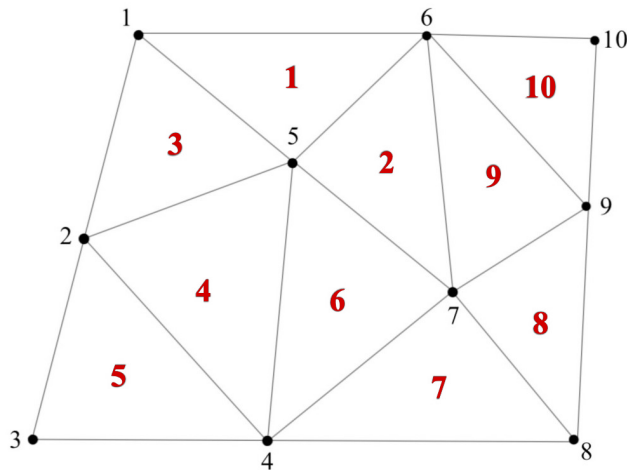
Figure 2.4: Example of subdivision of a two-dimensional domain

Once the domain has been discretized, the unknown function u within each element has to be found. If linear triangular elements are used, the unknown function u related to all the elements of the domain is defined as:

$$u^e(x, y) = \alpha_1^e + \alpha_2^e x + \alpha_3^e y \tag{2.9}$$

where α_1^e, α_2^e and α_3^e are unknown constant coefficients and e denotes the e-th element of the domain.

If we impose (2.9) on the three nodes of each linear element, we obtain:

$$\begin{aligned}
u_i^e &= \alpha_1^e + \alpha_2^e x_i^e + \alpha_3^e y_i^e \\
u_j^e &= \alpha_1^e + \alpha_2^e x_j^e + \alpha_3^e y_j^e \\
u_k^e &= \alpha_1^e + \alpha_2^e x_k^e + \alpha_3^e y_k^e
\end{aligned} \tag{2.10}$$

where x^e and y^e are the coordinates of the nodes related to the e-th element.

Solving the previous equations, we obtain the values of α_1^e, α_2^e and α_3^e and consequently the unknown function u^e expressed as:

$$u^e(x, y) = \sum_{n=1}^{3} u_n^e \varphi_n^e(x, y) \tag{2.11}$$

where $\varphi_n^e(x, y)$ defines the **interpolation functions**. These functions are given by:

$$\varphi_n^e(x, y) = \frac{1}{2A^e}(\alpha_{1n}^e + \alpha_{2n}^e x + \alpha_{3n}^e y) \qquad n = 1, 2, 3 \tag{2.12}$$

where α_{1n}^e, α_{2n}^e, α_{3n}^e depend on the values of the coordinates of the e-th element.

In (2.12), A^e is the area of the e-th element:

$$A^e = \frac{1}{2} \begin{vmatrix} 1 & x_i^e & y_i^e \\ 1 & x_j^e & y_j^e \\ 1 & x_k^e & y_k^e \end{vmatrix} \tag{2.13}$$

The problem can be formulated by using one of the following methods to obtain the system of equations: the Ritz method [10] or the Galerkin method [11]. The first considers the **homogeneous Neumann boundary condition**. This condition is a particular case of (2.4) in which $\gamma = t_0 = 0$. The total variational functional is represented as the summation of the variational functional of each element of the domain:

$$F(u) = \sum_{e=1}^{M} F^e(u^e) \tag{2.14}$$

where M denotes the total number of elements.

The functional related to each element is denoted as:

$$F^e(u^e) = \frac{1}{2} \iint_{\Omega^e} \left[a_x \left(\frac{\partial u^e}{\partial x} \right)^2 + a_y \left(\frac{\partial u^e}{\partial y} \right)^2 + b(u^e)^2 \right] d\Omega \tag{2.15}$$

$$- \iint_{\Omega^e} f u^e d\Omega$$

If we substitute (2.11) into the equation and differentiate F^e with respect to u_m^e, yields:

$$\frac{\partial F^e}{\partial u_m^e} = \sum_{n=1}^{3} u_n^e \iint_{\Omega^e} \left(a_x \frac{\partial \varphi_m^e}{\partial x} \frac{\partial \varphi_n^e}{\partial x} + a_y \frac{\partial \varphi_m^e}{\partial y} \frac{\partial \varphi_n^e}{\partial y} + b \varphi_m^e \varphi_n^e \right) d\Omega$$

$$- \iint_{\Omega^e} f \varphi_m^e d\Omega \tag{2.16}$$

$$with \quad m = 1,2,3$$

13

In matrix form, this is indicated as:

$$\left\{\frac{\partial F^e}{\partial u^e}\right\} = [K^e]\{u^e\} - \{r^e\} \tag{2.17}$$

where the elements of the matrix K^e and of the vector r^e are provided by the following integrals:

$$K_{mn}^e = \iint_{\Omega^e} \left(a_x \frac{\partial \varphi_m^e}{\partial x}\frac{\partial \varphi_n^e}{\partial x} + a_y \frac{\partial \varphi_m^e}{\partial y}\frac{\partial \varphi_n^e}{\partial y} + b\varphi_m^e \varphi_n^e\right) dxdy \qquad m, n = 1, 2, 3 \tag{2.18}$$

$$r_m^e = \iint_{\Omega^e} f\varphi_m^e dxdy \qquad m = 1, 2, 3 \tag{2.19}$$

The system of equations can be found: it is expressed as the summation over all the triangular elements, into which the domain is partitioned, of the derivatives of the subfunctional F^e respect to the unknown function u^e. The stationarity requirement on F is imposed:

$$\left\{\frac{\partial F}{\partial u}\right\} = \sum_{e=1}^{M}\left\{\overline{\frac{\partial F^e}{\partial u^e}}\right\} = \sum_{e=1}^{M}\left([\overline{K^e}]\{\overline{u^e}\} - \{\overline{r^e}\}\right) = \{0\} \tag{2.20}$$

The matrix $\overline{K^e}$ and the vector $\overline{r^e}$ are assembled to find the matrix and the vector associated to the entire domain:

$$[K] = \sum_{e=1}^{M}[\overline{K^e}] \tag{2.21}$$

$$\{r\} = \sum_{e=1}^{M}\{\overline{r^e}\} \tag{2.22}$$

14

So, the system of equations can be written compactly as:

$$[K]\{u\} = \{r\} \tag{2.23}$$

The derivation of the system assumed that u satisfies the homogeneous Neumann boundary condition on Γ_2. We can now extend the analysis to the general case in which $\gamma \neq 0$ and $t_0 \neq 0$. It is necessary to add an extra term to the functional $F(u)$ expressed as:

$$F_c(u) = \int_{\Gamma_2} \left(\frac{\gamma}{2}u^2 - t_0 u\right) d\Gamma \tag{2.24}$$

Assuming that Γ_2 comprises N segments, $F_c(u)$ can be rewritten with a summation:

$$F_c(u) = \sum_{s=1}^{N} F_c^s(u^s) \tag{2.25}$$

where F_c^s denotes the functional linked to the s-th segment of the surface examined.

The unknown function u within each segment is approximated in a way similar to the unknown function within each triangular element of the entire domain studied:

$$u^s = \sum_{n=1}^{2} u_n^s \varphi_n^s \tag{2.26}$$

where:

$$\varphi_1^s = 1 - \xi \qquad \varphi_2^s = \xi \tag{2.27}$$

15

and ξ is the normalized distance measured from node 1 to node 2 on the s-th segment.

Following the same mathematical steps adopted to find the derivative of F^e, the derivative of the functional associated to the s-th segment is obtained:

$$\frac{\partial F_c^s}{\partial u_m^s} = \sum_{n=1}^{2} u_n^s \int_0^1 \gamma \varphi_m^s \varphi_n^s l^s d\xi - \int_0^1 t_0 \varphi_m^s l^s d\xi \qquad (2.28)$$

where l^s is the length of the s-th segment.

In matrix form the above expression becomes:

$$\left\{ \frac{\partial F_c^s}{\partial u^s} \right\} = [K^s] \{u^s\} - \{r^s\} \qquad (2.29)$$

with the elements of K^s and r^s given by:

$$K_{mn}^s = \int_0^1 \gamma \varphi_m^s \varphi_n^s l^s d\xi \qquad m, n = 1, 2 \qquad (2.30)$$

$$r_m^s = \int_0^1 t_0 \varphi_m^s l^s d\xi \qquad m = 1, 2 \qquad (2.31)$$

The general system of equations is given by the union of all the derivatives calculated on the triangular elements into which the domain is splitted and all the derivatives evaluated on the segments that form the contour:

$$\begin{aligned}
\left\{ \frac{\partial F}{\partial u} \right\} &= \sum_{e=1}^{M} \left\{ \overline{\frac{\partial F^e}{\partial u^e}} \right\} + \sum_{s=1}^{N} \left\{ \overline{\frac{\partial F_c^s}{\partial u^s}} \right\} = \\
&= \sum_{e=1}^{M} \left(\left[\overline{K^e} \right] \{\overline{u^e}\} - \{\overline{r^e}\} \right) + \sum_{s=1}^{N} \left(\left[\overline{K^s} \right] \{\overline{u^s}\} - \{\overline{r^s}\} \right) = \{0\}
\end{aligned} \qquad (2.32)$$

16

Now that the system has been set up, it can be solved by imposing the Dirichlet boundary condition for the nodes on Γ_1.

After considering the Dirichlet boundary condition, the system will give us the unknowns u_m. There are several methods for solving the system which are divided into two large groups: **direct methods** and **iterative methods** [12]. The former are based on the Gaussian elimination and guarantee a correct solution to the system, the latter start from an initial guess and then minimize the residual error through various iterations. Usually, the iterative methods provide an approximate solution with some degree of accuracy. Then, there are other iterative methods that instead are able to give an exact solution after a certain number of iterations. Both methods have advantages and disadvantages so, the choice of the method depends on the problem we are interested into. We will describe these methods in a more detailed way later. It is necessary to keep in mind that the choice of the method is fundamental because it influences the efficiency of the Finite Element Method.

2.1.3   Higher-Order Elements

Once the method has been established, the next step is how to improve the accuracy. In Finite Element Method, two different approaches are commonly taken into account: one consists to split out the elements into smaller elements, the other uses higher-order elements.

A quadratic triangular element has six nodes, three of which are located in the center of its sides while the others are represented by the vertices.

In this case, the unknown function related to the e-th element is expressed as:

$$u^e(x, y) = \alpha_1^e + \alpha_2^e x + \alpha_3^e y + \alpha_4^e x^2 + \alpha_5^e xy + \alpha_6^e y^2 \qquad (2.33)$$
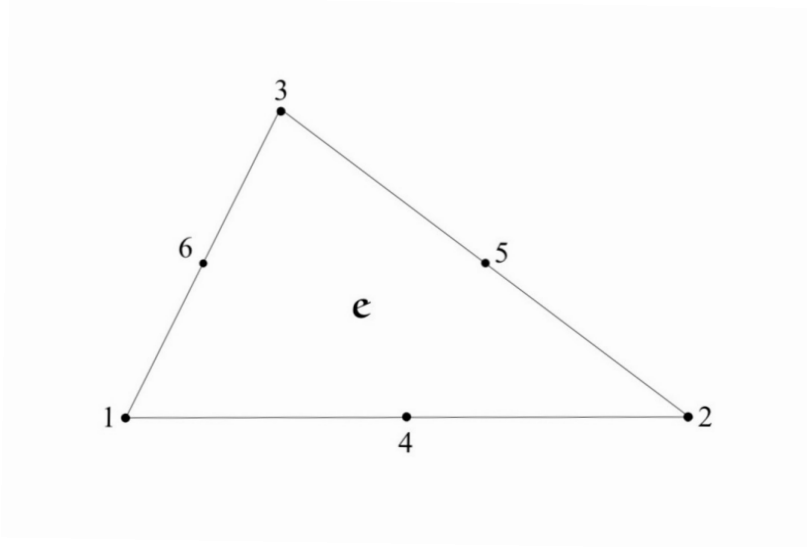
Figure 2.5: Quadratic triangular element

where the six coefficients $\alpha_1^e, \alpha_2^e, ..., \alpha_6^e$ are solved by imposing this equation at the six nodes:

$$u^e(x, y) = \sum_{n=1}^{6} u_n^e \varphi_n^e(x, y) \tag{2.34}$$

φ_n^e are the interpolation functions of the e-th element and they depend on L_n^e functions expressed as:

$$L_n^e(x, y) = \frac{1}{2A^e}(\alpha_{1n}^e + \alpha_{2n}^e x + \alpha_{3n}^e y) \qquad n = 1, 2, 3 \tag{2.35}$$

These functions are the same as the interpolation functions defined in the linear case and they can be examined by considering any point P within a triangular element. The area of the triangle defined by this point and nodes 2 and 3 is:

$$A_1 = \frac{1}{2} \begin{vmatrix} 1 & x & y \\ 1 & x_j^e & y_j^e \\ 1 & x_k^e & y_k^e \end{vmatrix} \tag{2.36}$$

18

From the expression of the area, it can be found that:

$$L_1^e = \frac{A_1}{A^e} = \frac{1}{2A^e} \left(\alpha_{11}^e + \alpha_{21}^e x + \alpha_{31}^e y \right) \tag{2.37}$$

We can do the same by looking at the other two areas formed by P. This leads to:

$$L_2^e = \frac{A_2}{A^e} = \frac{1}{2A^e} \left(\alpha_{12}^e + \alpha_{22}^e x + \alpha_{32}^e y \right) \tag{2.38}$$

$$L_3^e = \frac{A_3}{A^e} = \frac{1}{2A^e} \left(\alpha_{13}^e + \alpha_{23}^e x + \alpha_{33}^e y \right) \tag{2.39}$$

Once the interpolation functions have been constructed, one can obtain the elemental matrix K^e and the elemental vector r^e by using a numerical integration. A common integration scheme is Gaussian quadrature. For an integral evaluated on a triangular element:

$$\iint_{\Omega^e} F \left(L_1^e, L_2^e, L_3^e \right) dx dy = \sum_{m=1}^{M_q} A^e w_m F \left(L_{1m}^e, L_{2m}^e, L_{3m}^e \right) \tag{2.40}$$

where $(L_{1m}^e, L_{2m}^e, L_{3m}^e)$ are the sampling points and w_m are the weights.

2.1.4 Isoparametric Elements

As mentioned in the previous paragraph, the most important advantage of higher-order elements is that for a certain accuracy, they can use larger elements and smaller number of unknowns. However, elements with straight lines cannot model curved domains precisely. This problem can be overcome by using isoparametric elements which present curved lines.

One can define a set of barycentric coordinates which are more suitable respect to the cartesian ones to describe curved sides. It is important to define a mapping between xy-plane and $\xi\eta$-plane: the first illustrates an element with curved lines while the second represents a regular element with straight sides.
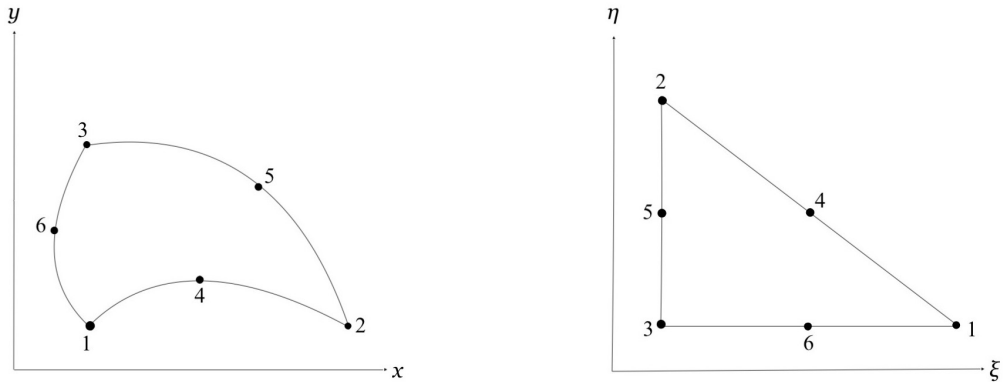
Figure 2.6: Two-dimensional element with curved sides in the xy-plane and its transformation in the $\xi\eta$-plane

The domain transformation is pointed out by the Jacobian matrix $\mathbf{J}$:

$$\mathbf{J} = \left[\begin{array}{cc} \frac{\partial x}{\partial \xi} & \frac{\partial y}{\partial \xi} \\ \frac{\partial x}{\partial \eta} & \frac{\partial y}{\partial \eta} \end{array} \right] \tag{2.41}$$

To introduce the concept of isoparametric elements, we can start considering triangular elements with curved sides in the xy-plane. Using the quadratic transformation, one can obtain:

$$x = \alpha_1 + \alpha_2\xi + \alpha_3\eta + \alpha_4\xi^2 + \alpha_5\xi\eta + \alpha_6\eta^2 \tag{2.42}$$

$$y = \alpha_1' + \alpha_2'\xi + \alpha_3'\eta + \alpha_4'\xi^2 + \alpha_5'\xi\eta + \alpha_6'\eta^2 \tag{2.43}$$

The unknown coefficients can be found by applying these two equations to the six nodes of the element. We obtain:

20

$$x = \sum_{n=1}^{6} x_n \varphi_n^e \left(\xi, \eta \right) \tag{2.44}$$

$$y = \sum_{n=1}^{6} y_n \varphi_n^e \left(\xi, \eta \right) \tag{2.45}$$

The mapping defined by (2.44) and (2.45) describes the geometry accurately to second order. One can achieve more accurate mappings by using higher-order mappings.

After the mapping of the element in the $\xi\eta$-plane, it is useful to express the unknown function u in terms of ξ and η. In the quadratic case:

$$u^e \left(\xi, \eta \right) = \sum_{n=1}^{6} u_n^e \varphi_n^e \left(\xi, \eta \right) \tag{2.46}$$

The interpolation functions depend on the regular domain and they can be identified starting from the interpolation functions associated to the deformed domain. It is necessary to point out the derivatives of these functions in the $\xi\eta$-plane to show the elements of the K^e matrix and of the r^e vector:

$$\frac{\partial \varphi_m^e}{\partial \xi} = \frac{\partial \varphi_m^e}{\partial x} \frac{\partial x}{\partial \xi} + \frac{\partial \varphi_m^e}{\partial y} \frac{\partial y}{\partial \xi} \tag{2.47}$$

$$\frac{\partial \varphi_m^e}{\partial \eta} = \frac{\partial \varphi_m^e}{\partial x} \frac{\partial x}{\partial \eta} + \frac{\partial \varphi_m^e}{\partial y} \frac{\partial y}{\partial \eta} \tag{2.48}$$

These equations can be written as:

$$\left\{ \begin{array}{c} \frac{\partial \varphi_m^e}{\partial \xi} \\ \frac{\partial \varphi_m^e}{\partial \eta} \end{array} \right\} = (\mathbf{J}) \left\{ \begin{array}{c} \frac{\partial \varphi_m^e}{\partial x} \\ \frac{\partial \varphi_m^e}{\partial y} \end{array} \right\} \tag{2.49}$$

where $\mathbf{J}$ is the Jacobian matrix defined above.

The definition of isoparametric elements can be considered also regarding quadrilaterals.
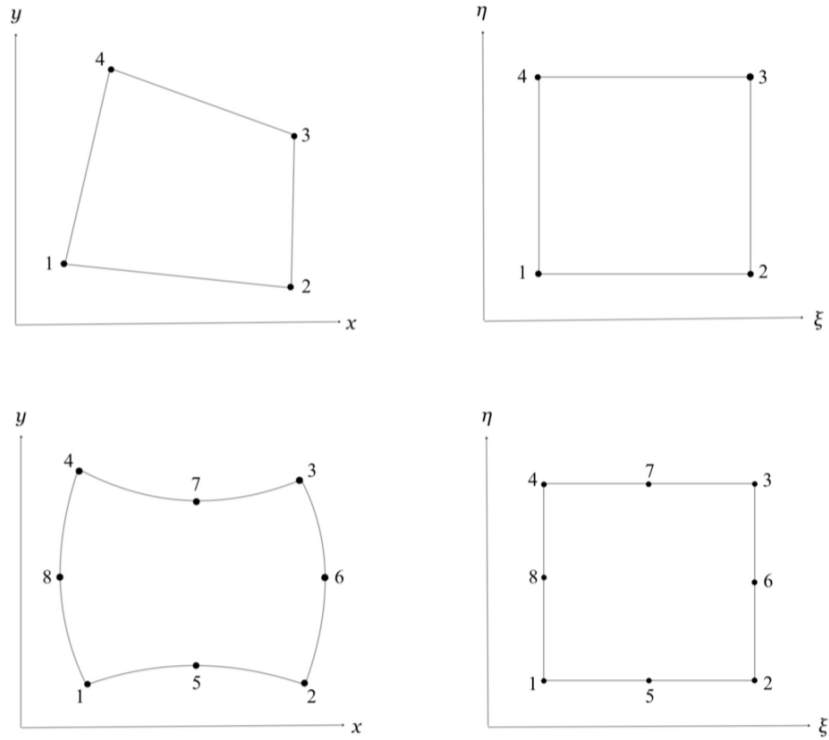
Figure 2.7: Quadrilateral linear and quadratic elements with curved sides in the xy-plane and their transformations in the $\xi\eta$-plane

A quadrilateral with straight lines is defined in the $\xi\eta$-plane in this way:

$$x = \sum_{n=1}^{4} x_n \varphi_n^e (\xi, \eta) \tag{2.50}$$

$$y = \sum_{n=1}^{4} y_n \varphi_n^e (\xi, \eta) \tag{2.51}$$

A quadrilateral element can be found out also through a biquadratic transformation. The transformation functions are:

$$\varphi_n^e (\xi, \eta) = \varphi_n^e (\xi) \, \varphi_n^e (\eta) \tag{2.52}$$

22

Starting from the interpolation functions, as it has already been seen in the case of triangular elements, one can define the elements of the K^e matrix and of the r^e vector through the Jacobian matrix which determines the domain transformation.

2.2 Application to the Acoustic Field

2.2.1 The Helmholtz Equation

As discussed previously, the Finite Element Method is one of the most common methods for describing and solving various problems in the engineering field. Our interest is directed to the field of acoustic waves. The goal is to calculate the sound pressure in different points of a pipe affected by geometrical deformations to identify them and to monitor the condition of the duct. Therefore we use the acoustic transformation and obtain the structure of the duct without deformation. In this case, the second-order differential equation which defines the boundary-value problem is delineated by the **Helmholtz equation**. Implemented by the German physicist Hermann von Helmholtz (1821-1894), a pioneer in acoustics, electromagnetism and physiology, the Helmholtz equation is used to study physical problems involving partial differential equations (PDEs) in both space and time. It describes a time-independent form of the wave equation and it can be carried out from the **linear continuity equation** and the **linear Euler equation** [1]. Given $p(\mathbf{r})$ the pressure at a particular point $\mathbf{r}$, one can obtain:

$$\nabla p = -j\omega \rho_0 \mathbf{v} \tag{2.53}$$

$$j\omega p = -B_0 \nabla \cdot \mathbf{v} \tag{2.54}$$

where $\mathbf{v}$ is the fluid speed, ρ_0 is the rest density and B_0 is the compression modulus.

Applying the divergence to the first equation, we find:

$$\nabla^2 p = -j\omega\rho_0\left(-\frac{j\omega p}{B_0}\right) \qquad (2.55)$$

and this yields the Helmholtz equation:

$$\nabla^2 p + k^2 p = 0 \qquad (2.56)$$

where:

$$k = \omega\sqrt{\frac{\rho_0}{B_0}} = \frac{\omega}{v_0} \qquad (2.57)$$

k is the wavenumber. It is known as the spatial frequency of a wave measured in cycles per unit distance.

The Helmholtz equation must be accompanied by boundary conditions in order to be solved. The most common is the **hard boundary condition** given by:

$$\frac{\partial p}{\partial v} = 0 \qquad (2.58)$$

There are also non-homogeneous boundary conditions in which the pressure value or its derivative are taken as known values. These terms act as sources.

2.2.2 Finite Element Method for measuring the Sound Pressure

To solve the Helmholtz equation, the FEM is used. The Helmholtz equation is expressed as sum of integrals:

$$\int_S \nabla \psi \cdot \nabla p \, dS - k^2 \int_S \psi p \, dS = \int_{\partial S} \psi \frac{\partial p}{\partial v} \, dl \qquad (2.59)$$

The last integral illustrates the known term and it is a contour integral. $f = \frac{\partial p}{\partial v}$ is the source or excitation function which can be also equal to zero. The parts of the domain where the source function is nonzero are the ports.

2.2.3 Analysis of the Sound Pressure in the Planar Case

Of course, also in the acoustic waves field, it is necessary to adopt one of the two methods seen in the general case (Ritz method or Galerkin method) to formulate and solve the system. The pressure p, associated with a particular element into which the domain is divided, is provided by the summation of the product between the pressure related to all the element nodes and some functions related to the nodes called interpolation functions:

$$p = \sum_{n=1}^{N} p_n \varphi_n \qquad (2.60)$$

Therefore the pressure p_n corresponds to the unknown function u_n^e and φ_n is the interpolation function seen previously in the description of FEM. Using Galerkin's method, the system of equation to solve, in matrix form, is given by:

$$\left(\mathbf{A} - k^2 \mathbf{B} \right) \mathbf{p} = \mathbf{C} \qquad (2.61)$$

where $\mathbf{A} = [A_{m,n}]$, $\mathbf{B} = [B_{m,n}]$, $\mathbf{C} = [C_{m,1}]$ and:

$$A_{m,n} = \int_S \nabla\varphi_m \cdot \nabla\varphi_n dS = \int_S \left(\frac{\partial\varphi_m}{\partial x}\frac{\partial\varphi_n}{\partial x} + \frac{\partial\varphi_m}{\partial y}\frac{\partial\varphi_n}{\partial y} \right) dS \qquad (2.62)$$

$$B_{m,n} = \int_S \varphi_m \varphi_n dS \qquad (2.63)$$

$$C_{m,1} = \int_{\partial S} \varphi_m f dl \qquad (2.64)$$

The elements of the matrices $\mathbf{A}$ and $\mathbf{B}$ correspond to the elements of the matrix K^e_{mn} of the general case evaluated previously, while the elements of the vector $\mathbf{C}$ match with the elements of the vector r^e_m.

This leads to:

$$\mathbf{p} = \left(\mathbf{A} - k^2 \mathbf{B} \right)^{-1} \mathbf{C} \qquad (2.65)$$

Once the coefficients have been obtained, it is therefore possible to express the pressure related to each element of the domain.

2.2.4 Analysis of the Sound Pressure in the Radial Case

One can analyze also the problem from the cylindrical coordinates point of view. Cylindrical coordinates are a generalization of two-dimensional polar coordinates to three dimension by adding a height z. These coordinates are defined by ρ which is the distance between the origin and the projection of a chosen point in xy-plane, by ϕ known as azimuth which is the angle between ρ and the reference direction on the xy-plane and by z which is the distance from the xy-plane to the chosen point in the space. The presence of ρ which is, in simple terms, the radius of the cylinder, and of the angle ϕ

which defines the base surface of the cylinder, cause this analysis to define a rotary behavior.
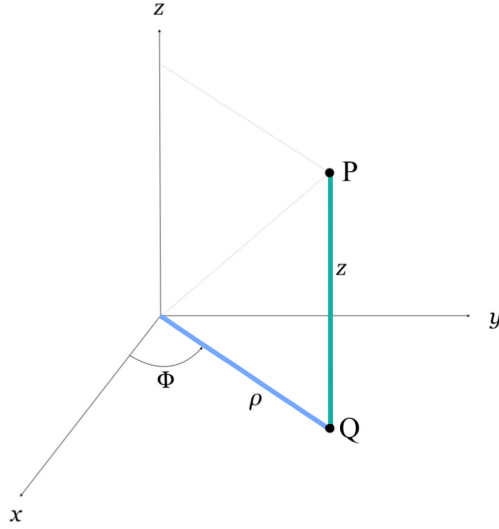
Figure 2.8: Cylindrical coordinates

In this case we have $dV = \rho d\rho d\phi dz$ and $dS = \rho d\rho d\phi$, the volume element and the surface element respectively. The pressure p delineating every element of the domain, is given by the same expression of the planar case:

$$p = \sum_{n=1}^{N} p_n \varphi_n \qquad (2.66)$$

The elements of matrix $\mathbf{A}$, $\mathbf{B}$ and of the vector $\mathbf{C}$ are:

$$A_{m,n} = \int_V \nabla \varphi_m \cdot \nabla \varphi_n dV = 2\pi \int \left(\frac{\partial \varphi_m}{\partial \rho} \frac{\partial \varphi_n}{\partial \rho} + \frac{\partial \varphi_m}{\partial z} \frac{\partial \varphi_n}{\partial z} \right) \rho d\rho dz \qquad (2.67)$$

$$B_{m,n} = 2\pi \int \varphi_m \varphi_n \rho d\rho dz \qquad (2.68)$$

27

$$C_{m,1} = 2\pi \int \varphi_m f \rho d\rho \qquad (2.69)$$

With these new matrix expressions, we can now determine the pressure at each point of the domain as in the planare case.

2.2.5 Acoustic Transformation

As we have already mentioned, our aim is the determination of sound pressure in geometries affected by deformations and their transformation into regular domains. The first transformation is linked to the mapping of a triangle into another. The reference geometry is defined by the coordinates x and y while the deformed one is managed by x' and y'.
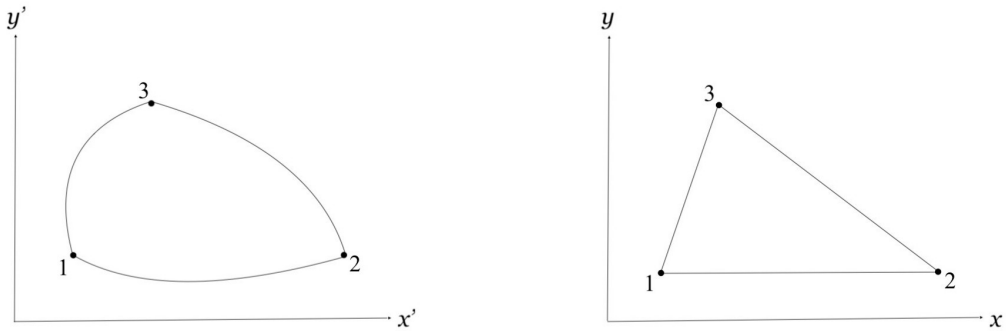
Figure 2.9: Mapping of a deformed triangle in the $x'y'$-plane to the reference one in the xy-plane

This mapping yields:

$$\mathbf{r}' = \overline{\mathbf{T}}' \boldsymbol{\lambda} \qquad (2.70)$$

where $\overline{\mathbf{T}}'$ is a matrix specified by:

$$\overline{\mathbf{T}}' = \begin{bmatrix} x'_1 & x'_2 & x'_3 \\ y'_1 & y'_2 & y'_3 \\ 1 & 1 & 1 \end{bmatrix} \tag{2.71}$$

We can calculate the inverse matrix as follows:

$$\left(\overline{\mathbf{T}}'\right)^{-1} = \frac{1}{\det \overline{\mathbf{T}}'} \begin{bmatrix} y'_2 - y'_3 & x'_3 - x'_2 & x'_2 y'_3 - x'_3 y'_2 \\ y'_3 - y'_1 & x'_1 - x'_3 & x'_3 y'_1 - x'_1 y'_3 \\ y'_1 - y'_2 & x'_2 - x'_1 & x'_1 y'_2 - x'_2 y'_1 \end{bmatrix} \tag{2.72}$$

Now the mapping can be expressed more linearly:

$$\mathbf{r} = \overline{\mathbf{T}} \left(\overline{\mathbf{T}}'\right)^{-1} \mathbf{r}' = \boldsymbol{\tau} \mathbf{r}' \tag{2.73}$$

where $\mathbf{r}'$ shows the system connected to the deformed geometry, $\mathbf{r}$ implements the reference geometry and $\boldsymbol{\tau}$ is the transformation.

Once the mapping has been obtained, the reference coordinates can thus be performed:

$$x = \tau_{xx} x' + \tau_{xy} y' + \tau_{13} \tag{2.74}$$

$$y = \tau_{yx} x' + \tau_{yy} y' + \tau_{23} \tag{2.75}$$

The transformation is governed by the Jacobian matrix:

$$\mathbf{J} = \begin{bmatrix} \tau_{xx} & \tau_{xy} & 0 \\ \tau_{yx} & \tau_{yy} & 0 \\ 0 & 0 & 1 \end{bmatrix} \tag{2.76}$$

29

where:

$$\tau_{xx} = x_1 \frac{(y_2' - y_3')}{\det \overline{\mathbf{T}}'} + x_2 \frac{(y_3' - y_1')}{\det \overline{\mathbf{T}}'} + x_3 \frac{(y_1' - y_2')}{\det \overline{\mathbf{T}}'} \qquad (2.77)$$

$$\tau_{xy} = x_1 \frac{(x_3' - x_2')}{\det \overline{\mathbf{T}}'} + x_2 \frac{(x_1' - x_3')}{\det \overline{\mathbf{T}}'} + x_3 \frac{(x_2' - x_1')}{\det \overline{\mathbf{T}}'} \qquad (2.78)$$

$$\tau_{yx} = y_1 \frac{(y_2' - y_3')}{\det \overline{\mathbf{T}}'} + y_2 \frac{(y_3' - y_1')}{\det \overline{\mathbf{T}}'} + y_3 \frac{(y_1' - y_2')}{\det \overline{\mathbf{T}}'} \qquad (2.79)$$

$$\tau_{yy} = y_1 \frac{(x_3' - x_2')}{\det \overline{\mathbf{T}}'} + y_2 \frac{(x_1' - x_3')}{\det \overline{\mathbf{T}}'} + y_3 \frac{(x_2' - x_1')}{\det \overline{\mathbf{T}}'} \qquad (2.80)$$

In conclusion, the matrix $\overline{\mathbf{T}}$ which defines the transformation can be pointed out:

$$\overline{\mathbf{T}} = \frac{\mathbf{J}\mathbf{J}^T}{\det \mathbf{J}} = \frac{1}{\det \mathbf{J}} \begin{bmatrix} \tau_{xx}^2 + \tau_{xy}^2 & \tau_{xx}\tau_{yx} + \tau_{xy}\tau_{yy} & 0 \\ \tau_{xx}\tau_{yx} + \tau_{xy}\tau_{yy} & \tau_{yx}^2 + \tau_{yy}^2 & 0 \\ 0 & 0 & 1 \end{bmatrix} \qquad (2.81)$$

where:

$$\det \mathbf{J} = \tau_{xx}\tau_{yy} - \tau_{xy}\tau_{yx} \qquad (2.82)$$

2.2.6 Transformation on Quadrilaterals

Now suppose we have a quadrilateral having the following coordinates: $(x_i', y_{1,i}')$, $(x_i', y_{2,i}')$, $(x_{i+1}', y_{1,i+1}')$, $(x_{i+1}', y_{2,i+1}')$. The goal is to convert it into another quadrilateral showing these new points: (x_i, y_1), (x_i, y_2), (x_{i+1}, y_1), (x_{i+1}, y_2). In addition, it is pointed out that:

$$x_i' = x_i \qquad (2.83)$$

$$x'_{i+1} = x_{i+1} \tag{2.84}$$

where i determines the point and the region between i and $i+1$. These formulas imply that the transformation affects only the y side.
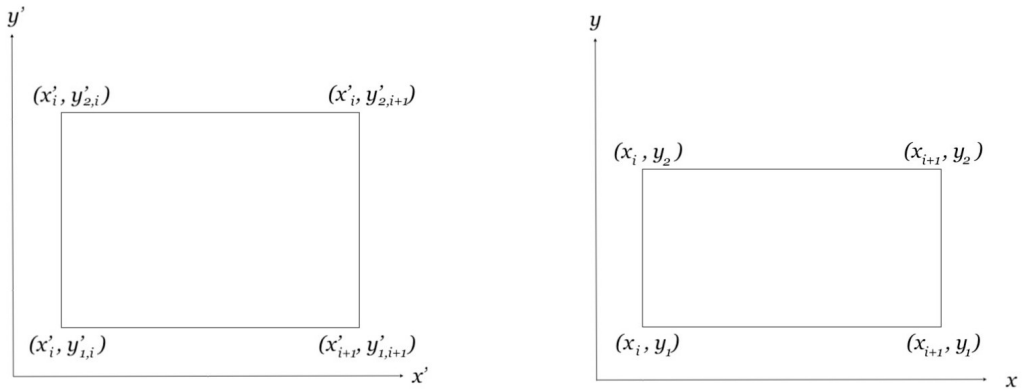
Figure 2.10: Mapping of a quadrilateral into another

The equation that express this change of geometry is the following:

$$y = \frac{y' - y'_1}{h'} h \tag{2.85}$$

where $h = y_2 - y_1$ denotes the height of the resulting quadrilateral and $h' = y'_2 - y'_1$ stands for the height of the deformed one.

The two values along the y direction associated to the deformation are achieved thanks to a procedure known as **linear interpolation**. It is one of the simplest interpolation method. To interpolate means to estimate a particular value of a function starting from certain known values of the function. With the linear interpolation any pair of adiacent point is simply joined by a segment. In general, denoting the known values as (x_i, y_i) and (x_{i+1}, y_{i+1}), the linear interpolation function can be finally written:

$$y = f(x) = \frac{x_{i+1} - x}{x_{i+1} - x_i} y_i + \frac{x - x_i}{x_{i+1} - x_i} y_{i+1} = y_i X_i + y_{i+1} X_{i+1} \qquad (2.86)$$
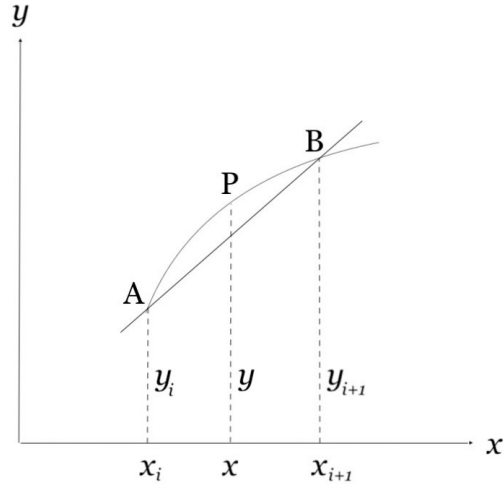
Figure 2.11: Linear interpolation to estimate the value of the point P starting from A and B points

Employing this function, we find the values that characterize the height of the quadrilateral:

$$y_1' = y_{1,i}' X_i + y_{1,i+1}' X_{i+1} \qquad (2.87)$$

$$y_2' = y_{2,i}' X_i + y_{2,i+1}' X_{i+1} \qquad (2.88)$$

Substituting these values into (2.85):

$$y = \frac{y' - y_{1,i}' X_i - y_{1,i+1}' X_{i+1}}{h_i' X_i + h_{i+1}' X_{i+1}} h \qquad (2.89)$$

The inverse transformation is given by:

$$y' = y\frac{\left(h_i'X_i + h_{i+1}'X_{i+1}\right)}{h} + y_{1,i}'X_i + y_{1,i+1}'X_{i+1} \qquad (2.90)$$

After getting these expressions, the elements of the Jacobian matrix are thus identified:

$$J_{yy} = \frac{\partial y}{\partial y'} = \frac{h}{h_i'X_i + h_{i+1}'X_{i+1}} \qquad (2.91)$$

$$J_{yx} = \frac{\partial y}{\partial x'} = \left[\frac{\left(y_{1,i}' - y_{1,i+1}'\right)}{h_i'X_i + h_{i+1}'X_{i+1}} - \frac{\left(y' - y_{1,i}'X_i - y_{1,i+1}'X_{i+1}\right)}{\left(h_i'X_i + h_{i+1}'X_{i+1}\right)^2}\left(h_{i+1}' - h_i'\right)\right]\frac{h}{\Delta_i} \qquad (2.92)$$

The Jacobian matrix can be finally expressed:

$$\mathbf{J} = \begin{bmatrix} 1 & 0 & 0 \\ J_{yx} & J_{yy} & 0 \\ 0 & 0 & 1 \end{bmatrix} \qquad (2.93)$$

where the determinant is:

$$\det \mathbf{J} = J_{yy} \qquad (2.94)$$

The matrix $\overline{\mathbf{T}}$ that describes the transformation on quadrilaterals is thus obtained:

$$\overline{\mathbf{T}} = \frac{\mathbf{J}\mathbf{J}^T}{\det \mathbf{J}} = \frac{1}{\det \mathbf{J}} \begin{bmatrix} 1 & J_{yx} & 0 \\ J_{yx} & J_{yx}^2 + J_{yy}^2 & 0 \\ 0 & 0 & 1 \end{bmatrix} \qquad (2.95)$$

33

2.2.7 Anisotropic Case

In the previous two sections we have seen how the acoustic transformation takes place in the two-dimensional domains. In particular, we have evaluated the mapping between a deformed triangle and a regular one and we have done the same also considering quadrilaterals. Defining the elements that make up the mesh and therefore allowing us to perform the geometric transformation is of fundamental importance. The accuracy of the results depends on the elements we are going to use and on their properties. As we have already seen, the transformation is based on linear interpolation and our task is to find an approximation between the values of the deformed structure and the same values related to the regular structure and we want the convergence between these values to be equal to zero. To satisfy this request, it is necessary to emphasize that the considered element must be **anisotropic**. In the isotropic mesh case, if we want to have a smaller mesh along one of the two directions, we have to deal with smaller equilateral triangles. However, in the anisotropic case, if we want smaller elements along a direction, we can modify their shape by going to stretch them. These triangles are able to cover a larger area respect to the equilateral triangles within our geometry [13]. Furthermore, the analysis of an anisotropic mesh is also convenient from the computational point of view because it requires the use of a smaller quantity of elements given their ability to spread within the structure.

Chapter 3

Guided Propagation of Sound

The Finite Element Method is one of the most important methods that are used for the detailed analysis of the behavior of a system. In particular, we have used it to determine the different sound pressure points inside a deformed pipe with consequent transformation of the geometry. Sound is a set of pressure waves and it can propagate through various media. During their propagation, waves can be reflected, refracted or attenuated by the medium. All media have three properties which affect the behavior of sound propagation [14]:

- The speed of sound which is given by the relationship between density and pressure
- The motion of the medium
- The viscosity of the medium which determines the rate at which sound is attenuated

What we are interested into is the propagation of sound waves in particular regions. In this chapter we will therefore describe guided propagation from a general point of view, in particular we will discuss the rectangular and the circular waveguide whose parameters will help us to determine the solution of our problem and then consider the multimode acoustics which is based on the modal analysis of the geometry from the acoustic point of view. We will evaluate the importance of normalization and the main concepts of impedance and scattering matrix and then conclude the chapter with the definition of acoustic power and its importance in calculating the pressure at the ports.

3.1 A General Description of Guided Propagation

The study of guided propagation is based on the analysis of waves that propagate in cylindrical regions. The cylindrical region, delimited by walls that can be metallic, is known as a **waveguide**. The name is linked to the ability to guide the wave along the axis of this region.
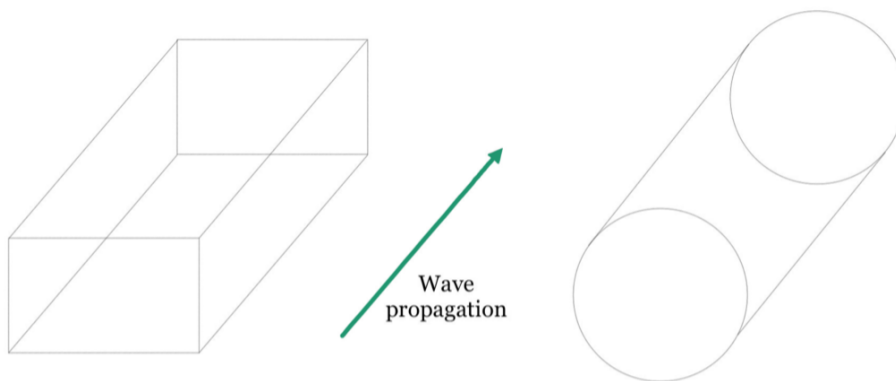
Figure 3.1: Examples of waveguides

The waves that propagate along a structure are characterized by an exponential dependence on the direction of propagation, which we assume is indicated by x: $e^{\mp\gamma x}$, where γ is known as the **propagation constant**. The propagation constant defines the phase and amplitude of each component of the wave. Guided propagation has the following characteristics:

- The transverse dimensions of the guide must be in the order of the wavelength and the frequency at which we operate must be positive
- The fields that can be propagated with the exponential law described above are particular field configurations known as **modes**. For this reason, guided propagation is also called **modal propagation**

To examine these modes and their properties, it is necessary to consider also the boundary conditions. Given the difficulty of obtaining a direct solution, we must consider a set of auxiliary functions called potentials [15]. The

different types of modes are specified with subscripts. These are integers represented as m and n and can take values from 0 to infinity. The combination of these two integers defines a particular field configuration. In particular, the mode defined with subscript equal to 00 is known as the **fundamental mode**. For each mode there is a lower frequency limit. This is known as the **cut-off frequency**. Below this frequency no signals can propagate along the waveguide.

In reality, there are waveguides of different types and shapes. The rectangular waveguide is probably the most used due to its simplicity and good electromagnetic properties and it is employed in many applications.
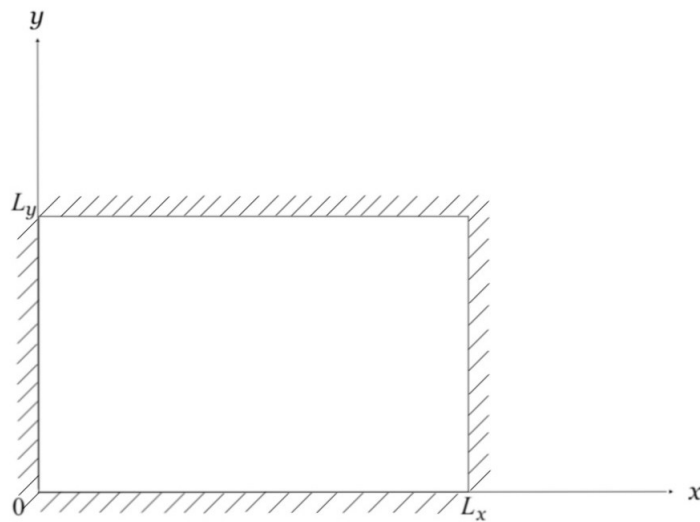
Figure 3.2: Rectangular guide

In this case, the potential function is:

$$\varphi\left(x, y\right) = X\left(x\right) Y\left(y\right) \tag{3.1}$$

Starting from this function, it is possible to calculate X and Y:

$$X = A \cos\left(k_x x\right) + B \sin\left(k_x x\right) \tag{3.2}$$

$$Y = C \cos{(k_y y)} + D \sin{(k_y y)} \tag{3.3}$$

where:

$$k_x = \frac{m\pi}{L_x} \quad m = 0, 1, ... \tag{3.4}$$

$$k_y = \frac{n\pi}{L_y} \quad n = 0, 1, ... \tag{3.5}$$

k_x and k_y introduce the eigenvalues linked to the x and y direction respectively while m and n are the integers which represent the possible combinations of modes. The generic mode i is therefore associated with a pair (m, n). Considering an arbitrary constant C_{mn}, we can write:

$$\varphi_i(x, y) = \varphi_{mn}(x, y) = C_{mn} \cos{\frac{m\pi x}{L_x}} \cos{\frac{n\pi y}{L_y}} \tag{3.6}$$

$$k_{mn} = \sqrt{\left(\frac{m\pi}{L_x}\right)^2 + \left(\frac{n\pi}{L_y}\right)^2} \tag{3.7}$$

$$\gamma_{mn} = \sqrt{\left(\frac{m\pi}{L_x}\right)^2 + \left(\frac{n\pi}{L_y}\right)^2 - k^2} \tag{3.8}$$

where k_{mn} is the eigenvalue associated with each pair of integers that define the modes, γ_{mn} is the propagation constant and k is the wavenumber [15].

Another type of guide particularly used is the circular one [15]. It is employed to propagate circular polarization signals, to feed circular horns and it is widely used especially with regards to antennas.
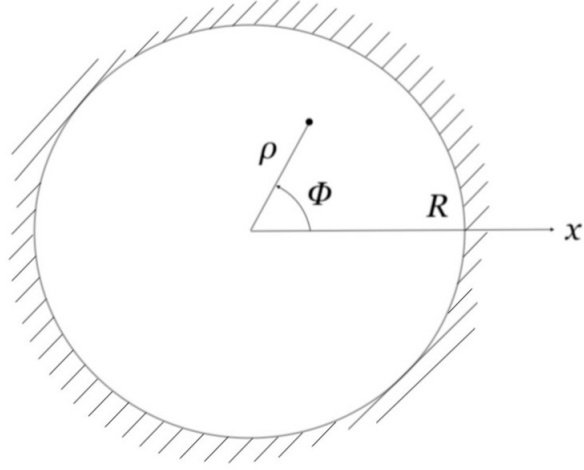
Figure 3.3: Circular guide

As for the rectangular guide, we write the potential function:

$$\varphi\left(\rho, \phi\right) = J_m\left(k_{mn}\rho\right) \begin{bmatrix} \cos\left(m\phi\right) \\ \sin\left(m\phi\right) \end{bmatrix} \tag{3.9}$$

where J_m specifies a group of functions known as Bessel functions.

Bessel functions are a set of mathematical functions derived around 1817 by the German astronomer Bessel [16]. Nowadays, these functions are spent for the description of many physical phenomena including the flow of heat in a cylinder and the motion of fluids. The zeros of Bessel functions are known and therefore also the zeros of the derivatives of these functions will be known. From the values of these zeros, we can find the expression of the eigenvalues k_{mn}:

$$k_{mn} = \frac{\chi'_{mn}}{R} \tag{3.10}$$

where χ'_{mn} is the n-th zero of J'_m and R is the radius of the circular guide.

χ'_{mn}	$n = 1$	2	3
$m = 0$	3.8317	7.0156	10.1735
1	1.8412	5.3314	8.5363
2	3.0542	6.7061	9.9695
3	4.2012	8.0152	11.3459
4	5.3176	9.2824	12.6819
5	6.4156	10.5199	13.9872
6	7.5013	11.7349	15.2682

Figure 3.4: Values of the zeros of Bessel functions

The potential function will become:

$$\varphi\left(\rho,\phi\right) = A_{mn} J_m\left(\frac{\chi'_{mn}}{R}\rho\right)\left[\begin{array}{c}\cos\left(m\phi\right)\\\sin\left(m\phi\right)\end{array}\right] \tag{3.11}$$

where A_{mn} is an arbitrary constant.

Finally, the propagation constant is expressed as follows:

$$\gamma_{mn} = \sqrt{\left(\frac{\chi'_{mn}}{R}\right)^2 - k^2} \tag{3.12}$$

3.2 Multimode Acoustics

After having described the concept of guided propagation and some of its properties and characteristics, it is now possible to specify the particular case related to sound propagation in pipes. Modes in circular pipes can be classified according to the two indices, also mentioned in the previous section: m, known as the azimuthal index, and n, which is the radial one. As before, the potential function is found out, in this case it is a pressure wave:

$$p_{mn}\left(\rho, \phi\right) = A_{mn} J_m \left(\frac{\chi'_{mn}}{R}\rho\right) \left[\begin{array}{c} \cos\left(m\phi\right) \\ \sin\left(m\phi\right) \end{array}\right] \qquad (3.13)$$

where R is the radius of the pipe, χ'_{mn} is the n-th zero of the derivative of J_m and A_{mn} are normalization constants such that:

$$\int_S p_{mn}^2 dS = 1 \qquad (3.14)$$

Introducing the expression of the eigenvalues related to the modes as $k_{mn} = \frac{\chi'_{mn}}{R}$, the propagation constant is calculated:

$$\gamma_{mn} = \sqrt{k_{mn}^2 - k^2} \qquad (3.15)$$

where $k = \frac{\omega}{v}$ is the wavenumber. Dealing with sound waves, the speed v is the speed of sound [17].

The fundamental mode is the most important mode and it is the only capable of propagating in the absence of the other modes. In this case, the fundamental mode is given by $m = 0$ and $n = 0$ and conventionally $\chi'_{00} = 0$. However, a generic mode propagates along the axial direction, assumed to be z, as $e^{-\gamma_{mn}z}$.

In general, wave propagation can be described as an electrical circuit characterized by a certain voltage and a certain current value. In the sound

41

field, voltage equals pressure, while current equals sound speed [1]. The relationship between pressure and sound velocity is given by the linear Euler equation that we have already expressed in the previous chapter:

$$\nabla p = -j\omega\rho_0 \mathbf{v} \tag{3.16}$$

where ρ_0 is the rest density.

The component of the speed of the sound wave directed along the direction of propagation z is given by the following expression:

$$v_z = -\frac{1}{j\omega\rho_0}\frac{\partial p}{\partial z} \tag{3.17}$$

The pipe in which the sound wave will flow, represents a cavity. The sound pressure in any cavity is closely related to the atmospheric pressure p_0, in more details, to the pressure that we find inside the cavity in total absence of sound field:

$$p(z) = p_0 e^{-\gamma z} \tag{3.18}$$

Deriving the pressure with respect to space and substituting the result into (3.17), we find out:

$$v_z = \frac{\gamma}{j\omega\rho_0}p \tag{3.19}$$

We get the relationship between pressure and speed, which, referring to electronics, corresponds to the link between voltage and current. In an electronic circuit, the ratio between voltage and current is known as **impedance**. Impedance performs the total opposition to alternating current by an electronic circuit [18]. In the sound field case, it is a constant related to the propagation of sound waves in an acoustic medium. The reciprocal of impedance

is **admittance**. Therefore, the ratio between speed and pressure can be determined and gives birth to the wave admittance:

$$Y = \frac{\gamma}{j\omega\rho_0} \tag{3.20}$$

In case we are dealing with the fundamental mode, in which the eigenvalue is equal to zero, the propagation constant is $\gamma = j\frac{\omega}{v}$ and the wave admittance will be simplified:

$$Y = \frac{1}{v\rho_0} \tag{3.21}$$

The expression of the wave admittance will prove to be fundamental for the calculation of the pressure. It is therefore necessary to pay careful attention.

3.2.1 Normalization

Previously, we pointed out the pressure wave equation. This depends on a series of normalization coefficients A_{mn} for which it results:

$$\int_S p_i^2 dS = \int_S p_{mn}^2 dS = 1 \tag{3.22}$$

where i is the index of the generic mode associated to the pair (m, n).

The normalization constants are therefore expressed as [17]:

$$A_{mn} = \frac{1}{\sqrt{2\pi \int_0^R \rho J_m^2 (k_{mn}\rho)\, d\rho}} \quad if \quad m = 0 \tag{3.23}$$

$$A_{mn} = \frac{1}{\sqrt{\pi \int_0^R \rho J_m^2 (k_{mn}\rho) \, d\rho}} \quad if \quad m > 0 \tag{3.24}$$

In evaluating our geometry, using the FEM procedure and referring in particular to the radial case as described in the previous chapter, we will consider Bessel functions but with the azimuthal index $m = 0$ [1]. At each port yields:

$$p = \left(F_0^+ + F_0^-\right) Q_0 + \sum_{n=1} \left(F_n^+ + F_n^-\right) Q_n J_0 \left(k_{0n}\rho\right) \tag{3.25}$$

$$v_z = \frac{k}{\omega \rho_0} \left(F_0^+ - F_0^-\right) Q_0 + \sum_{n=1} \frac{\gamma_{0n}}{j\omega \rho_0} \left(F_n^+ - F_n^-\right) Q_n J_0 \left(k_{0n}\rho\right) \tag{3.26}$$

where p is the sound pressure, v_z is the sound speed in the direction of propagation, Q_0 and Q_n are the normalization components referred to a null radial index and to any radial index respectively and finally we find F_0^+ and F_n^+ which describe the incident wave flowing in the pipe and F_0^- and F_n^- characterizing the reflected wave.

The normalization is such that:

$$2\pi Q_n^2 \int_0^R \rho J_0^2 \left(k_{0n}\rho\right) d\rho = 1 \tag{3.27}$$

From this expression, the normalization constants are thus derived:

$$Q_0 = \frac{1}{\sqrt{\pi R^2}} \tag{3.28}$$

$$Q_n = \frac{1}{\sqrt{2\pi \int_0^R \rho J_0^2 \left(k_{0n}\rho\right) d\rho}} \tag{3.29}$$

Our analysis also concerns a planar case, which therefore is modeled by using a set of Cartesian coordinates and it is defined by a rectangular two-dimensional structure. To describe the normalization, we must consider the definition of rectangular guide. The generic mode is expressed by an index i and it is associated with a function $\cos\left(\frac{i\pi s}{L}\right)$ where L is the length of the port and s is a curvilinear coordinate defined on the port that varies from 0 and L. The eigenvalue, as it happens for the rectangular guide, is given by the following expression:

$$k_i = \frac{i\pi}{L} \tag{3.30}$$

At each port, we obtain the pressure and the sound velocity:

$$p = \sum_n \left(F_n^+ + F_n^-\right) \sqrt{\frac{\varepsilon_{n0}}{L}} \cos\left(\frac{n\pi s}{L}\right) \tag{3.31}$$

$$v_z = \sum_n \frac{\gamma_n}{j\omega\rho_0} \left(F_n^+ - F_n^-\right) \sqrt{\frac{\varepsilon_{n0}}{L}} \cos\left(\frac{n\pi s}{L}\right) \tag{3.32}$$

where:

$$\varepsilon_{n0} = \begin{cases} 1 & if \quad n = 0 \\ 2 & otherwise \end{cases} \tag{3.33}$$

The term under root is used to have the normalization, in fact it results:

$$\int_0^L \left(\sqrt{\frac{\varepsilon_{n0}}{L}} \cos\left(\frac{n\pi s}{L}\right)\right)^2 ds = 1 \tag{3.34}$$

3.2.2 Voltage and Current Matrices

Previously, we have mentioned that the pressure analysis within a pipe can be interpreted in a more general way as a circuit analysis in which voltage and current are the parameters to be evaluated. This similarity leads us to model pressure and velocity at each domain port so that they depend on voltage and current values [17]. In formulas:

$$p\left(x, y, z'\right) = \sum_i p_i\left(x, y\right) \left[V_i^+ e^{-\gamma_i z'} + V_i^- e^{\gamma_i z'}\right] \tag{3.35}$$

$$
\begin{aligned}
v_z\left(x, y, z'\right) &= \sum_i v_{zi}\left(x, y\right) \left[I_i^+ e^{-\gamma_i z'} + I_i^- e^{\gamma_i z'}\right] = \\
&= \sum_i \frac{\gamma_i}{j\omega\rho_0} p_i\left(x, y\right) \left[V_i^+ e^{-\gamma_i z'} - V_i^- e^{\gamma_i z'}\right]
\end{aligned}
\tag{3.36}
$$

where $\frac{\gamma_i}{j\omega\rho_0} = Y_i$ is the wave admittance, z' is a coordinate that enters into the ports, V_i^+ and V_i^- are the incident and reflected voltage waves respectively and finally I_i^+ and I_i^- are the current waves. At the first port it turns out $z = z'$ while at the other port we have $z = -z'$.

The problem is then expressed in matrix form:

$$\mathbf{V}^\pm = \begin{bmatrix} V_1^\pm \\ V_2^\pm \\ \dots \\ V_N^\pm \end{bmatrix} \qquad \mathbf{I}^\pm = \begin{bmatrix} I_1^\pm \\ I_2^\pm \\ \dots \\ I_N^\pm \end{bmatrix} \tag{3.37}$$

From this expression, the general voltage and current matrices are obtained:

$$\mathbf{V} = \mathbf{V}^+ + \mathbf{V}^- \tag{3.38}$$

$$\mathbf{I} = \mathbf{I}^+ + \mathbf{I}^- \tag{3.39}$$

We can therefore determine the impedance matrix:

$$\mathbf{V} = \mathbf{ZI} \qquad (3.40)$$

Finally, we impose the condition of absence of velocity at each point of the domain and the pressure term p_j for each mode and each port that we are going to consider. Then, we test the result with the normalized functions p_i previously analyzed. The generic term Z_{ij} is thus obtained by imposing p_j as a velocity at the ports:

$$Z_{ij} = \int_{S_i} p_i\left(x,y\right) p_{tot_j}\left(x,y,z_{port}\right) dS \qquad (3.41)$$

3.2.3 Scattering Matrix

In the previous paragraph, we identified the matrices that define voltage and current as the sum of incident and reflected waves:

$$\mathbf{V} = \mathbf{V}^+ + \mathbf{V}^- \qquad (3.42)$$

$$\mathbf{I} = \mathbf{I}^+ + \mathbf{I}^- = \frac{\mathbf{V}^+}{\mathbf{Z}_c} - \frac{\mathbf{V}^-}{\mathbf{Z}_c} \qquad (3.43)$$

where $\mathbf{Z}_c$ is known as the characteristic impedance. It is the most important parameter for a waveguide and it is represented as the ratio of magnitude of voltage and current waves in an infinite transmission line at zero reflection wave condition.

Now we introduce the following normalized variables [19]:

$$\mathbf{v} = \frac{\mathbf{V}}{\sqrt{\mathbf{Z}_c}} \qquad (3.44)$$

$$i = \sqrt{\mathbf{Z}_c}\mathbf{I} \tag{3.45}$$

$$\mathbf{a} = \frac{\mathbf{V}^+}{\sqrt{\mathbf{Z}_c}} = \sqrt{\mathbf{Z}_c}\mathbf{I}^+ \tag{3.46}$$

$$\mathbf{b} = \frac{\mathbf{V}^-}{\sqrt{\mathbf{Z}_c}} = \sqrt{\mathbf{Z}_c}\mathbf{I}^- \tag{3.47}$$

where $\mathbf{a}$ and $\mathbf{b}$ point out the incident and reflected normalized waves respectively. It yields:

$$\mathbf{a} = \frac{\mathbf{v} + \mathbf{i}}{2} = \frac{1}{2\sqrt{\mathbf{Z}_c}}[\mathbf{V} + \mathbf{Z}_c\mathbf{I}] \tag{3.48}$$

$$\mathbf{b} = \frac{\mathbf{v} - \mathbf{i}}{2} = \frac{1}{2\sqrt{\mathbf{Z}_c}}[\mathbf{V} - \mathbf{Z}_c\mathbf{I}] \tag{3.49}$$

All the elements in these equations are column vectors whose number of rows equals the number of ports we have. In our case, there are two ports and one can therefore manage the elements a_1 and b_1 referred to the first port and a_2 and b_2 associated with the second one. It turns out:

$$b_1 = S_{11}a_1 + S_{12}a_2 \tag{3.50}$$

$$b_2 = S_{21}a_1 + S_{22}a_2 \tag{3.51}$$

where S_{ij} determines the elements of an $\mathbf{S}$ matrix known as **scattering matrix**. The scattering matrix combines incident and reflected waves. It is what allows us to describe the properties of complicated networks. Thanks to the scattering matrix, it is possible to know the amount of signal that is transmitted from one port to the other and the amount of signal that is reflected. The scattering matrix requires the definition of a characteristic impedance for each port and can be represented as follows:

$$\mathbf{S} = \begin{bmatrix} S_{11} & S_{12} \\ S_{21} & S_{22} \end{bmatrix} \tag{3.52}$$

Its components constitute the **S parameters**. In general, these parameters describe the input-output relationship between ports in an electrical system. In particular, S_{11} term represents the contribution of the reflected wave b_1 due to the incident wave a_1 at port 1, S_{12} expresses the contribution of the reflected wave b_1 due to the incident wave a_2 at port 2, S_{21} is the term related to the contribution of the reflected wave b_2 due to the incident wave a_1 at port 1 and finally S_{22} is the contribution of the reflected wave b_2 due to the incident wave a_2 at port 2. In formulas:

$$S_{11} = \left.\frac{b_1}{a_1}\right|_{a_2=0} \tag{3.53}$$

$$S_{12} = \left.\frac{b_1}{a_2}\right|_{a_1=0} \tag{3.54}$$

$$S_{21} = \left.\frac{b_2}{a_1}\right|_{a_2=0} \tag{3.55}$$

$$S_{22} = \left.\frac{b_2}{a_2}\right|_{a_1=0} \tag{3.56}$$
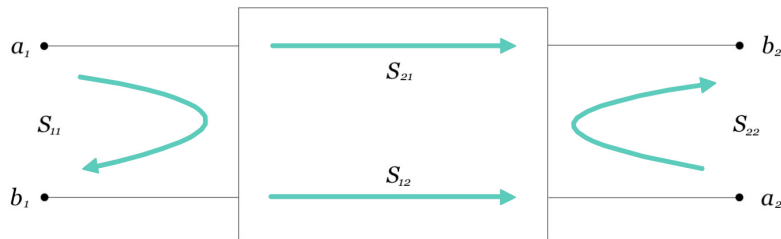
Figure 3.5: Scattering parameters in a two port network

The concept of scattering parameters is closely related to the concept of power: for example, the term S_{12} is known as the power transferred from port 1 to port 2. So, in general, S_{ij} is the power transferred from port i to port j. S parameters are performed as functions of frequency and vary with frequency variation. In our case, we want to calculate the S parameters to

identify the behavior of a deformed pipe under the stimulation of a sound wave and to observe what happens in function of a certain frequency range. In practice, the most commonly quoted parameter is S_{11}. This term shows how much power is reflected and it is known also as **reflection coefficient**. For example, if $S_{11} = 0$ dB, then all the power is reflected and nothing is radiated. The more the dB value goes below the 0 dB, the more the power is transmitted.

3.2.4   Voltage Scattering Matrix

Returning to the definition of voltage matrix as the sum of the voltage incident matrix and reflected matrix, it is possible to express the scattering matrix as the ratio between the reflected voltage matrix and the incident one [17]. It turns out:

$$\mathbf{V}^- = \mathbf{S}\mathbf{V}^+ \tag{3.57}$$

The scattering matrix can be also called "voltage" scattering matrix and it can be represented with the subscript v. It is necessary to make this clarification in order to not confuse it with the "power" scattering matrix that we will consider next.

From (3.40), we obtain:

$$\mathbf{V}^+ + \mathbf{V}^- = \mathbf{Z}\left(\mathbf{I}^+ + \mathbf{I}^-\right) = \mathbf{Z}\mathbf{Y}_c\left(\mathbf{V}^+ - \mathbf{V}^-\right) \tag{3.58}$$

where $\mathbf{Y}_c$ is the diagonal matrix of wave admittances Y_i. By replacing the voltage scattering matrix formula in the previous equation, yields:

$$\left(\mathbf{U} + \mathbf{S}_v\right)\mathbf{V}^+ = \mathbf{Z}\mathbf{Y}_c\left(\mathbf{U} - \mathbf{S}_v\right)\mathbf{V}^+ \tag{3.59}$$

where $\mathbf{U}$ is the identity matrix. Because of the arbitrariness of $\mathbf{V}^+$, one gets:

$$\mathbf{U} + \mathbf{S}_v = \mathbf{Z}\mathbf{Y}_c \left(\mathbf{U} - \mathbf{S}_v \right) \tag{3.60}$$

Solving for $\mathbf{S}_v$, we obtain the voltage scattering matrix:

$$\mathbf{S}_v = \left(\mathbf{Z}\mathbf{Y}_c + \mathbf{U} \right)^{-1} \left(\mathbf{Z}\mathbf{Y}_c - \mathbf{U} \right) \tag{3.61}$$

Practically, this matrix specifies the relationship between the different incident and reflected voltage values that we find at the two ports of the domain but it is not able to give us complete information about the problem we are interested into.

3.2.5 Power Scattering Matrix

So far we have dealt with the voltage scattering matrix. This matrix is representative but it cannot give us the same amount of information as the power scattering matrix. When the main interest is in the power relationship between the various circuits in which the sources are not correlated, the voltage waves are not considered the best independent variables to be used for the analysis. A different concept of waves is introduced, which is that of power waves. These waves are defined by the power scattering matrix [17]. The coefficients of this matrix in square magnitude represents relative reflected powers. We can therefore determine the acoustic power associated with each mode:

$$P_i^+ = \frac{1}{2} \int_S V_i^+ p_i \left(I_i^+ v_{zi} \right)^* dS = \frac{1}{2} Y_i^* \left| V_i^+ \right|^2 \int_S \left| p_i \right|^2 dS = \frac{1}{2} Y_i^* \left| V_i^+ \right|^2 \tag{3.62}$$

51

The power is connected to the other quantities analyzed and it is generally expressed as the product between the voltage and the current. For each mode, it turns out:

$$\left| W_i^+ \right|^2 = V_i^+ I_i^+ \tag{3.63}$$

where the superscript "+" refers to the incident wave. This term produces the peak power. It is the maximum power that the power supply can sustain for a short time. By applying the square root and multiplying and dividing by the voltage root, we obtain a new expression for the term W_i^+ which represents the square root of the peak power associated with each generic mode denoted by the i index:

$$W_i^+ = \sqrt{|Y_i|} V_i^+ \tag{3.64}$$

At this point, the acoustic power is calculated as follows:

$$P_i^+ = \frac{1}{2} \left| W_i^+ \right|^2 \tag{3.65}$$

All those coefficients that correspond to the modes that do not propagate, do not contribute to the power calculation.

To better understand the topic of power scattering matrix, it is necessary to start from the definition of voltage scattering matrix mentioned previously. Knowing that:

$$\mathbf{V}^- = \mathbf{S}_v \mathbf{V}^+ \tag{3.66}$$

Substituting the following expression into (3.66):

$$\mathbf{V}^\pm = \sqrt{|\mathbf{Z}_c|} \mathbf{W}^\pm \tag{3.67}$$

It is found:

$$\sqrt{|\mathbf{Z}_c|}\mathbf{W}^- = \mathbf{S}_v\sqrt{|\mathbf{Z}_c|}\mathbf{W}^+ \tag{3.68}$$

$$\mathbf{W}^- = \sqrt{|\mathbf{Y}_c|}\mathbf{S}_v\sqrt{|\mathbf{Z}_c|}\mathbf{W}^+ = \mathbf{S}_p\mathbf{W}^+ \tag{3.69}$$

Finally, we derive the relationship between the power and the voltage scattering matrix:

$$\mathbf{S}_p = \sqrt{|\mathbf{Y}_c|}\mathbf{S}_v\sqrt{|\mathbf{Z}_c|} \tag{3.70}$$

The elements of the two matrices are therefore related by:

$$S_{p(i,j)} = \sqrt{|Y_i|}S_{v(i,j)}\sqrt{|Z_j|} \tag{3.71}$$

Starting from the voltage scattering matrix and from the definition of wave impedance and admittance, we obtain the matrix that expresses the bonds between powers. The power waves are more suitable quantities than the conventional traveling waves.

3.2.6   Measuring the Pressure

In the previous chapter, we described the Finite Element Method to analyze different pressure values in particular geometries. For this measurement and to determine the behavior of our object, we considered the voltage scattering matrix first and then the power scattering matrix, which offers us more information about it. Once this matrix and its elements have been found, it is possible to calculate the total scattered pressure [17]:

53

$$p_{sca}(x, y) = \sum_i V_i^- p_i(x, y) = V_j^+ \sum_i S_{v(i,j)} p_i(x, y) \qquad (3.72)$$

Knowing that:

$$S_{v(i,j)} = \sqrt{|Z_i|} S_{p(i,j)} \sqrt{|Y_j|} \qquad (3.73)$$

One can obtain:

$$p_{sca}(x, y) = V_j^+ \sqrt{|Y_j|} \sum_i S_{p(i,j)} \sqrt{|Z_i|} p_i(x, y) \qquad (3.74)$$

For the purpose of computing the pressure, the term $V_j^+ \sqrt{|Y_j|}$ can be omitted since it is just a scaling factor.

Therefore, all the results that we are going to obtain following the steps of the FEM method of the previous chapter will be related also to the concepts of scattering matrix, propagation and modal analysis. The S parameters that describe the behavior of the domain are obtained as a function of frequency. The analysis of the modes and of the pressure waves propagation of the two-dimensional Finite Element Method is now clearer. In the next chapter, we will study a new calculation method for the description of the deformed geometry and its transformation, which will replace the Finite Element Method. It is a method still being tested which allows us, however, to obtain a more efficient resolution in terms of computational time. This speeding up will be especially useful when we will investigate the three dimensions.

Chapter 4

Hierarchical Model Reduction

So far, we have described the two-dimensional finite element technique to solve the Helmholtz equation and to find the pressure values of the sound wave of our interest. However, the different models we can study, can be extremely complex, especially when we are dealing with the three-dimensional case, and, as a consequence, the computational costs become very high. In order to accelerate the numerical simulation, we can personalize standard methods, such as the Finite Element Method, to achieve particular features to figure out the solution. To solve this problem, a new method has been adopted, known as **Hierarchical Model (HiMod) reduction** [20, 21]. The basic idea is to consider the axial and the transverse directions in different ways: a one-dimensional finite element discretization is used for the axial direction, while different modal bases are used for the transverse ones.

Figure 4.1: One-dimensional Finite Element Method on the axial direction
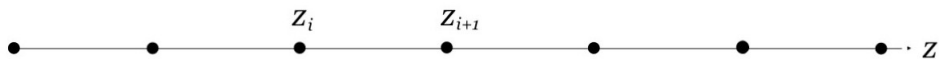
Doing this, we obtain the reduction of the two-dimensional or three-dimensional problem to a one-dimensional problem. This reduces the size of the problem while still ensuring accuracy [22]. This method is called "hierarchical" because the selection of the number of the modes can be hierarchically performed [23]. The number of modes can be selected with an a

priori approach and the basis functions collected, incorporate the information on the boundary conditions. Selection of the modal basis is crucial in this context [24]. We will start analyzing Bessel polynomials for measuring the sound pressure in pipes, then we will see the results obtained by considering other basis functions, thus underlining the importance of the choice.

However, this approach has been evaluated in various fields such as the medical one and in details, to develop models for the circulatory system in patients with coronary artery disease [25]. Other study fields concern oil pipelines, internal combustion engines and river systems [21].

This new method was mainly tested for domains with straight lines but it is important to examine more complex geometries that have smooth lines and therefore come closer to the problems of reality. One of the limitations of this procedure relies in fact on the rectilinear nature of the centerline defining the axial direction of the domain. As a matter of fact, for curved pipes, the method consists of a mapping of the centerline with a straight line [26]. HiMod reduction is however motivated by the simplicity of one-dimensional Finite Element Method and of the representation of pipes with a generic centerline.

In this chapter, we will see how to apply this new method to the two-dimensional case: we will start with the general geometric description of the domain and then we will determine the pressure at each point of the domain, both considering the planar case, which involves Cartesian coordinates, and the radial case, where polar coordinates are employed.

4.1 Geometric Setting of the Domain

Suppose $\Omega \subset \mathbb{R}^d$ is the domain of the problem, where d can be equal to 2 or 3 and represents the dimension of the domain. We assume that the domain can be performed as:

$$\Omega = \cup_{x \in \Omega_{1D}} \{x\} \times \gamma_x \tag{4.1}$$

where Ω_{1D} is the one-dimensional supporting fiber and γ_x is the transverse fiber associated with the generic point $x \in \Omega_{1D}$.

The supporting fiber is the x axis while γ_x is the transverse direction centered at x. The dimension of γ_x is related to the dimension of Ω : when $\Omega \subset \mathbb{R}^d$, $\gamma_x \subset \mathbb{R}^{d-1}$.

The axial direction associated with Ω_{1D} is dominant with respect to the transverse ones. In fact we can consider $L_x \gg L_y, L_z$, where L_x, L_y and L_z are the lengths of the three dimensions of the domain [22].
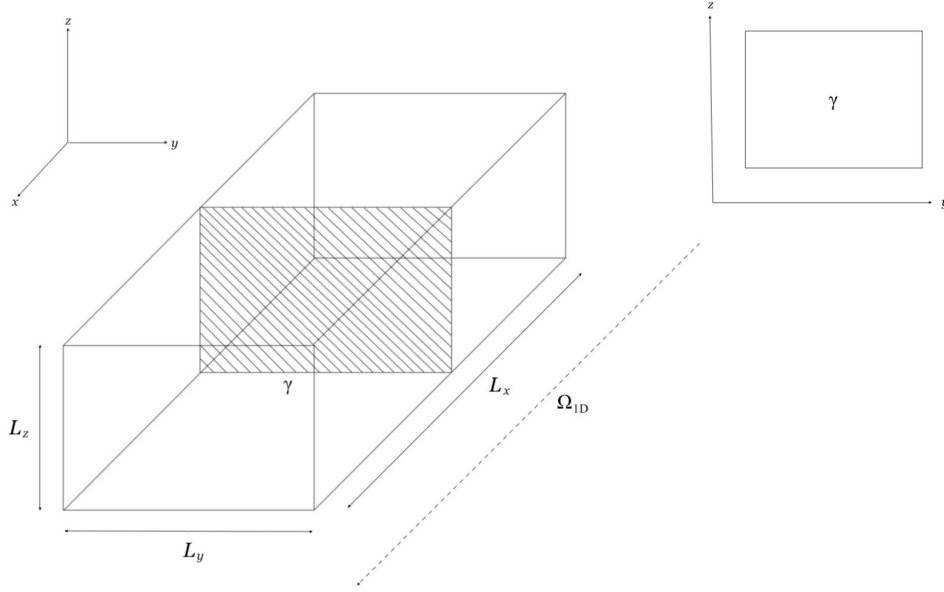
Figure 4.2: Example of a three-dimensional domain

For each $x \in \Omega_{1D}$, we can introduce a mapping between the original domain and the reference one we want to obtain with the transformation:

$$\psi_x : \gamma_x \to \widehat{\gamma}_x \tag{4.2}$$

Hereafter, we choose $\Omega_{1D} = (0, L_x)$ and $\gamma_x = \gamma = (0, L_y)$ for the two-dimensional case and $\gamma_x = \gamma = (0, L_y) \times (0, L_z)$ for the three-dimensional one.

In particular, we have assumed that Ω_{1D} is a curve where x is a curvilinear abscissa, while fibers γ_x represent regular functions of x.

Ω is the image of $\widehat{\Omega} = [0, L_x] \times \gamma$, so we can express the global map of the domain as:

$$\Psi : \Omega \to \widehat{\Omega} \tag{4.3}$$

where Ω is the original domain and $\widehat{\Omega}$ is the transformed domain.

The deformed domain is represented as:

$$\Omega = \Omega_{1D} \times \gamma_x \tag{4.4}$$

while the reference domain will be:

$$\widehat{\Omega} = \widehat{\Omega}_{1D} \times \widehat{\gamma}_x \tag{4.5}$$

With the transformation, we get the new supporting fiber $\widehat{\Omega}_{1D}$, which is a straight line, and $\widehat{\gamma}_x$, the new transverse fiber of the same dimension as γ_x.
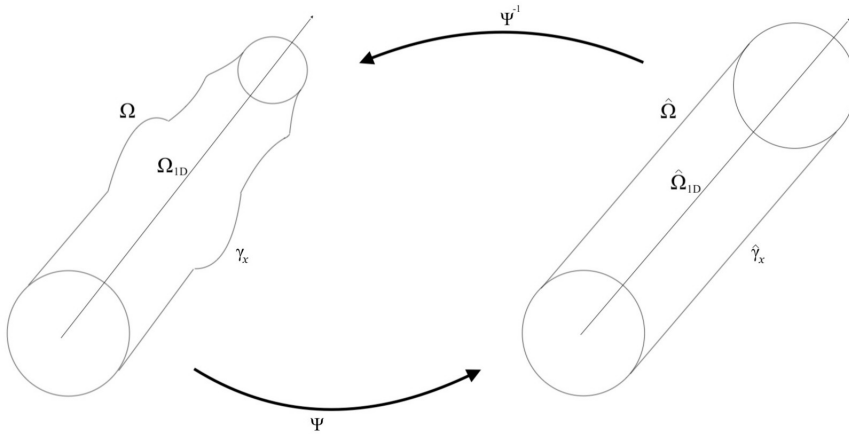

Figure 4.3: A physical domain of interest mapped to the reference cylindrical domain

In our case, the original geometry is given by a deformed pipe. It is therefore a cylindrical domain with variable radius. This geometry must be transformed into a regular cylinder. A simple approach is to map the circle into a square: in this way, we can perform the calculations by referring to the Cartesian coordinates. However this procedure lacks accuracy especially with regard to the vertices and the contours. An approach that uses a cylindrical structure is therefore more suitable from this point of view. This is also quite obvious given the geometric shape of a pipe. However, the spectral approximation of partial differential equations in polar coordinates suffers from several issues resulting from the conversion from the Cartesian frame.

Regularity and boundary condition enforcement add requirements to the spectral basis to use. The selection of a basis function is thus very difficult [24]. What we want to do is to find out which are the modal functions that present the best conditions for our problem to be tested.

4.2   Model Reduction

Now we want to formulate the reduced model. We introduce the function space $V_{1D} \subseteq H^1(\Omega_{1D})$ on Ω_{1D}, such that the related functions vanish on Dirichlet boundaries. On the transverse fiber, we set a modal basis $\{\varphi_k\}_{k\in\mathbb{N}} \in H^1(\gamma_x)$. These functions will be such that:

$$\int_{\widehat{\gamma}_x} \varphi_i\left(y\right) \varphi_j\left(y\right) dy = \delta_{ij} \quad \forall i,j \in \mathbb{N} \tag{4.6}$$

There are different choices for these modal bases and we will specify them later.

Through the combination of the function space and the modal functions, we can define the reduced space:

$$V_m = \left\{ v_m(\mathbf{z}) = \sum_{k=1}^{m} v_k(\Psi_1(\mathbf{z}))\varphi_k(\Psi_2(\mathbf{z})) \quad v_k \in V_{1D} \right\} \tag{4.7}$$

59

where $m \in \mathbb{N}$ is a priori fixed number. For the orthonormality of the basis we also have:

$$v_k \left(\Psi_1 \left(\mathbf{z} \right) \right) = \int_{\gamma_x} v_m \left(\Psi_1 \left(\mathbf{z} \right), \Psi_2 \left(\mathbf{z} \right) \right) \varphi_k \left(\Psi_2 \left(\mathbf{z} \right) \right) d\Psi_2 \left(\mathbf{z} \right) \quad k = 1, ..., m \quad (4.8)$$

To build a basis, two different procedures can be considered [24]:

1) The "top-down" approach in which we can construct directly the basis function through the solution of a Sturm-Liouville eigenvalue (SLE) problem together with homogeneous boundary conditions. The Sturm-Liouville theory is based on the analysis of the behavior of the eigenvalues and on the consideration of the eigenfunctions in the function space.

2) The "bottom-up" approach in which we can construct the basis by operating separately on the coordinates. To do this, there are several procedures discussed [27].

By considering the second procedure, two scalar problems are solved: one for the angular component and the other for the radial one. The radial basis, determined as $\{\xi_n \left(\widehat{r} \right)\}_{n=0}^{\infty}$, is therefore obtained and we can use it to denote the two-dimensional spectral basis [24]:

$$\widehat{\varphi}_k \left(\widehat{r}, \widehat{\theta} \right) = \widehat{\varphi}_{j,n}^{\sin,\cos} \left(\widehat{r}, \widehat{\theta} \right) = \xi_n \left(\widehat{r} \right) \begin{cases} \cos \left(j\widehat{\theta} \right) \\ \sin \left(j\widehat{\theta} \right) \end{cases} \quad (4.9)$$

where the superscript is referred to the trigonometric function analyzed and j, n are the two indices that highlight the dependence of the basis functions.

As mentioned above, the basis functions $\{\xi_n\}$ can be of different types depending on the problem we are dealing with. These functions are polynomials that will be analyzed in details when we will discuss the results related to the HiMod two-dimensional radial case.

4.3 Hierarchical Model Reduction Evaluation: Planar Case

As we have already said, HiMod reduction was implemented to increase the computational efficiency of the FEM.

In the two-dimensional case, both the supporting fiber and the transverse one are in one dimension. In fact, we will have $\Omega \subset \mathbb{R}^2$ and $\gamma_x \subset \mathbb{R}^1$.

After the transformation done by following the steps described before, the domain is a rectangle with height h and length equal to the length of the original domain [1]. We can define the transformation with the matrix $\overline{\mathbf{T}}$ which turns out to be the same matrix specified for the transformation in the two-dimensional Finite Element Method. By considering for example y as the transverse direction and z as the axial direction which defines the direction of propagation:

$$\overline{\mathbf{T}} = \left[\begin{array}{cc} T_{yy}(y,z) & T_{yz}(y,z) \\ T_{zy}(y,z) & T_{zz}(y,z) \end{array} \right] \tag{4.10}$$

with $T_{zy} = T_{yz}$.

The pressure can be expressed as:

$$p\left(y,z\right) = \sum_q c_q p_q\left(y,z\right) = \sum_m \sum_n c_{m,n} \varphi_m\left(y\right) u_n\left(z\right) \tag{4.11}$$

where φ_m are the modal functions defined as $A_m \cos \frac{m\pi y}{h}$ and u_n are the elements obtained from the FEM of the axial direction.

By using the one-dimensional FEM for the axial direction, the segment over the z direction will be divided into N elements. Therefore, it is necessary to match each index q with a pair (m,n) such that $m = m_q$ and $n = n_q$. Now it is possible to determine the A and B matrices needed to figure out the pressure at every point of the domain.

The elements of matrix B are:

$$B\left(p,q\right) = \sum_i A^{(z)}w_i^{(z)}u_{n_p}\left(z_i\right)u_{n_q}\left(z_i\right)\beta\left(z_i\right) \tag{4.12}$$

where:

$$\beta\left(z_i\right) = \sum_k A^{(y)}w_k^{(y)}\frac{\varphi_{m_p}\left(y_k\right)\varphi_{m_q}\left(y_k\right)}{\det \mathbf{J}\left(z_i,y_k\right)} \tag{4.13}$$

The elements of matrix A are:

$$A(p,q) = A_{yy}(p,q) + A_{yz}(p,q) + A_{zy}(p,q) + A_{zz}(p,q) \tag{4.14}$$

where:

$$A_{yy}(p,q) = \sum_i A^{(z)}w_i^{(z)}u_{n_p}(z_i)u_{n_q}(z_i)\alpha_{yy}\left(z_i\right) \tag{4.15}$$

$$A_{yz}(p,q) = \sum_i A^{(z)}w_i^{(z)}u_{n_p}(z_i)\left.\frac{\partial u_{n_q}}{\partial z}\right|_{z_i}\alpha_{yz}(z_i) \tag{4.16}$$

$$A_{zy}(p,q) = \sum_i A^{(z)}w_i^{(z)}\left.\frac{\partial u_{n_p}}{\partial z}\right|_{z_i}u_{n_q}(z_i)\alpha_{zy}(z_i) \tag{4.17}$$

$$A_{zz}(p,q) = \sum_i A^{(z)}w_i^{(z)}\left.\frac{\partial u_{n_p}}{\partial z}\right|_{z_i}\left.\frac{\partial u_{n_q}}{\partial z}\right|_{z_i}\alpha_{zz}(z_i) \tag{4.18}$$

Now we can express the α coefficients:

$$\alpha_{yy}(z_i) = \sum_k A^{(y)}w_k^{(y)}T_{yy}(z_i,y_k)\left.\frac{\partial\varphi_{m_p}}{\partial y}\right|_{y_k}\left.\frac{\partial\varphi_{m_q}}{\partial y}\right|_{y_k} \tag{4.19}$$

$$\alpha_{yz}(z_i) = \sum_k A^{(y)}w_k^{(y)}T_{yz}(z_i,y_k)\left.\frac{\partial\varphi_{m_p}}{\partial y}\right|_{y_k}\varphi_{m_q}(y_k) \tag{4.20}$$

$$\alpha_{zy}(z_i) = \sum_k A^{(y)} w_k^{(y)} T_{zy}(z_i, y_k) \varphi_{m_p}(y_k) \left. \frac{\partial \varphi_{m_q}}{\partial y} \right|_{y_k} \qquad (4.21)$$

$$\alpha_{zz}(z_i) = \sum_k A^{(y)} w_k^{(y)} T_{zz}(z_i, y_k) \varphi_{m_p}(y_k) \varphi_{m_q}(y_k) \qquad (4.22)$$

The numerical integration has been used. It is the approximate computation of an integral using numerical techniques. It can be called also quadrature. We can recall that the gaussian quadrature is given by:

$$\int_S f(x, y) dS \simeq A \sum_{q=1}^{Q} f(x_q, y_q) w_q \qquad (4.23)$$

where A is the area of the considered element and w_q represent the weights related to the various contributions.

In the expressions of the elements of the two matrices, we have seen $A^{(z)}$, $A^{(y)}$, z_i and y_k:

$$A^{(z)} = \frac{L_z}{2} \qquad (4.24)$$

$$A^{(y)} = \frac{h}{2} \qquad (4.25)$$

$$z_i = \xi_i \frac{L_z}{2} + \frac{z_a + z_b}{2} \qquad (4.26)$$

$$y_k = \xi_k \frac{h}{2} + \frac{h}{2} \qquad (4.27)$$

where L_z is the length of each segment into which z is divided through the one-dimensional FEM, h is the height of the transverse direction, ξ_i and ξ_k are the integration points related to the axial and transverse direction respectively.

4.4 Hierarchical Model Reduction Evaluation: Radial Case

In the two-dimensional radial case we have a similar situation. In this case, we have the parameter ρ instead of y to represent the transverse direction. The transformation matrix $\overline{\mathbf{T}}$ is given by:

$$\overline{\mathbf{T}} = \begin{bmatrix} T_{\rho\rho}(\rho, z) & T_{\rho z}(\rho, z) \\ T_{z\rho}(\rho, z) & T_{zz}(\rho, z) \end{bmatrix} \tag{4.28}$$

with $T_{z\rho} = T_{\rho z}$.

The pressure p related to the domain is:

$$p(\rho, z) = \sum_q c_q p_q(\rho, z) = \sum_m \sum_n c_{m,n} \varphi_m(\rho) u_n(z) \tag{4.29}$$

As before, φ_m expresses the modal functions and u_n are the elements related to the dominant direction of the domain.

The elements of the matrices A and B are calculated by using the numerical integration:

$$B(p, q) = \sum_i A^{(z)} w_i^{(z)} u_{n_p}(z_i) u_{n_q}(z_i) \beta(z_i) \tag{4.30}$$

$$A_{\rho\rho}(p, q) = \sum_i A^{(z)} w_i^{(z)} u_{n_p}(z_i) u_{n_q}(z_i) \alpha_{\rho\rho}(z_i) \tag{4.31}$$

$$A_{\rho z}(p, q) = \sum_i A^{(z)} w_i^{(z)} u_{n_p}(z_i) \left.\frac{\partial u_{n_q}}{\partial z}\right|_{z_i} \alpha_{\rho z}(z_i) \tag{4.32}$$

$$A_{z\rho}(p, q) = \sum_i A^{(z)} w_i^{(z)} \left.\frac{\partial u_{n_p}}{\partial z}\right|_{z_i} u_{n_q}(z_i) \alpha_{z\rho}(z_i) \tag{4.33}$$

$$A_{zz}(p, q) = \sum_i A^{(z)} w_i^{(z)} \left.\frac{\partial u_{n_p}}{\partial z}\right|_{z_i} \left.\frac{\partial u_{n_q}}{\partial z}\right|_{z_i} \alpha_{zz}(z_i) \tag{4.34}$$

where:

$$\beta(z_i) = 2\pi \sum_k A^{(\rho)} w_k^{(\rho)} \rho_k \frac{\varphi_{m_p}(\rho_k)\varphi_{m_q}(\rho_k)}{\det \mathbf{J}(z_i, \rho_k)} \tag{4.35}$$

$$\alpha_{\rho\rho}(z_i) = 2\pi \sum_k A^{(\rho)} w_k^{(\rho)} \rho_k T_{\rho\rho}(z_i, \rho_k) \left.\frac{\partial \varphi_{m_p}}{\partial \rho}\right|_{\rho_k} \left.\frac{\partial \varphi_{m_q}}{\partial \rho}\right|_{\rho_k} \tag{4.36}$$

$$\alpha_{\rho z}(z_i) = 2\pi \sum_k A^{(\rho)} w_k^{(\rho)} \rho_k T_{\rho z}(z_i, \rho_k) \left.\frac{\partial \varphi_{m_p}}{\partial \rho}\right|_{\rho_k} \varphi_{m_q}(\rho_k) \tag{4.37}$$

$$\alpha_{z\rho}(z_i) = 2\pi \sum_k A^{(\rho)} w_k^{(\rho)} \rho_k T_{z\rho}(z_i, \rho_k) \varphi_{m_p}(\rho_k) \left.\frac{\partial \varphi_{m_q}}{\partial \rho}\right|_{\rho_k} \tag{4.38}$$

$$\alpha_{zz}(z_i) = 2\pi \sum_k A^{(\rho)} w_k^{(\rho)} \rho_k T_{zz}(z_i, \rho_k) \varphi_{m_p}(\rho_k) \varphi_{m_q}(\rho_k) \tag{4.39}$$

ρ_k, z_i, $A^{(\rho)}$, $A^{(z)}$ are obtained by considering different quadrature rules such as, for example, Gauss quadrature rule or Simpson quadrature rule. If Gauss rule is used, we can find that:

$$\rho_k = \xi_k \frac{\rho_b - \rho_a}{2} + \frac{\rho_a + \rho_b}{2} \tag{4.40}$$

$$z_i = \xi_i \frac{L_z}{2} + \frac{z_a + z_b}{2} \tag{4.41}$$

$$A^{(\rho)} = \frac{\rho_b - \rho_a}{2} \tag{4.42}$$

$$A^{(z)} = \frac{L_z}{2} \tag{4.43}$$

The quadrature rules related to the axial and the transverse direction can be also different. For example, we can use the Gauss quadrature for the dominant direction and the Simpson quadrature for the transverse one and viceversa.

Chapter 5

Two-Dimensional Case Numerical Results

In the previous chapters, we described the two-dimensional finite element calculation procedure which can be used for the simulation of any physical phenomenon using mathematical steps. In particular, our analysis focuses on the computation of the acoustic pressure in different points of a cylindrical pipe in order to identify any geometric deformations. Thanks to our study, we can continuously monitor the status of these structures. After having determined the Finite Element Method case in details, we went on to examine a new calculation method, still under study, known as Hierarchical Model Reduction. This method allows us to obtain an optimization regarding the calculation time. In this chapter, we will evaluate the results obtained with both the FEM and the new HiMod method and then we will determine the comparison between the results obtained in both cases with the resolution of any problems. In particular, we will deal with the convergence problem of the S curves between the HiMod radial case and the Finite Element Method without transformation of the geometry. Our goal will be to find the modal functions that make these curves overlap as much as possible and that the convergence is guaranteed. Finally, we will draw the necessary conclusions and try to understand the advantage obtained by using the HiMod procedure compared to the Finite Element Method.

5.1 Two-Dimensional FEM Numerical Results

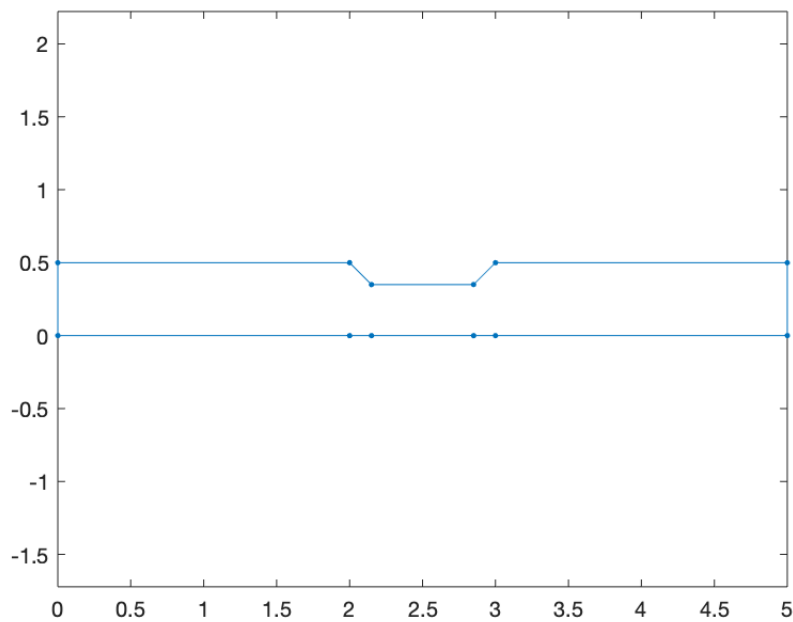We start with the analysis of a deformed two-dimensional domain of this type:

Figure 5.1: Example of deformed geometry

By adopting this geometry and by applying the Finite Element Method, one can therefore observes how the discretization and the division of the structure into triangles takes place. Of course, by changing the density value of the mesh, the triangulation will undergo changes. For example, by considering a higher density value, we will have a denser mesh and consequently an increase in the accuracy of the results but also an increase in the memory demand.
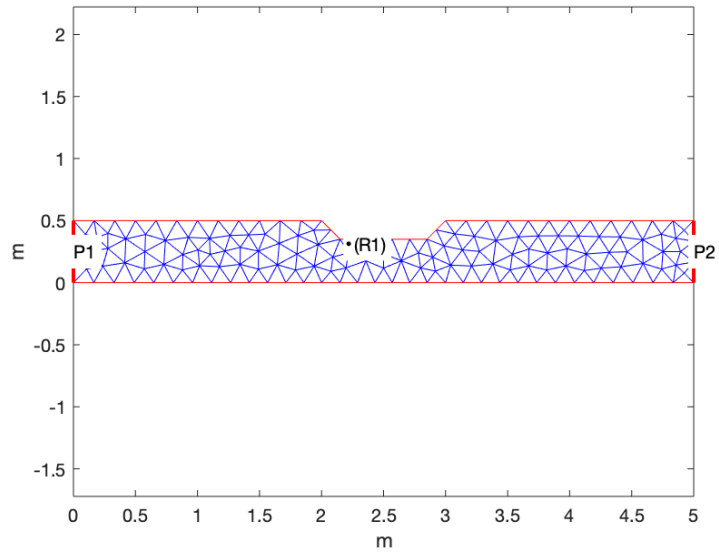
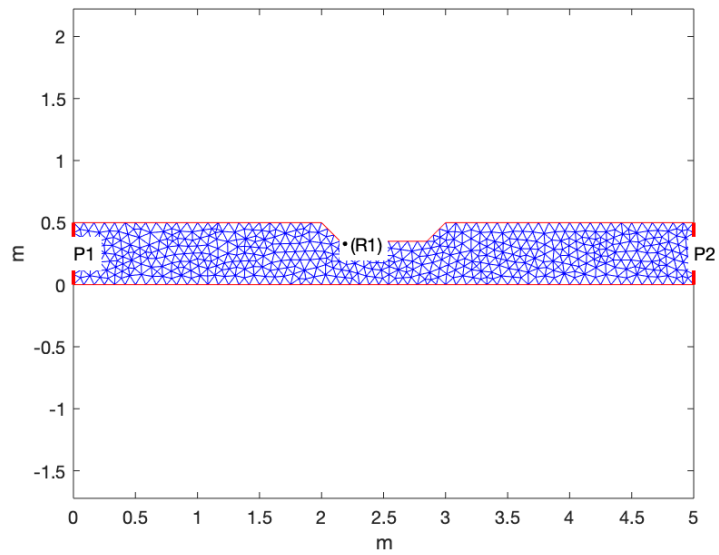Figure 5.2: Mesh discretization with a density value $= 10$

Figure 5.3: Mesh discretization with a density value $= 20$

Starting from the computation of the two-dimensional planar case, after having carried out the acoustic transformation by using the formulas show in the previous chapters, we come to the final results. In this case, we obtain the scattering parameter S_{11} to perform the modal analysis and therefore to understand the behavior of the structure, at each point, subject to the pressure. If we want, we can also represent the other scattering parameters in the plot. As we have already mentioned before, the S parameters are expressed as a function of frequency. For example, one can consider a range from 1Hz to 200Hz and observe the performance of the curve in the FEM case without transformation and in the FEM case with geometry transformation and overlap the two curves.
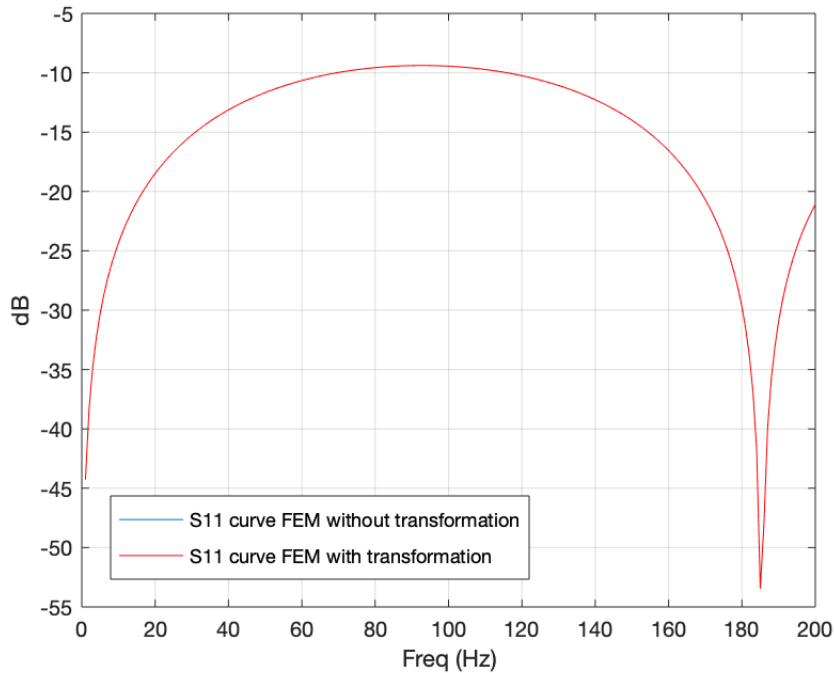

Figure 5.4: S_{11} curves overlap between the FEM case without transformation and with transformation of the geometry

In figure 5.4, we can see the superposition of the two curves S_{11} for a density value equal to 10 and quadratic triangular elements for the discretization and we can note that they overlap almost perfectly. By increasing the order of the elements, the overlap is even more precise.

The degree of accuracy also increases by increasing the density value of these elements. We can numerically evaluate the correctness of the overlap by figuring out the error curve as a function of frequency:
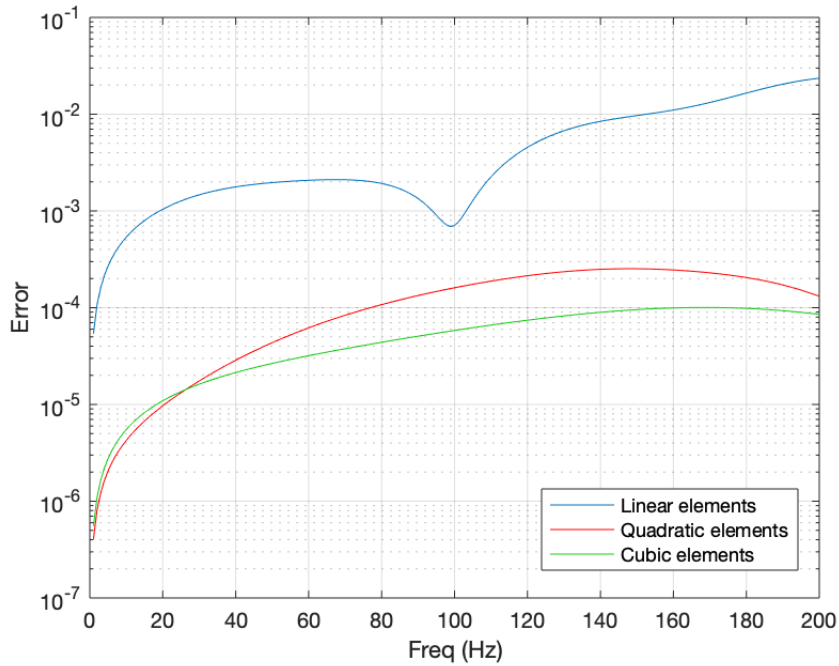

Figure 5.5: Logarithmic error curves for linear, quadratic and cubic elements

In figure 5.5, we note that by evaluating higher-order elements, the error decreases for all the frequencies considered except for the lower ones where the curves related to the quadratic and cubic elements have more or less the same values.

The two-dimensional geometries of our interest may also present different deformations with respect to the one just considered. One can study a deformation that displays the following model:

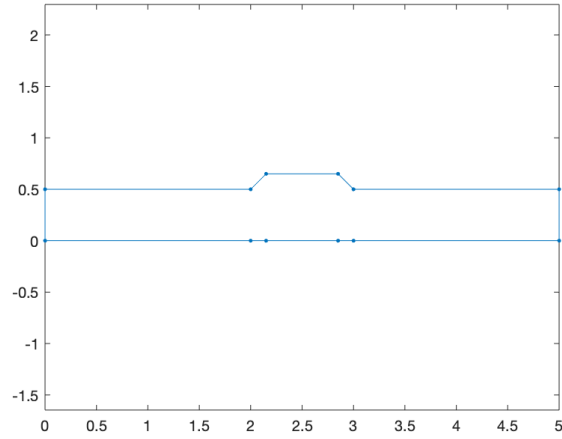Figure 5.6: Example of a geometry deformed by a bulge at its center

In this example, all the considerations made in the previous case are valid, that is, by increasing density and by using cubic elements for the mesh, we obtain more rigorous results. This statement is also proven by the error curve.
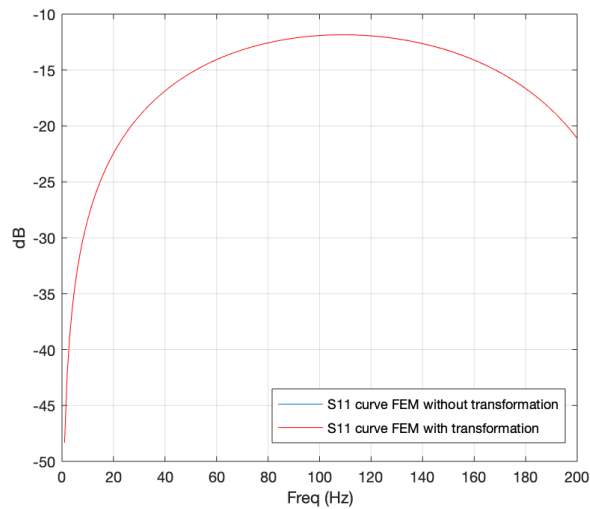

Figure 5.7: S_{11} curves overlap in the FEM case considering a geometry with a bulge at the center

71

By examining this type of geometry, which has a central deformation characterized by a bulge, we obtain the overlap shown in figure 5.7. As the previous example, the figure shows the curves for quadratic triangular elements. Also in this case, we can see how the overlap between the curves is perfect.

After highlighting the acoustic transformation in the two-dimensional FEM planar case, it is possible to make the same assessments also for the radial case. By choosing any two-dimensional domains, we note that the accuracy increases hand in hand with the increase in the values of the parameters mentioned above. We can analyze a geometry similar to that of figure 5.1 with a density value equal to 10. The mesh discretization and the structure have the following design:
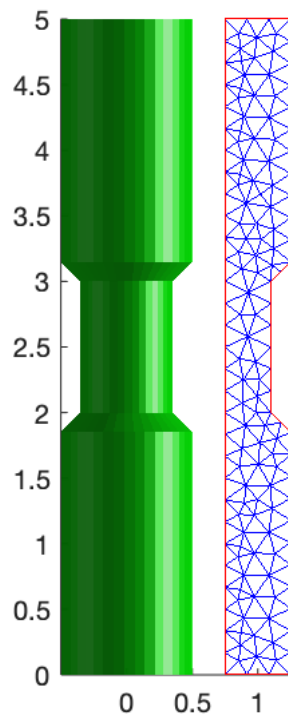

Figure 5.8: Structure of the deformed pipe with its mesh discretization

As before, we evaluate the overlap between the S_{11} curves:
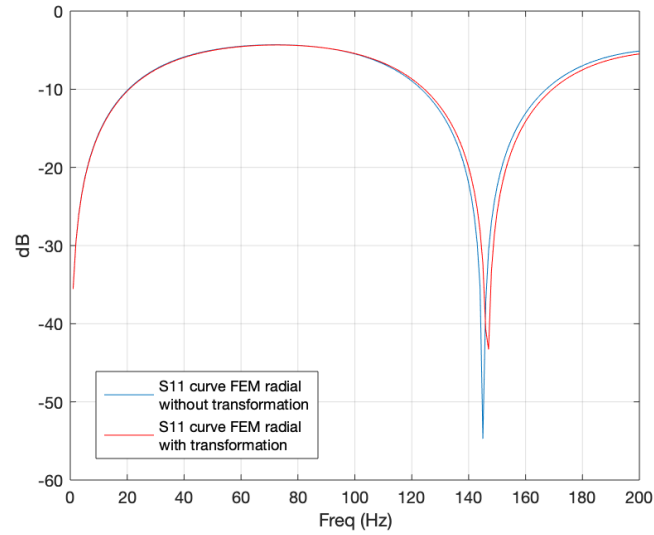
Figure 5.9: S_{11} curves overlap considering linear triangular elements for the discretization
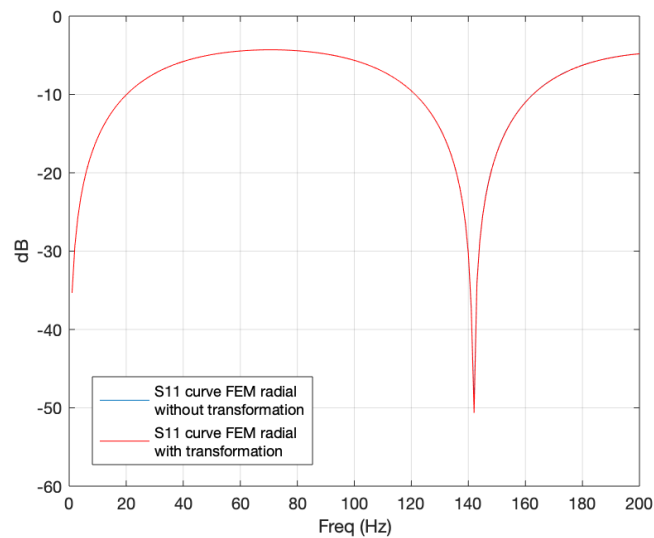
Figure 5.10: S_{11} curves overlap considering quadratic triangular elements for the discretization

We have demonstrated also for the radial case that the accuracy of the results increases by using higher-order elements for triangulation. In the figures above, we have in fact determined the overlap in case of linear and quadratic elements and it is obtained that with quadratic elements, the final result is far better. Clearly in the second case, the calculation time is slightly higher and it will be even more higher using cubic elements but obtaining more precise results at the expense of a longer operating time is a fair compromise.

We can also check out another geometry that raises the following structure:
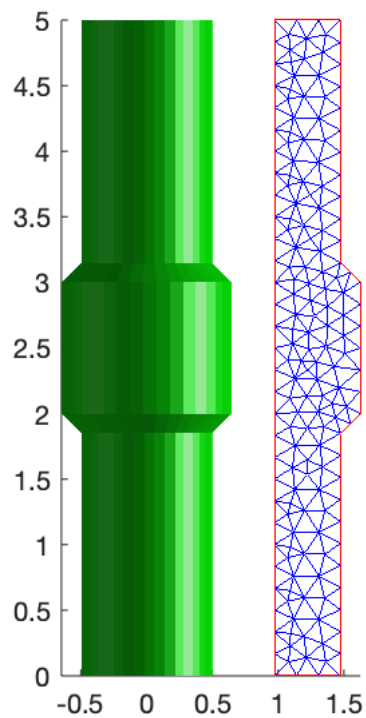
Figure 5.11: Deformed pipe with a bulge at its center and its mesh discretization

The solution is given by the following graph:
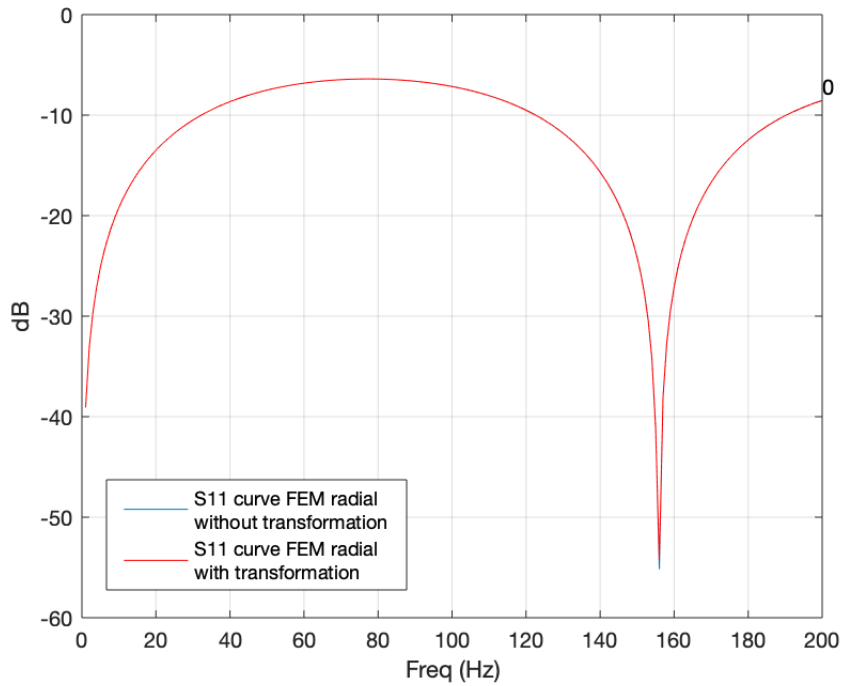
Figure 5.12: S_{11} curves overlap related to the pipe with a bulge at the center

In conclusion, by using the FEM for both planar and radial cases, a perfect overlap of the curves representing the scattering parameters is obtained. In all the cases considered, we have analyzed the S_{11} parameter which represents the quantity of the sound wave reflected at port 1.

At this point, after analyzing the s curves, we can display the elements of the transformation matrix and, based on their values, understand how the acoustic transformation takes place. Dealing with the geometry of figure 5.1, we carry out the following plot:
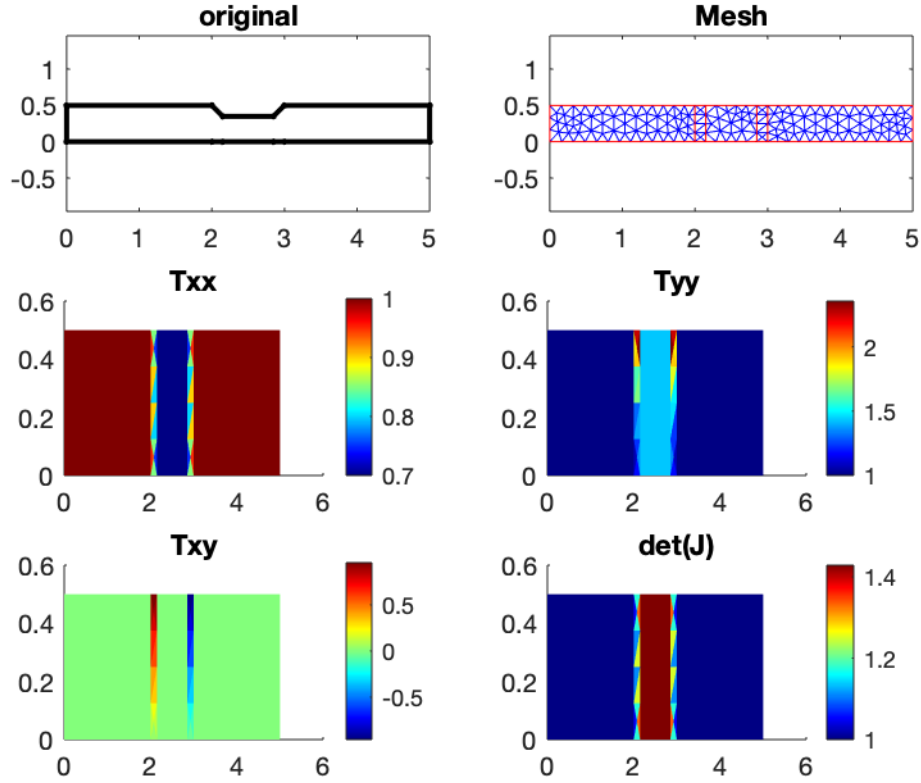
Figure 5.13: Deformed geometry, geometry mesh after transformation, T_{xx}, T_{yy}, T_{xy}, dJ

The figure 5.13 shows that the values of the elements T_{xx}, T_{yy} and T_{xy} are respectively 1, 1 and 0 where the geometry undergoes no transformation. The values change near the deformation where we apply the acoustic transformation and then find a stability within the deformation itself. Practically, the values are not steady when we employ the modification of the structure to then stabilize on a single value different from the starting one (except T_{xy} which returns to 0) once the contour change has been applied. Furthermore, the values of the elements of T depend on the mesh density and also on the frequency range considered: the denser the mesh and the wider the frequency range, the more the T values will change because the complexity of the problem calculation increases.

For the geometry of figure 5.6, it turns out:

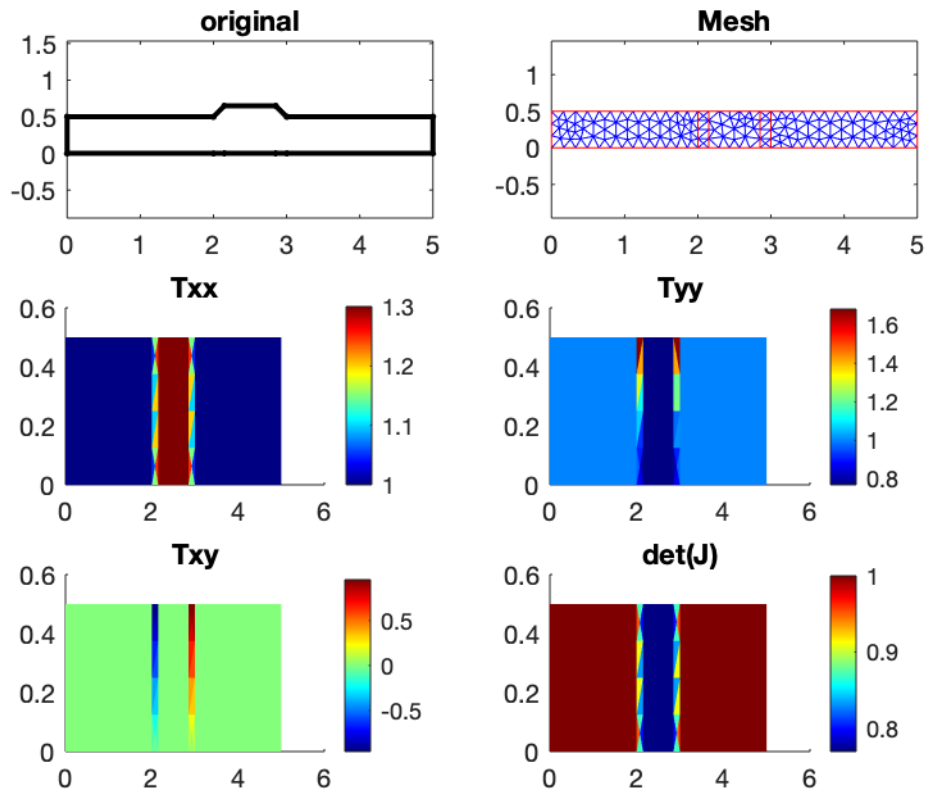Figure 5.14: Second example of deformed geometry, geometry mesh after transformation, T_{xx}, T_{yy}, T_{xy}, dJ

The same considerations made in the previous example apply.

5.2 Two-Dimensional HiMod Numerical Results

In the previous section, we analyzed the results related to the S parameters, obtained as a function of a certain frequency range, in relation to the Finite Element Method. In particular, we have seen that for all the examples considered, both for the two-dimensional planar case and radial case, the overlap between the s curve associated with the FEM considered without any transformation of the geometry and the FEM with the transformation, is more and more precise with the growth of parameters such as, for example, the mesh density that generates the domain and the order of the elements considered which can be linear, quadratic or cubic. The main problem of the FEM, as already mentioned previously, is given by the fact that, especially in the case of more complex geometries, it turns out to be obsolete in terms of computational efficiency. For this reason, we decided to evaluate the HiMod method, whose characteristics have already been illustrated.

By evaluating the same two-dimensional domain shown previously in figure 5.1, we can notice, as regards the planar case, that the computational time is significantly reduced and this allows us to optimize the monitoring of the deformation and solve any problems in time faster. Also according to the HiMod method, the considerations made previously regarding the parameters, such as the mesh density and the order of the elements, apply. In general, the overlap between the s curve linked to the case without transformation and that of the HiMod case is almost perfect.
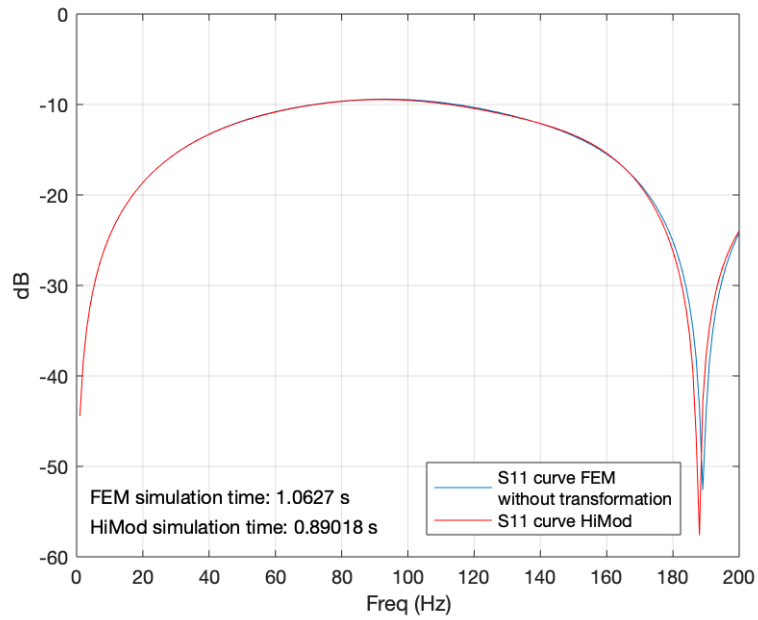
Figure 5.15: S_{11} curves overlap in HiMod with linear triangular elements
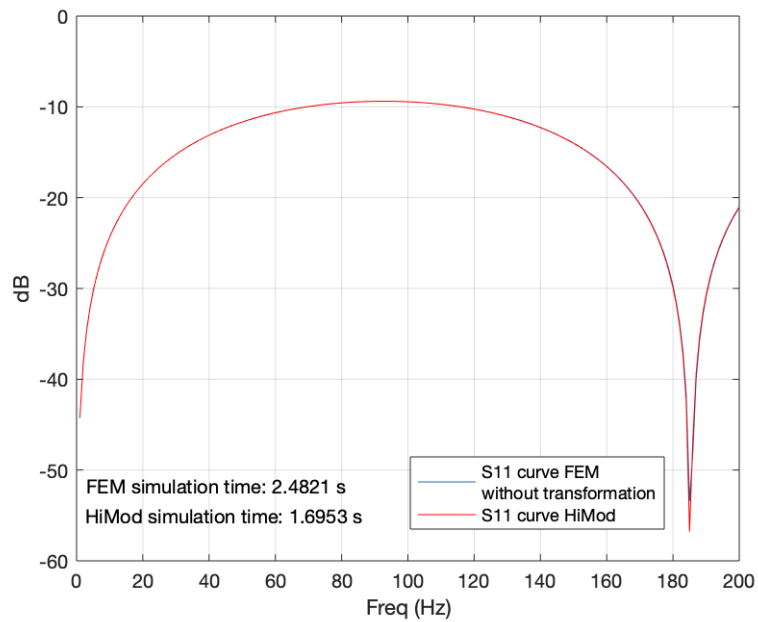
Figure 5.16: S_{11} curves overlap in HiMod with quadratic triangular elements

79
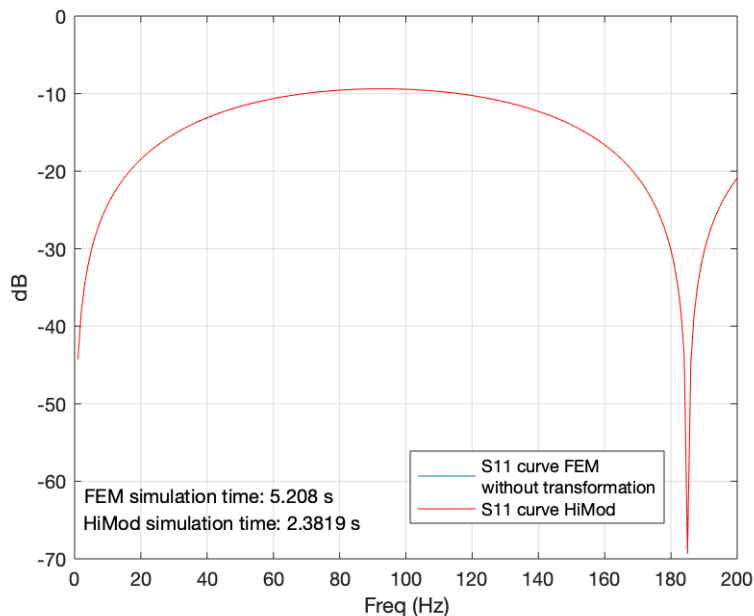
Figure 5.17: S_{11} curves overlap in HiMod with cubic triangular elements

In figures 5.15, 5.16 and 5.17 the overlaps between the curves S_{11} relating to linear, quadratic and cubic triangular elements respectively are shown. As in the FEM case, it turns out that by using higher-order elements, the solution will be more accurate. In the examples, we can also notice the different simulation times both in FEM and HiMod. In particular, as previously stated, the computational time using HiMod turns out to be much faster and the timing difference is recognized mostly by increasing the order of the elements. Considering, for example, cubic elements, we observe HiMod a simulation time equal to half the FEM simulation time. These properties can also be seen by examining other examples. Considering the geometry in figure 5.6, we obtain the following result:
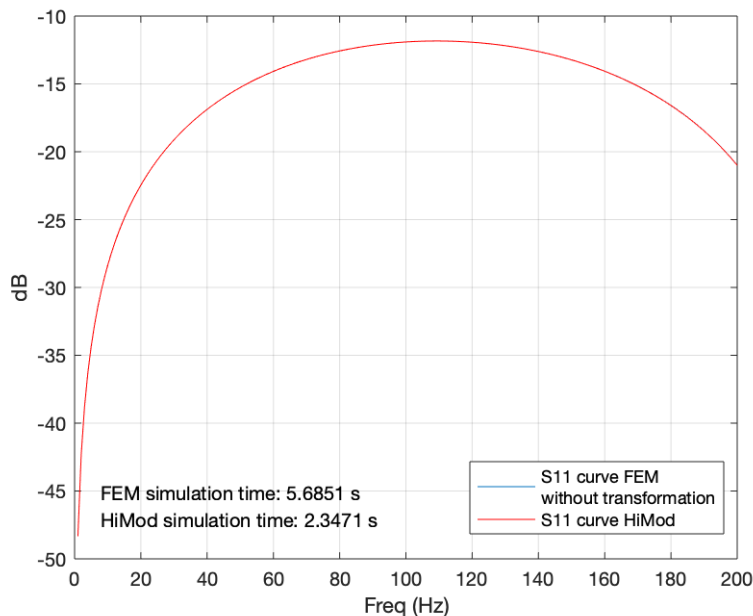
Figure 5.18: S_{11} curves overlap in HiMod related to a pipe with a bulge in the center

The figure 5.18 shows the overlap by analyzing a mesh density value of 10 and cubic elements. We can therefore conclude by saying that considering a two-dimensional geometry, with the HiMod method we obtain the result we were looking for and these are achieved in much less time. With the HiMod method we are therefore able to optimize the calculations.

5.2.1 Convergence Problem

Once we have found the solution regarding the two-dimensional planar case by using HiMod, we do the same for the radial case. In the radial case, the modal bases are expressed in a different way respect to the planar case. However, if in the planar case everything went smoothly, here instead we notice a problem related to the convergence between the s curve in the two-dimensional FEM in which we don't have any transformation of the domain and the same curve obtained with the two-dimensional HiMod reduction. In fact, if we consider the radial case that deals with Bessel functions, we can

81

clearly identify the lack of convergence for any value of parameters considered.
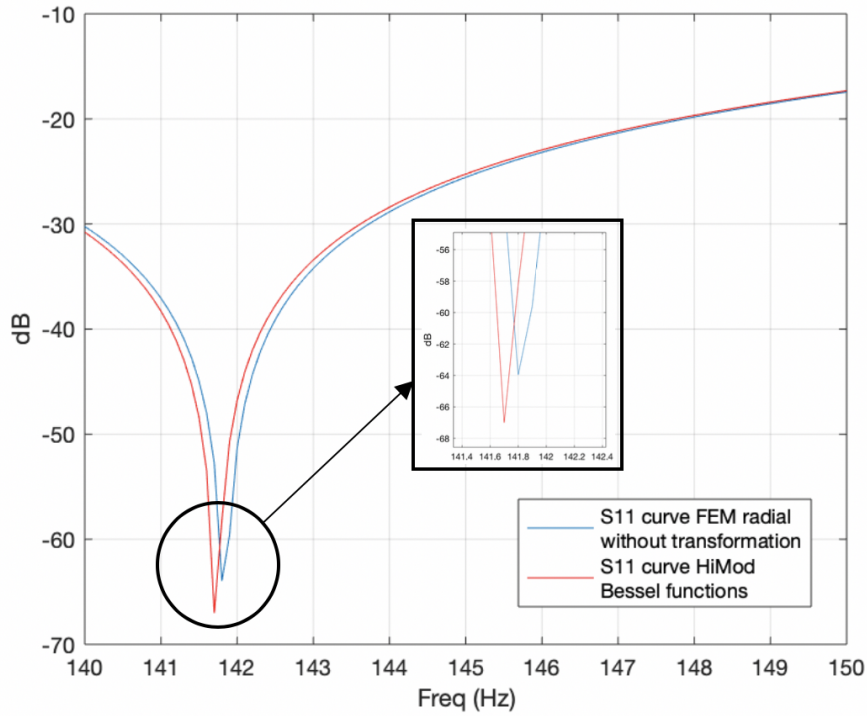
Figure 5.19: Convergence problem in the two-dimensional HiMod radial case

We have examined the geometry of figure 5.8 with quadratic elements and Bessel functions. In this case we note the lack of convergence at the frequency that hover around 141 and 142Hz. If, for all the results previously evaluated, a perfect overlap between the two curves was observed both for the FEM and HiMod planar cases and both in the case of quadratic and cubic elements (the linear elements do not show a perfect overlap given their extreme simplicity), now we note that also handling with quadratic elements, the overlap is not respected. The optimal result we would like to obtain is the perfect overlap between these two curves as happened in the comparison between the s curves in the FEM radial case and in the planar HiMod case. To try to achieve the perfect overlap, we have examined other modal functions different from the Bessel ones. In particular, we have tested a group of polynomials known as Chebyshev polynomials. The Chebyshev polynomials are a sequence of

orthogonal polynomials related to De Moivre's formula. They have many properties and they are useful in various areas such as the approximation field [28]. We usually distinguish between Chebyshev polynomials of the first kind denoted as T_n and Chebyshev polynomials of the second kind denoted as U_n. The Chebyshev polynomials are polynomials of degree n. The first few Chebyshev polynomials of the first kind are:

$$
\begin{aligned}
T_0(x) &= 1 \\
T_1(x) &= x \\
T_2(x) &= 2x^2 - 1 \\
T_3(x) &= 4x^3 - 3x \\
T_4(x) &= 8x^4 - 8x^2 + 1 \\
T_5(x) &= 16x^5 - 20x^3 + 5x
\end{aligned}
\tag{5.1}
$$

Starting from these equations, we can also define their derivatives. In general:

$$
\begin{aligned}
T_0^{'}(x) &= 0 \\
T_1^{'}(x) &= 1 \\
T_{k+1}^{'}(x) &= 2T_k(x) + 2xT_k^{'}(x) - T_{k-1}^{'}(x)
\end{aligned}
\tag{5.2}
$$

where $k = 0, 1, 2, ..., n$.

Figure 5.20: Chebyshev polynomials of the first kind $T_n(x)$
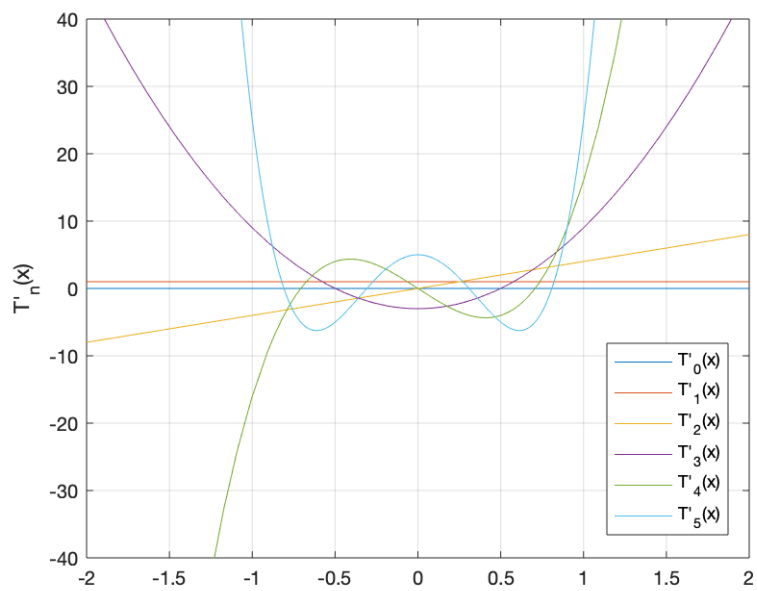
Figure 5.21: Derivatives of Chebyshev polynomials of the first kind $T_n^{'}(x)$

The Chebyshev polynomials can be described also by the following system:

$$T_n(x) = \begin{cases} \cos(n \arccos x) & |x| \leq 1 \\ \cosh(nar \cosh x) & x \geq 1 \\ (-1)^n \cosh(nar \cosh(-x) & x \leq -1 \end{cases} \tag{5.3}$$

To choose the Chebyshev polynomial of our interest, it is important that the derivative of this function is equal to zero in 0 and in R which are the ends of our domain. We can choose for example the Chebyshev polynomials related only to even indices, with a translation on the x axis. From the properties of these functions:

$$T_{2n}(x) = T_n(2x^2 - 1) \tag{5.4}$$

so:

$$T_{2n}(x^2 - 1) = T_n(2x^4 - 4x^2 + 1) \tag{5.5}$$

which represent the Chebyshev polynomials we are going to use. In the radial case, $x = \frac{\rho}{R}$.

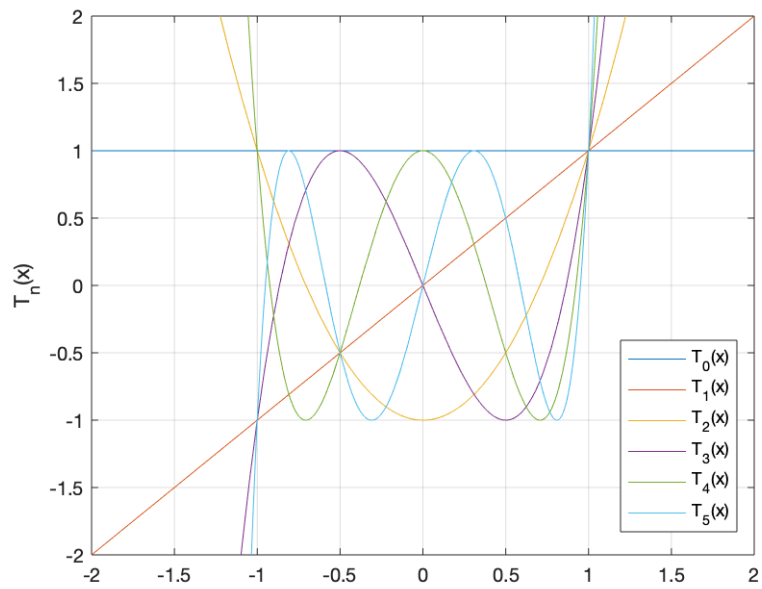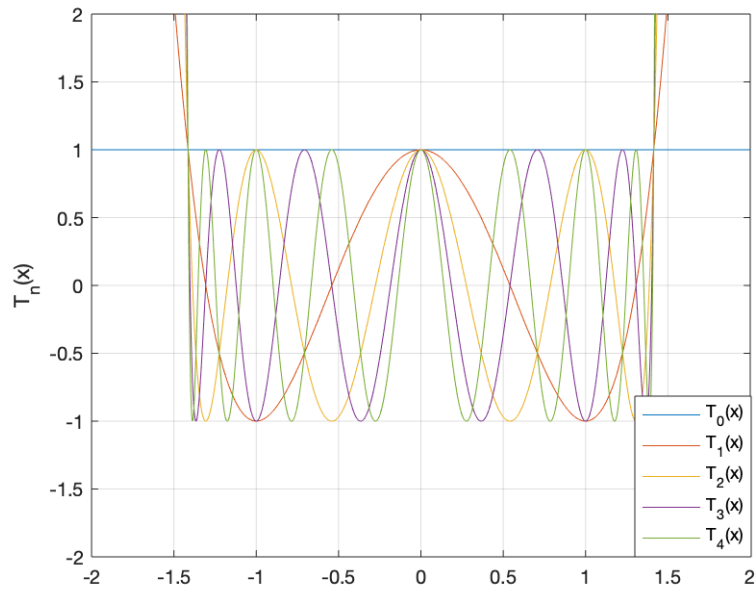Figure 5.22: Chebyshev polynomials of the first kind $T_{2n}(x^2 - 1)$
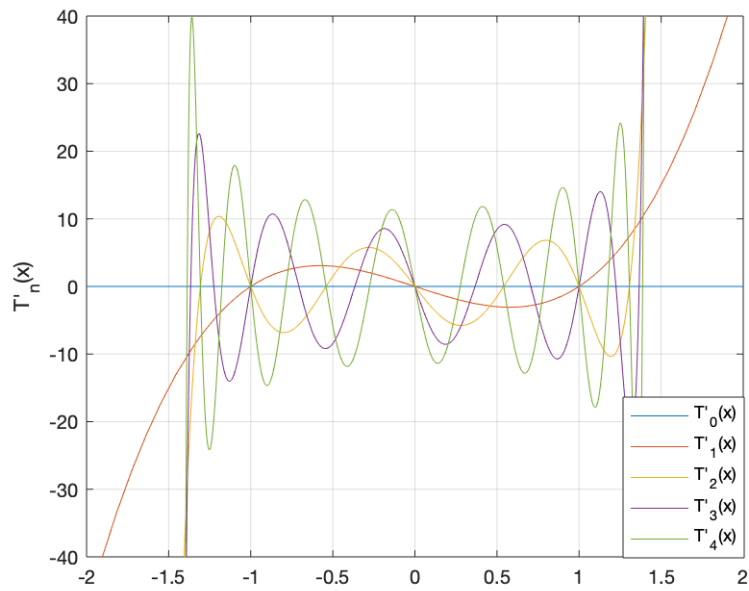
Figure 5.23: Derivatives of Chebyshev polynomials of the first kind $T'_{2n}(x^2-1)$

The transverse functions obtained are given by the following expression:

$$\varphi_n\left(\rho\right) = \frac{1}{\sqrt{2\pi \int_0^R \rho T_n^2 \left(2\left(\frac{\rho}{R}\right)^4 - 4\left(\frac{\rho}{R}\right)^2 + 1\right) d\rho}} T_n\left(2\left(\frac{\rho}{R}\right)^4 - 4\left(\frac{\rho}{R}\right)^2 + 1\right)$$

(5.6)

After the evaluation of Chebyshev polynomials to describe the transverse direction of the domain, we have considered also the Zernike polynomials. Zernike polynomials were implemented by Zernike in 1934 [29]. These mathematical functions are used to describe wavefront data. In particular, they are applied to fit irregular and non-rotationally symmetric surfaces over a circular region. The fields in which these functions are employed concern mostly atmospheric turbulence, corneal topography and interferometer measurements. Zernike polynomials present different advantages: they are orthogonal over the continuous unit circle and they efficiently represent common errors related to the optics field. Zernike polynomials are used not only for the observation of certain kinds of aberrations, but also for a complete representation of any wavefront, which can be also very complex. In general, Zernike polynomials are defined as:

$$Z_n^j\left(\rho, \theta\right) = R_n^j\left(\rho\right) \begin{cases} \sin\left(j\theta\right) \\ \cos\left(j\theta\right) \end{cases}$$

(5.7)

where ρ is the radial distance, θ is the azimuthal angle, $R_n^j\left(\rho\right)$ is the radial function, j is the index describing the azimuthal frequency and n represents the order of the radial polynomial [30].

These functions are also known as 1-sided Jacobi basis because they derive from the Jacobi polynomials and in general, are given by the following expression:

$$\left(\frac{\rho}{R}\right)^j P_{\frac{n-j}{2}}^{0,j}\left(2\left(\frac{\rho}{R}\right)^2 - 1\right)$$

(5.8)

87

where $P_{\frac{n-j}{2}}^{0,j}$ is the Jacobi polynomial of degree $\frac{n-j}{2}$ and order $(0,j)$. Thanks to the orthogonality constraint, these polynomials oscillate mostly near $\frac{\rho}{R} = 1$, and consequently, the roots move closer and closer to the outer boundary for a fixed degree and by increasing j, allowing for longer time steps. In our particular case, the index j seen before is null.

As before, we want to consider polynomials which show a derivative equal to zero in 0 and R. A function with these characteristics is provided by the polynomials with even subscript and a translation on the axis $\frac{\rho}{R}$:

$$P_{2n}\left(\left(\frac{\rho}{R}\right)^2 - 1\right) \tag{5.9}$$
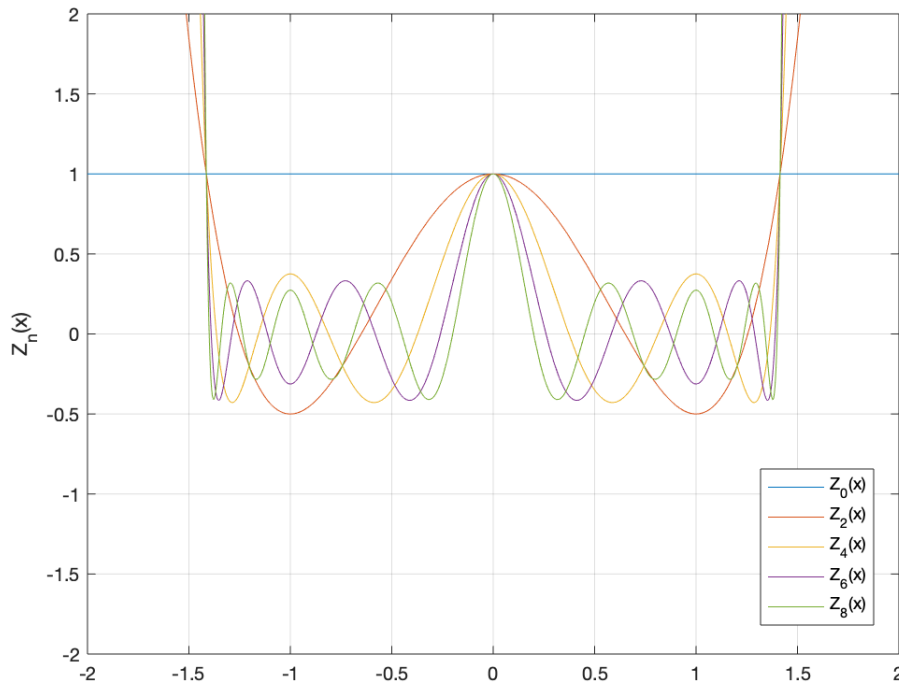
Figure 5.24: Zernike polynomials $Z_n(x) = P_{2n}(x^2 - 1)$

From this basis set, the transverse functions are obtained:

$$\varphi_n(\rho) = \frac{1}{\sqrt{2\pi \int_0^R \rho P_{2n}^2\left(\left(\frac{\rho}{R}\right)^2 - 1\right) d\rho}} P_{2n}\left(\left(\frac{\rho}{R}\right)^2 - 1\right) \qquad (5.10)$$

In both cases where we exploit Chebyshev and Zernike polynomials, a normalization is applied:

$$2\pi Q_n^2 \int_0^R \rho T_n^2\left(2\left(\frac{\rho}{R}\right)^4 - 4\left(\frac{\rho}{R}\right)^2 + 1\right) d\rho = 1 \qquad (5.11)$$

$$2\pi Q_n^2 \int_0^R \rho P_{2n}^2\left(\left(\frac{\rho}{R}\right)^2 - 1\right) d\rho = 1 \qquad (5.12)$$

where:

$$Q_n = \frac{1}{\sqrt{2\pi \int_0^R \rho T_n^2\left(2\left(\frac{\rho}{R}\right)^4 - 4\left(\frac{\rho}{R}\right)^2 + 1\right) d\rho}} \qquad (5.13)$$

$$Q_n = \frac{1}{\sqrt{2\pi \int_0^R \rho P_{2n}^2\left(\left(\frac{\rho}{R}\right)^2 - 1\right) d\rho}} \qquad (5.14)$$

Once we have analyzed these functions, we can use them to find the final solution. Considering the geometry seen in figure 5.8 and cubic triangular elements as elements of the domain discretization, we obtain the following curves:
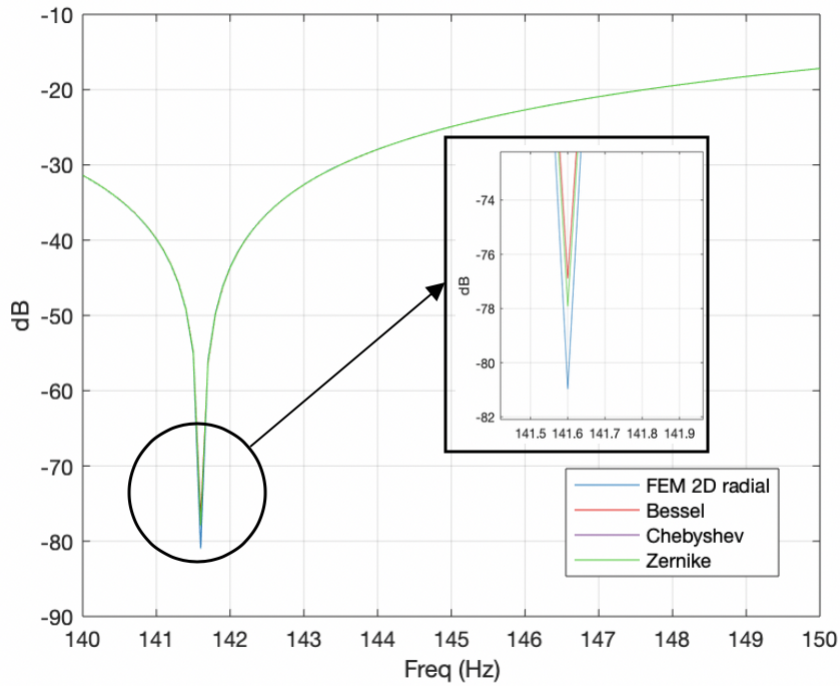
Figure 5.25: Comparison between S_{11} curves in the two-dimensional FEM radial case and HiMod radial case with Bessel, Chebyshev and Zernike functions

From the figure, we can see that the s curves linked to the Chebyshev and Zernike polynomials, which are superimposed on each other, tend to approach the FEM s curve, while the curve associated with the Bessel functions has worse results in terms of convergence.

By examining also the geometry of figure 5.11, we can make the same statements and, always dealing with cubic elements, we figure out:
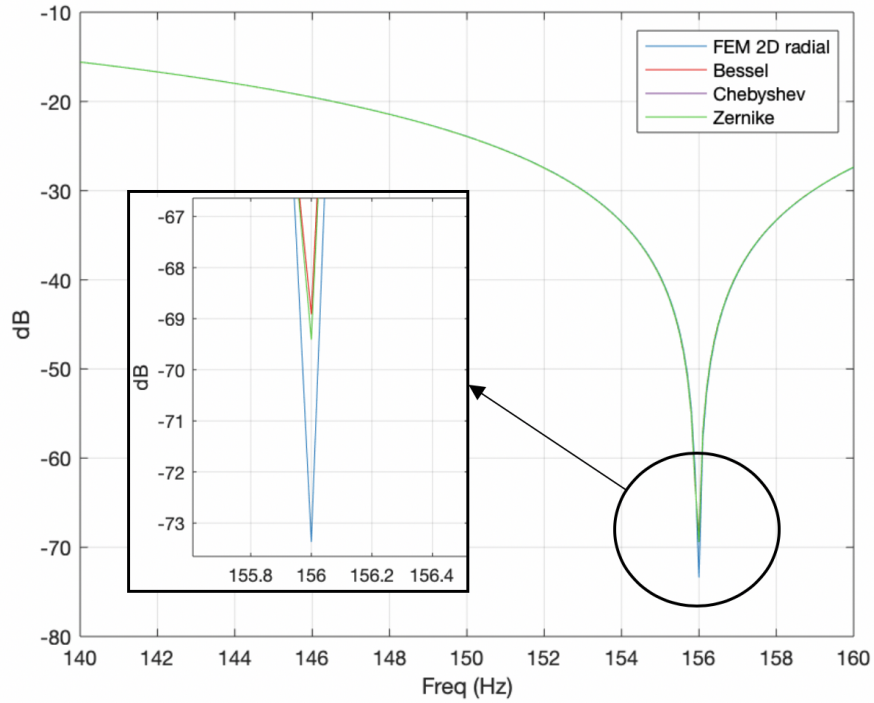
Figure 5.26: Second example of comparison between S_{11} curves in the two-dimensional FEM radial case and HiMod radial case with Bessel, Chebyshev and Zernike functions

In conclusion, we succeeded in our aim of obtaining better results than those given by analyzing the Bessel functions. By studying the nature of these two new polynomials and by using their translated versions, we approached the FEM curve without transformation.

Chapter 6

Extension to the Three-Dimensional Case

So far, the two-dimensional case has been evaluated. We first evaluated the Finite Element Method, considering a planar case and, in particular, a geometry characterized by a rectangle with different deformations and then we transformed it into a regular structure. We did the same considering the polar coordinates. After the detailed description of the Finite Element Method, the new HiMod reduction method has been implemented, because it is able to provide the same results but in less computational time and, in particular, we have focused on the problem of the convergence of the curves by representing the modes in the radial case and we have examined several modal functions to find a better result. Hence, some physical problems can be approximated with a mathematical model in one or two dimensions. However, it is now necessary to expand our study to the three dimensions because, all existing physical problems can be classified in space. When a one- or two-dimensional representation is not possible, it is necessary to consider the three-dimensional case. In this chapter we will describe the basics of the Finite Element Method in three dimensions by following the steps provided in [8] , just to better understand the analysis of a three-dimensional structure, then we will go through the description of the 3D HiMod reduction, still in the experimental phase, to figure out its advantages as regards the evaluation of the sound pressure in pipes affected by deformations.

6.1 Three-Dimensional Finite Element Method

6.1.1 The Boundary-Value Problem and the Variational Formulation

The boundary-value problem is defined by the following second-order differential equation:

$$-\frac{\partial}{\partial x}\left(a_x\frac{\partial u}{\partial x}\right) - \frac{\partial}{\partial y}\left(a_y\frac{\partial u}{\partial y}\right) - \frac{\partial}{\partial z}\left(a_z\frac{\partial u}{\partial z}\right) + bu = f \qquad in \quad V \qquad (6.1)$$

The boundary conditions that accompany the above equation are:

$$u = u_0 \quad on \quad S_1 \qquad (6.2)$$

$$\left(a_x\frac{\partial u}{\partial x}\widehat{x} + a_y\frac{\partial u}{\partial y}\widehat{y} + a_z\frac{\partial u}{\partial z}\widehat{z}\right)\cdot\widehat{n} + \gamma u = t_0 \quad on \quad S_2 \qquad (6.3)$$

where $S = S_1 + S_2$ denotes the surface enclosing the volume V while $\widehat{n}$ is the normal vector.

The variational problem [9] equivalent to (6.1) is performed by the following system of equations:

$$\begin{cases} \delta F\left(u\right) = 0 \\ u = u_0 \quad on \quad S_1 \end{cases} \qquad (6.4)$$

where:

$$F(u) = \frac{1}{2}\iiint_V\left[a_x\left(\frac{\partial u}{\partial x}\right)^2 + a_y\left(\frac{\partial u}{\partial y}\right)^2 + a_z\left(\frac{\partial u}{\partial z}\right)^2 + bu^2\right]dV$$
$$+ \iint_{S_2}\left(\frac{\gamma}{2}u^2 - t_0u\right)dS - \iiint_V fudV \qquad (6.5)$$

If a_x, a_y and a_z present discontinuities inside the volume, u satisfies the **continuity conditions** given by:

$$u^+ = u^- \quad on \quad S_d \tag{6.6}$$

and

$$\left(a_x^+ \frac{\partial u^+}{\partial x} \widehat{x} + a_y^+ \frac{\partial u^+}{\partial y} \widehat{y} + a_z^+ \frac{\partial u^+}{\partial z} \widehat{z} \right) \cdot \widehat{n} = \left(a_x^- \frac{\partial u^-}{\partial x} \widehat{x} + a_y^- \frac{\partial u^-}{\partial y} \widehat{y} + a_z^- \frac{\partial u^-}{\partial z} \widehat{z} \right) \cdot \widehat{n} \quad on \quad S_d \tag{6.7}$$

where S_d represents the discontinuity interface, the superscript ”+” describes the observation point that approaches the interface from the ”+” side and the superscript ”−” describes the observation point that approaches the interface from the ”−” side. The continuity conditions, naturally, are valid for both the boundary-value problem and the variational one.
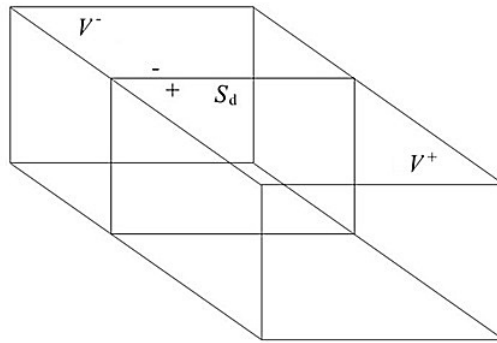
Figure 6.1: Three-dimensional domain with a discontinuity interface denoted by S_d

6.1.2 Three-Dimensional Finite Element Method Calculation

After the delineation of these two problems, the different steps of Finite Element Method in the three-dimensional case can be described. In this case, the geometrical domain is composed by a volume and this volume must be divided into a number of smaller volume elements, as, for example, tetrahedral elements. Consequently, the surface S is divided into different triangular elements. Once the mesh has been generated, it is necessary to consider the unknown function u in each element of the subdivision. This function is expressed by:

$$u^e (x, y, z) = \alpha_1^e + \alpha_2^e x + \alpha_3^e y + \alpha_4^e z \tag{6.8}$$

The coefficients $\alpha_1^e, \alpha_2^e, \alpha_3^e$ and α_4^e are obtained by applying (6.8) to the element nodes.

$$u_i^e = \alpha_1^e + \alpha_2^e x_i^e + \alpha_3^e y_i^e + \alpha_4^e z_i^e \tag{6.9}$$

$$u_j^e = \alpha_1^e + \alpha_2^e x_j^e + \alpha_3^e y_j^e + \alpha_4^e z_j^e \tag{6.10}$$

$$u_k^e = \alpha_1^e + \alpha_2^e x_k^e + \alpha_3^e y_k^e + \alpha_4^e z_k^e \tag{6.11}$$

$$u_l^e = \alpha_1^e + \alpha_2^e x_l^e + \alpha_3^e y_l^e + \alpha_4^e z_l^e \tag{6.12}$$

From these equations, one can achieve the coefficients given above in function of the nodes coordinates and express the volume of each tetrahedral element:

$$V^e = \frac{1}{6} \begin{vmatrix} 1 & 1 & 1 & 1 \\ x_i^e & x_j^e & x_k^e & x_l^e \\ y_i^e & y_j^e & y_k^e & y_l^e \\ z_i^e & z_j^e & z_k^e & z_l^e \end{vmatrix} \tag{6.13}$$

After finding the values of the coefficients and substituting them into (6.8), we obtain:

$$u^e(x, y, z) = \sum_{n=1}^{4} u_n^e \varphi_n^e(x, y, z) \tag{6.14}$$

where $\varphi_n^e(x, y, z)$ represent the **interpolation functions**. They are given by:

$$\varphi_n^e(x, y, z) = \frac{1}{6V^e} \left(\alpha_{1n}^e + \alpha_{2n}^e x + \alpha_{3n}^e y + \alpha_{4n}^e z \right) \qquad n = 1, ..., 4 \tag{6.15}$$

Now, the problem can be formulated through two different methods: the Ritz method [10] or the Galerkin method [11].

For simplicity, we consider the special case of $\gamma = t_0 = 0$. The functional $F(u)$ can be found through the summation of all the functionals related to each element of the domain subdivision:

$$F(u) = \sum_{e=1}^{M} F^e(u^e) \tag{6.16}$$

where M is the total number of elements. The functional associated to each element is expressed as:

$$
\begin{aligned}
F^e(u^e) = \ & \frac{1}{2} \iiint_{V^e} \left[a_x \left(\frac{\partial u^e}{\partial x} \right)^2 + a_y \left(\frac{\partial u^e}{\partial y} \right)^2 + a_z \left(\frac{\partial u^e}{\partial z} \right)^2 + b \left(u^e \right)^2 \right] dV \\
& - \iiint_{V^e} f u^e dV
\end{aligned}
\tag{6.17}
$$

Substituting (6.14) into (6.17) and deriving with respect to u_m^e, the result is:

$$\frac{\partial F^e}{\partial u_m^e} = \sum_{n=1}^{4} u_n^e \iiint_{V^e} \left(a_x \frac{\partial \varphi_m^e}{\partial x} \frac{\partial \varphi_n^e}{\partial x} + a_y \frac{\partial \varphi_m^e}{\partial y} \frac{\partial \varphi_n^e}{\partial y} + a_z \frac{\partial \varphi_m^e}{\partial z} \frac{\partial \varphi_n^e}{\partial z} + b \varphi_m^e \varphi_n^e \right) dV$$

$$- \iiint_{V^e} f \varphi_m^e dV \tag{6.18}$$

$$with \quad m = 1, ..., 4$$

This can be written in matrix form:

$$\left\{ \frac{\partial F^e}{\partial u^e} \right\} = [K^e] \{u^e\} - \{r^e\} \tag{6.19}$$

where the elements of the matrix K^e and of the vector r^e are expressed as the following integrals:

$$K_{mn}^e = \iiint_{V^e} \left(a_x \frac{\partial \varphi_m^e}{\partial x} \frac{\partial \varphi_n^e}{\partial x} + a_y \frac{\partial \varphi_m^e}{\partial y} \frac{\partial \varphi_n^e}{\partial y} + a_z \frac{\partial \varphi_m^e}{\partial z} \frac{\partial \varphi_n^e}{\partial z} + b \varphi_m^e \varphi_n^e \right) dV$$

$$m, n = 1, ..., 4 \tag{6.20}$$

$$r_m^e = \iiint_{V^e} f \varphi_m^e dV \qquad m = 1, ..., 4 \tag{6.21}$$

Starting from (6.19), it is advisable to join the tetrahedra that divide the geometry and impose the stationarity condition on F to derive the system. In simple terms, we take the derivatives related to all the tetrahedral elements and we sum them together to obtain the general result:

$$\left\{ \frac{\partial F}{\partial u} \right\} = \sum_{e=1}^{M} \left\{ \overline{\frac{\partial F^e}{\partial u^e}} \right\} = \sum_{e=1}^{M} \left([\overline{K^e}] \{\overline{u^e}\} - \{\overline{r^e}\} \right) = \{0\} \tag{6.22}$$

We can also consider that:

$$[K] = \sum_{e=1}^{M} \left[\overline{K^e} \right] \tag{6.23}$$

$$\{r\} = \sum_{e=1}^{M} \{ \overline{r^e} \} \tag{6.24}$$

These expressions yield the compact form of the system:

$$[K] \{u\} = \{r\} \tag{6.25}$$

In the case of $\gamma \neq 0$ or $t_0 \neq 0$, we must add the surface integral to the functional:

$$F_c(u) = \iint_{S_2} \left(\frac{\gamma}{2} u^2 - t_0 u \right) dS \tag{6.26}$$

The surface S_2 is composed by N triangular elements. The functional F_c can be written as:

$$F_c(u) = \sum_{s=1}^{N} F_c^s(u^s) \tag{6.27}$$

where F_c^s represents the functional linked to the s-th triangle of the surface considered. The unknown function u within each triangular element can be expressed in a way similar to the unknown function related to the e-th tetrahedral element:

$$u^s = \sum_{n=1}^{3} u_n^s \varphi_n^s \tag{6.28}$$

Doing the same algebraic steps followed to find the derivative of F^e, one can find that:

$$\frac{\partial F_c^s}{\partial u_m^s} = \sum_{n=1}^{3} u_n^s \iint_{S^s} \gamma \varphi_m^s \varphi_n^s dS - \iint_{S^s} t_0 \varphi_m^s dS \qquad (6.29)$$

where S^s illustrates the surface of the s-th triangle.

In matrix form, the above expression is:

$$\left\{ \frac{\partial F_c^s}{\partial u^s} \right\} = [K^s] \{u^s\} - \{r^s\} \qquad (6.30)$$

The elements of the matrix K^s and of the vector r^s are given by the following integrals:

$$K_{mn}^s = \iint_{S^s} \gamma \varphi_m^s \varphi_n^s dS \qquad (6.31)$$

$$r_m^s = \iint_{S^s} t_0 \varphi_m^s dS \qquad (6.32)$$

To include F_c into the system, it is necessary to take the sum of all the derivatives of F_c^s, after considering the stationarity condition, and to add the summation to the expression of the derivative of F respect to u:

$$\left\{ \frac{\partial F}{\partial u} \right\} = \sum_{e=1}^{M} \left\{ \overline{\frac{\partial F^e}{\partial u^e}} \right\} + \sum_{s=1}^{N} \left\{ \overline{\frac{\partial F_c^s}{\partial u^s}} \right\} = \qquad (6.33)$$

$$= \sum_{e=1}^{M} \left([\overline{K^e}] \{\overline{u^e}\} - \{\overline{r^e}\} \right) + \sum_{s=1}^{N} \left([\overline{K^s}] \{\overline{u^s}\} - \{\overline{r^s}\} \right) = \{0\}$$

The final system is represented as in the two-dimensional problem and it can be solved for u after imposing the Dirichlet boundary condition.

6.1.3 Higher-Order Elements

So far, linear tetrahedral elements have been considered. Now, we can define higher-order elements related to the three-dimensional case as we did for the two-dimensional case. We start considering a point P inside a tetrahedral element and denoting V_n as the volume of the element defined by P. We define the following expression:

$$L_n^e(x, y, z) = \frac{V_n}{V^e} \tag{6.34}$$

This function is the same as the linear interpolation functions specified in the linear elements case. The values of the function L_n denote a point inside a tetrahedral element and they are called **volume coordinates**. Starting from (6.34), we can define the interpolation functions also for quadratic or cubic elements.
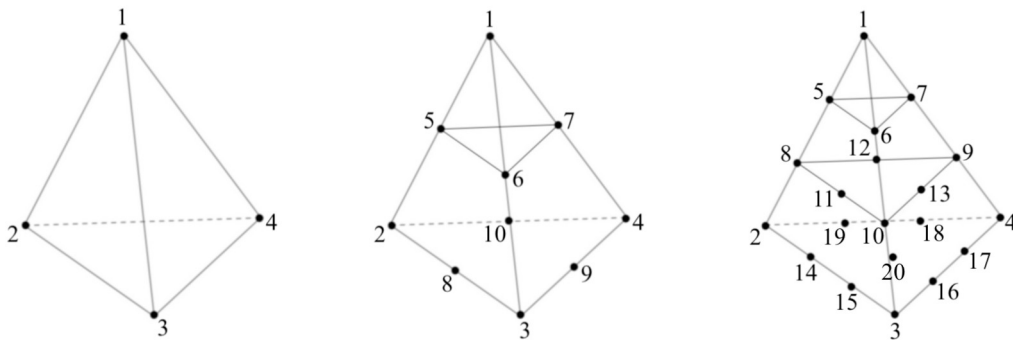

Figure 6.2: Linear, quadratic and cubic tetrahedral elements

Once we have the interpolation functions, the elemental matrix K^e and the vector r^e can be calculated by using the quadrature rules for the tetrahedron such as the Gaussian one [31]:

$$\iiint_{V^e} F(L_1^e, L_2^e, L_3^e, L_4^e)dV = \sum_{m=1}^{M_q} V^e w_m F(L_{1m}^e, L_{2m}^e, L_{3m}^e, L_{4m}^e) \tag{6.35}$$

where $L_{1m}^e, L_{2m}^e, L_{3m}^e, L_{4m}^e$ are the sampling points and w_m are the weights.

6.1.4 Isoparametric Elements

Such as the two-dimensional case, the barycentric coordinates, defined here by the triad (ξ, η, ς), are more suitable than the cartesian ones to describe curved geometries and lines and they give a more accurate modeling of the surfaces. This can be managed by first transforming an arbitrarily shaped element with curved sides in the xyz-space into a regularly shaped element with straight sides in the $\xi\eta\zeta$-space. The transformation is performed by using the following formulas:

$$x = \sum_{m=1}^{N_e} x_m \varphi_m^e (\xi, \eta, \zeta) \tag{6.36}$$

$$y = \sum_{m=1}^{N_e} y_m \varphi_m^e (\xi, \eta, \zeta) \tag{6.37}$$

$$z = \sum_{m=1}^{N_e} z_m \varphi_m^e (\xi, \eta, \zeta) \tag{6.38}$$

where N_e denotes the number of element nodes.

In this case, the elemental matrix and the vector are evaluated in the $\xi\eta\zeta$-space. Therefore, it is necessary to express the integrands in terms of ξ, η and ζ. This can be done in a way similar to the two-dimensional problem by using the Jacobian matrix to change variables:

$$\left\{ \begin{array}{c} \frac{\partial \varphi_m^e}{\partial x} \\ \frac{\partial \varphi_m^e}{\partial y} \\ \frac{\partial \varphi_m^e}{\partial z} \end{array} \right\} = (\mathbf{J})^{-1} \left\{ \begin{array}{c} \frac{\partial \varphi_m^e}{\partial \xi} \\ \frac{\partial \varphi_m^e}{\partial \eta} \\ \frac{\partial \varphi_m^e}{\partial \zeta} \end{array} \right\} \tag{6.39}$$

where:

$$\mathbf{J} = \begin{bmatrix} \frac{\partial x}{\partial \xi} & \frac{\partial y}{\partial \xi} & \frac{\partial z}{\partial \xi} \\ \frac{\partial x}{\partial \eta} & \frac{\partial y}{\partial \eta} & \frac{\partial z}{\partial \eta} \\ \frac{\partial x}{\partial \zeta} & \frac{\partial y}{\partial \zeta} & \frac{\partial z}{\partial \zeta} \end{bmatrix} \qquad (6.40)$$

The interpolation functions will present different expressions according to the type of elements used to discretize the domain. These will be employed to derive the respective derivatives and thus to change the variables considering the Jacobian matrix above.
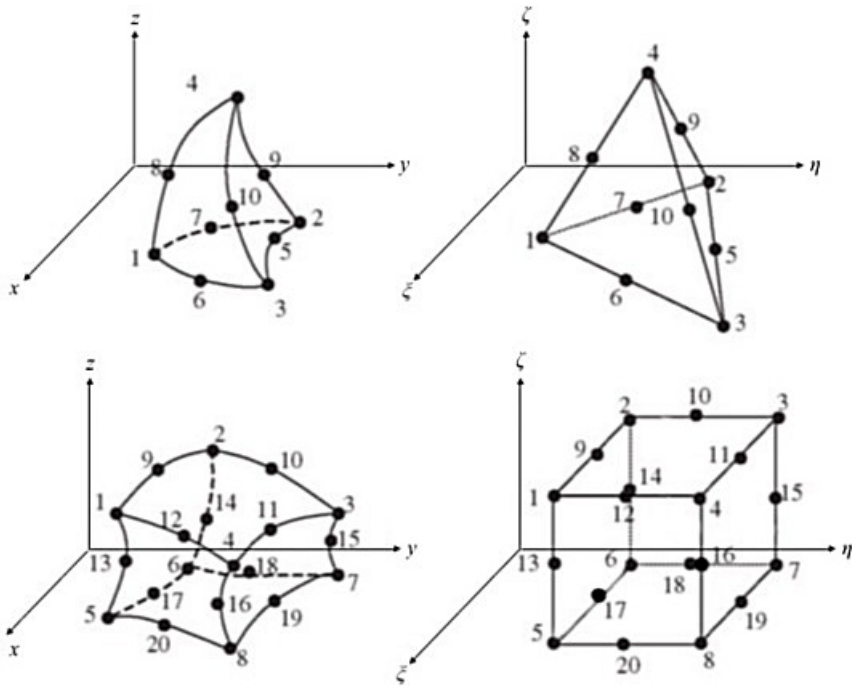
Figure 6.3: Quadratic tetrahedral and hexahedral elements in the xyz-space and their transformation in the $\xi\eta\zeta$-space

Through the Finite Element Method, it is therefore possible to analyze various problems of everyday reality. In particular the method is used for all those situations where it is not possible to reduce the problem to smaller dimensions. However, if the Finite Element Method was somewhat slow already in the two-dimensional case, all the more so for the three-dimensional

case. This is why it is important to evaluate the HiMod method also for 3D problems, to improve efficiency and speed up calculations.

6.2 Hierarchical Model Reduction in the Three-Dimensional Case

As previously mentioned, the Hierarchical Model (HiMod) reduction is a method introduced to effectively solve different engineering problems related to fluid dynamics [32] and also to the propagation of the sound pressure. With the two-dimensional case, we have already seen that by applying the HiMod method, the computational costs have decreased considerably compared to the Finite Element Method and, even more so, it will be for the three-dimensional case. In fact, one of the main difficulties of the 3D FEM is given by the use of a large number of elements to obtain accurate results. This implies a large number of equations to solve and many unknowns.

Considering the planar case, after the transformation, the domain is a parallelepiped with an height h_y, a length and a thickness equal to that of the original domain. The transformation acts at every point of the parallelepiped and it can be defined through a matrix $\overline{\mathbf{T}}$. In the general case, it is given by:

$$\overline{\mathbf{T}} = \begin{bmatrix} T_{xx}(x,y,z) & T_{xy}(x,y,z) & T_{xz}(x,y,z) \\ T_{yx}(x,y,z) & T_{yy}(x,y,z) & T_{yz}(x,y,z) \\ T_{zx}(x,y,z) & T_{zy}(x,y,z) & T_{zz}(x,y,z) \end{bmatrix} \qquad (6.41)$$

with $T_{yx} = T_{xy}$, $T_{zx} = T_{xz}$, $T_{zy} = T_{yz}$.

Therefore, the pressure will depend on three coordinates:

$$p(x,y,z) = \sum_q c_q p_q(x,y,z) = \sum_l \sum_m \sum_n c_{l,m,n} \varphi_l(x) \varphi_m(y) u_n(z) \qquad (6.42)$$

where φ are the modal functions associated to the transverse directions: along the x direction we have the thickness while along the y direction we have the height of the domain. The transverse functions are expressed as:

$$\varphi_l = A_l \cos \frac{l\pi x}{h_x} \tag{6.43}$$

$$\varphi_m = A_m \cos \frac{m\pi y}{h_y} \tag{6.44}$$

u_n are the one-dimensional FEM elements in which the dominant direction of the domain is divided.

The lattice is therefore a segment directed along the z direction divided into N elements. Therefore each index q will correspond to a triad (l, m, n) and one can obtain $l = l_q$, $m = m_q$ and $n = n_q$.

The elements of the matrices A and B are thus determined:

$$B(p, q) = \sum_i A^{(z)} w_i^{(z)} u_{n_p}(z_i) u_{n_q}(z_i) \beta(z_i) \tag{6.45}$$

where:

$$\beta(z_i) = \sum_j \sum_k A^{(x)} A^{(y)} w_j^{(x)} w_k^{(y)} \frac{\varphi_{l_p}(x_j)\varphi_{l_q}(x_j)\varphi_{m_p}(y_k)\varphi_{m_q}(y_k)}{\det \mathbf{J}(z_i, x_j, y_k)} \tag{6.46}$$

$$\begin{aligned} A(p, q) &= A_{xx}(p, q) + A_{xy}(p, q) + A_{xz}(p, q) + A_{yx}(p, q) + A_{yy}(p, q) + A_{yz}(p, q) \\ &+ A_{zx}(p, q) + A_{zy}(p, q) + A_{zz}(p, q) \end{aligned} \tag{6.47}$$

where:

$$A_{xx}(p, q) = \sum_i A^{(z)} w_i^{(z)} u_{n_p}(z_i) u_{n_q}(z_i) \alpha_{xx}(z_i) \tag{6.48}$$

$$A_{xy}(p, q) = \sum_i A^{(z)} w_i^{(z)} u_{n_p}(z_i) u_{n_q}(z_i) \alpha_{xy}(z_i) \qquad (6.49)$$

$$A_{xz}(p, q) = \sum_i A^{(z)} w_i^{(z)} u_{n_p}(z_i) \left. \frac{\partial u_{n_q}}{\partial z} \right|_{z_i} \alpha_{xz}(z_i) \qquad (6.50)$$

$$A_{yx}(p, q) = \sum_i A^{(z)} w_i^{(z)} u_{n_p}(z_i) u_{n_q}(z_i) \alpha_{yx}(z_i) \qquad (6.51)$$

$$A_{yy}(p, q) = \sum_i A^{(z)} w_i^{(z)} u_{n_p}(z_i) u_{n_q}(z_i) \alpha_{yy}(z_i) \qquad (6.52)$$

$$A_{yz}(p, q) = \sum_i A^{(z)} w_i^{(z)} u_{n_p}(z_i) \left. \frac{\partial u_{n_q}}{\partial z} \right|_{z_i} \alpha_{yz}(z_i) \qquad (6.53)$$

$$A_{zx}(p, q) = \sum_i A^{(z)} w_i^{(z)} \left. \frac{\partial u_{n_p}}{\partial z} \right|_{z_i} u_{n_q}(z_i) \alpha_{zx}(z_i) \qquad (6.54)$$

$$A_{zy}(p, q) = \sum_i A^{(z)} w_i^{(z)} \left. \frac{\partial u_{n_p}}{\partial z} \right|_{z_i} u_{n_q}(z_i) \alpha_{zy}(z_i) \qquad (6.55)$$

$$A_{zz}(p, q) = \sum_i A^{(z)} w_i^{(z)} \left. \frac{\partial u_{n_p}}{\partial z} \right|_{z_i} \left. \frac{\partial u_{n_q}}{\partial z} \right|_{z_i} \alpha_{zz}(z_i) \qquad (6.56)$$

The α coefficients are represented with two summations: one related to the transverse direction x and the other to the transverse direction y:

$$\alpha_{xx}(z_i) = \sum_j \sum_k A^{(x)} A^{(y)} w_j^{(x)} w_k^{(y)} T_{xx}(z_i, x_j, y_k) \left. \frac{\partial \varphi_{l_p}}{\partial x} \right|_{x_j} \left. \frac{\partial \varphi_{l_q}}{\partial x} \right|_{x_j} \varphi_{m_p}(y_k) \varphi_{m_q}(y_k)$$
$$(6.57)$$

$$\alpha_{xy}(z_i) = \sum_j \sum_k A^{(x)} A^{(y)} w_j^{(x)} w_k^{(y)} T_{xy}(z_i, x_j, y_k) \left. \frac{\partial \varphi_{l_p}}{\partial x} \right|_{x_j} \varphi_{l_q}(x_j) \varphi_{m_p}(y_k) \left. \frac{\partial \varphi_{m_q}}{\partial y} \right|_{y_k}$$
$$(6.58)$$

$$\alpha_{xz}(z_i) = \sum_j \sum_k A^{(x)} A^{(y)} w_j^{(x)} w_k^{(y)} T_{xz}(z_i, x_j, y_k) \left. \frac{\partial \varphi_{l_p}}{\partial x} \right|_{x_j} \varphi_{l_q}(x_j) \varphi_{m_p}(y_k) \varphi_{m_q}(y_k)$$
$$(6.59)$$

$$\alpha_{yx}(z_i) = \sum_j \sum_k A^{(x)} A^{(y)} w_j^{(x)} w_k^{(y)} T_{yx}(z_i, x_j, y_k) \varphi_{l_p}(x_j) \left. \frac{\partial \varphi_{l_q}}{\partial x} \right|_{x_j} \left. \frac{\partial \varphi_{m_p}}{\partial y} \right|_{y_k} \varphi_{m_q}(y_k)$$

$$(6.60)$$

$$\alpha_{yy}(z_i) = \sum_j \sum_k A^{(x)} A^{(y)} w_j^{(x)} w_k^{(y)} T_{yy}(z_i, x_j, y_k) \varphi_{l_p}(x_j) \varphi_{l_q}(x_j) \left. \frac{\partial \varphi_{m_p}}{\partial y} \right|_{y_k} \left. \frac{\partial \varphi_{m_q}}{\partial y} \right|_{y_k}$$

$$(6.61)$$

$$\alpha_{yz}(z_i) = \sum_j \sum_k A^{(x)} A^{(y)} w_j^{(x)} w_k^{(y)} T_{yz}(z_i, x_j, y_k) \varphi_{l_p}(x_j) \varphi_{l_q}(x_j) \left. \frac{\partial \varphi_{m_p}}{\partial y} \right|_{y_k} \varphi_{m_q}(y_k)$$

$$(6.62)$$

$$\alpha_{zx}(z_i) = \sum_j \sum_k A^{(x)} A^{(y)} w_j^{(x)} w_k^{(y)} T_{zx}(z_i, x_j, y_k) \varphi_{l_p}(x_j) \left. \frac{\partial \varphi_{l_q}}{\partial x} \right|_{x_j} \varphi_{m_p}(y_k) \varphi_{m_q}(y_k)$$

$$(6.63)$$

$$\alpha_{zy}(z_i) = \sum_j \sum_k A^{(x)} A^{(y)} w_j^{(x)} w_k^{(y)} T_{zy}(z_i, x_j, y_k) \varphi_{l_p}(x_j) \varphi_{l_q}(x_j) \varphi_{m_p}(y_k) \left. \frac{\partial \varphi_{m_q}}{\partial y} \right|_{y_k}$$

$$(6.64)$$

$$\alpha_{zz}(z_i) = \sum_j \sum_k A^{(x)} A^{(y)} w_j^{(x)} w_k^{(y)} T_{zz}(z_i, x_j, y_k) \varphi_{l_p}(x_j) \varphi_{l_q}(x_j) \varphi_{m_p}(y_k) \varphi_{m_q}(y_k)$$

$$(6.65)$$

As in the two-dimensional case, we used the numerical integration. The formulas which present the quadrature, provide the integration points and the weights necessary to determine $A^{(z)}$, $A^{(x)}$, $A^{(y)}$, z_i, x_j and y_k:

$$A^{(z)} = \frac{L_z}{2} \tag{6.66}$$

$$A^{(x)} = \frac{h_x}{2} \tag{6.67}$$

$$A^{(y)} = \frac{h_y}{2} \tag{6.68}$$

$$z_i = \xi_i \frac{L_z}{2} + \frac{z_a + z_b}{2} \tag{6.69}$$

$$x_j = \xi_j \frac{h_x}{2} + \frac{h_x}{2} \tag{6.70}$$

$$y_k = \xi_k \frac{h_y}{2} + \frac{h_y}{2} \tag{6.71}$$

where L_z is the length of each segment into which the direction z is divided using the one-dimensional FEM, h_x and h_y are the thickness and the height of the three-dimensional domain respectively. ξ_i, ξ_j and ξ_k are the integration points associated to the three directions.

6.2.1 Three-Dimensional Domain Transformation

We have shown the formulas that allow us to calculate the matrices A and B for the general three-dimensional HiMod case. In these formulas, we used the elements of the transformation matrix $\overline{\mathbf{T}}$ to determine the components we need. For simplicity, we evaluate the case where the transformation concerns only the height of the parallelepiped. This means that the transformation will be:

$$\begin{cases} x = x' \\ y = y'(x', y', z') \\ z = z' \end{cases} \tag{6.72}$$

Suppose we have a parallelepiped defined by the following coordinates: $\left(x'_j, y'_{1,i,j}, z'_i\right)$, $\left(x'_j, y'_{1,i+1,j}, z'_{i+1}\right)$, $\left(x'_{j+1}, y'_{1,i,j+1}, z'_i\right)$, $\left(x'_{j+1}, y'_{1,i+1,j+1}, z'_{i+1}\right)$, $\left(x'_j, y'_{2,i,j}, z'_i\right)$, $\left(x'_j, y'_{2,i+1,j}, z'_{i+1}\right)$, $\left(x'_{j+1}, y'_{2,i,j+1}, z'_i\right)$, $\left(x'_{j+1}, y'_{2,i+1,j+1}, z'_{i+1}\right)$. This solid must be transformed into another, which corresponds to its undeformed version. The new system of coordinates will be: (x_j, y_1, z_i), (x_j, y_1, z_{i+1}), (x_{j+1}, y_1, z_i),

(x_{j+1}, y_1, z_{i+1}), (x_j, y_2, z_i), (x_j, y_2, z_{i+1}), (x_{j+1}, y_2, z_i), (x_{j+1}, y_2, z_{i+1}). Knowing that the transformation only concerns the y direction, yields:

$$x'_j = x_j \tag{6.73}$$

$$x'_{j+1} = x_{j+1} \tag{6.74}$$

$$z'_i = z_i \tag{6.75}$$

$$z'_{i+1} = z_{i+1} \tag{6.76}$$

The geometric transformation related to the y direction is given by:

$$y = \frac{y' - y'_1}{h'_y} h_y \tag{6.77}$$

where $h'_y = y'_2 - y'_1$.

The two different points of the y direction in the deformed geometry are calculated through a procedure known as **bilinear interpolation**. It is an extension of the linear interpolation method adopted in the two-dimensional case for interpolating functions of two variables, $y = f(x, z)$, on a rectangular grid. Bilinear interpolation considers four vertex values, one on each edge of a rectangular cell, in order to obtain an approximate value inside the cell. The basic idea is to perform the linear interpolation first in one direction and then in the other direction [33].

We first calculate the linear interpolation in the x direction which gives:

$$f(x, z_i) = \frac{x_{j+1} - x}{x_{j+1} - x_j} f(x_j, z_i) + \frac{x - x_j}{x_{j+1} - x_j} f(x_{j+1}, z_i) \tag{6.78}$$

$$f(x, z_{i+1}) = \frac{x_{j+1} - x}{x_{j+1} - x_j} f(x_j, z_{i+1}) + \frac{x - x_j}{x_{j+1} - x_j} f(x_{j+1}, z_{i+1}) \tag{6.79}$$

Then we proceed by interpolating in the z direction:

$$f(x, z) = \frac{z_{i+1} - z}{z_{i+1} - z_i} f(x, z_i) + \frac{z - z_i}{z_{i+1} - z_i} f(x, z_{i+1}) \qquad (6.80)$$

Combining these three equations, it results in the desired estimate for $y = f(x, z)$:

$$\begin{aligned}
y &= f(x, z) = \frac{x_{j+1} - x}{x_{j+1} - x_j} \frac{z_{i+1} - z}{z_{i+1} - z_i} f(x_j, z_i) + \frac{x - x_j}{x_{j+1} - x_j} \frac{z_{i+1} - z}{z_{i+1} - z_i} f(x_{j+1}, z_i) + \\
&+ \frac{x_{j+1} - x}{x_{j+1} - x_j} \frac{z - z_i}{z_{i+1} - z_i} f(x_j, z_{i+1}) + \frac{x - x_j}{x_{j+1} - x_j} \frac{z - z_i}{z_{i+1} - z_i} f(x_{j+1}, z_{i+1}) \quad (6.81)
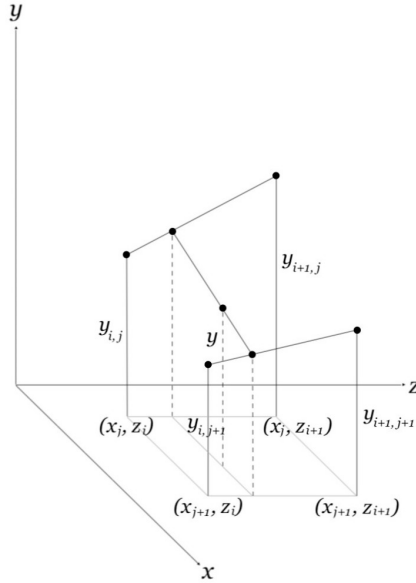\end{aligned}$$

Figure 6.4: Bilinear interpolation

Now, we can apply this formula to find the expression of y_1' and y_2' which define the height of the deformed geometry:

$$y'_1 = y'_{1,i,j} X_j Z_i + y'_{1,i+1,j} X_j Z_{i+1} + y'_{1,i,j+1} X_{j+1} Z_i + y'_{1,i+1,j+1} X_{j+1} Z_{i+1} \quad (6.82)$$

$$y'_2 = y'_{2,i,j} X_j Z_i + y'_{2,i+1,j} X_j Z_{i+1} + y'_{2,i,j+1} X_{j+1} Z_i + y'_{2,i+1,j+1} X_{j+1} Z_{i+1} \quad (6.83)$$

$$
\begin{aligned}
h'_y &= y'_2 - y'_1 = & (6.84) \\
&= h'_{y,i,j} X_j Z_i + h'_{y,i+1,j} X_j Z_{i+1} + h'_{y,i,j+1} X_{j+1} Z_i + h'_{y,i+1,j+1} X_{j+1} Z_{i+1}
\end{aligned}
$$

Replacing these equations in the expression of the transformation:

$$y = \frac{y' - y'_{1,i,j} X_j Z_i - y'_{1,i+1,j} X_j Z_{i+1} - y'_{1,i,j+1} X_{j+1} Z_i - y'_{1,i+1,j+1} X_{j+1} Z_{i+1}}{h'_{y,i,j} X_j Z_i + h'_{y,i+1,j} X_j Z_{i+1} + h'_{y,i,j+1} X_{j+1} Z_i + h'_{y,i+1,j+1} X_{j+1} Z_{i+1}} h_y$$
$$(6.85)$$

The inverse transformation is:

$$
\begin{aligned}
y' &= y \frac{h'_{y,i,j} X_j Z_i + h'_{y,i+1,j} X_j Z_{i+1} + h'_{y,i,j+1} X_{j+1} Z_i + h'_{y,i+1,j+1} X_{j+1} Z_{i+1}}{h_y} \quad (6.86) \\
&\quad + y'_{1,i,j} X_j Z_i + y'_{1,i+1,j} X_j Z_{i+1} + y'_{1,i,j+1} X_{j+1} Z_i + y'_{1,i+1,j+1} X_{j+1} Z_{i+1}
\end{aligned}
$$

Once the expression of the inverse transformation is obtained, the Jacobian matrix can be constructed. The elements of the Jacobian matrix associated to the three-dimensional case with only the transformation along y, are given by the following equations:

$$J_{xx} = \frac{\partial x}{\partial x'} = 1 \quad (6.87)$$

$$J_{xy} = \frac{\partial x}{\partial y'} = 0 \tag{6.88}$$

$$J_{xz} = \frac{\partial x}{\partial z'} = 0 \tag{6.89}$$

$$J_{yx} = \frac{\partial y}{\partial x'} = \tag{6.90}$$
$$= \left[\frac{(y'_{1,i,j} - y'_{1,i,j+1})(z_{i+1} - z) + (y'_{1,i+1,j} - y'_{1,i+1,j+1})(z - z_i)}{h'_{y,i,j}X_j Z_i + h'_{y,i+1,j}X_j Z_{i+1} + h'_{y,i,j+1}X_{j+1} Z_i + h'_{y,i+1,j+1}X_{j+1} Z_{i+1}} - \right.$$
$$- \frac{(y' - y'_{1,i,j}X_j Z_i - y'_{1,i+1,j}X_j Z_{i+1} - y'_{1,i,j+1}X_{j+1} Z_i - y'_{1,i+1,j+1}X_{j+1} Z_{i+1})}{(h'_{y,i,j}X_j Z_i + h'_{y,i+1,j}X_j Z_{i+1} + h'_{y,i,j+1}X_{j+1} Z_i + h'_{y,i+1,j+1}X_{j+1} Z_{i+1})^2} \cdot$$
$$\left. \cdot ((h'_{y,i,j+1} - h'_{y,i,j})(z_{i+1} - z) + (h'_{y,i+1,j+1} - h'_{y,i+1,j})(z - z_i)) \right] \frac{h_y}{\Delta_i \Delta_j}$$

$$J_{yy} = \frac{\partial y}{\partial y'} = \frac{h_y}{h'_{y,i,j}X_j Z_i + h'_{y,i+1,j}X_j Z_{i+1} + h'_{y,i,j+1}X_{j+1} Z_i + h'_{y,i+1,j+1}X_{j+1} Z_{i+1}}$$
$$\tag{6.91}$$

$$J_{yz} = \frac{\partial y}{\partial z'} = \tag{6.92}$$
$$= \left[\frac{(y'_{1,i,j} - y'_{1,i+1,j})(x_{j+1} - x) + (y'_{1,i,j+1} - y'_{1,i+1,j+1})(x - x_j)}{h'_{y,i,j}X_j Z_i + h'_{y,i+1,j}X_j Z_{i+1} + h'_{y,i,j+1}X_{j+1} Z_i + h'_{y,i+1,j+1}X_{j+1} Z_{i+1}} - \right.$$
$$- \frac{(y' - y'_{1,i,j}X_j Z_i - y'_{1,i+1,j}X_j Z_{i+1} - y'_{1,i,j+1}X_{j+1} Z_i - y'_{1,i+1,j+1}X_{j+1} Z_{i+1})}{(h'_{y,i,j}X_j Z_i + h'_{y,i+1,j}X_j Z_{i+1} + h'_{y,i,j+1}X_{j+1} Z_i + h'_{y,i+1,j+1}X_{j+1} Z_{i+1})^2} \cdot$$
$$\left. \cdot ((h'_{y,i+1,j} - h'_{y,i,j})(x_{j+1} - x) + (h'_{y,i+1,j+1} - h'_{y,i,j+1})(x - x_j)) \right] \frac{h_y}{\Delta_i \Delta_j}$$

$$J_{zx} = \frac{\partial z}{\partial x'} = 0 \tag{6.93}$$

$$J_{zy} = \frac{\partial z}{\partial y'} = 0 \tag{6.94}$$

$$J_{zz} = \frac{\partial z}{\partial z'} = 1 \tag{6.95}$$

Therefore the Jacobian matrix will be:

$$\mathbf{J} = \begin{bmatrix} 1 & 0 & 0 \\ J_{yx} & J_{yy} & J_{yz} \\ 0 & 0 & 1 \end{bmatrix}$$ (6.96)

and the determinant:

$$\det \mathbf{J} = J_{yy}$$ (6.97)

We can derive the transformation matrix, the elements of which will have to be replaced to obtain the matrices A and B previously seen:

$$\overline{\mathbf{T}} = \frac{\mathbf{J}\mathbf{J}^T}{\det \mathbf{J}} = \frac{1}{\det \mathbf{J}} \begin{bmatrix} 1 & J_{yx} & 0 \\ J_{yx} & J_{yx}^2 + J_{yy}^2 + J_{yz}^2 & J_{yz} \\ 0 & J_{yz} & 1 \end{bmatrix}$$ (6.98)

Chapter 7

Three-Dimensional Case Numerical Results

In the previous chapter, we have generally expressed the Finite Element Method in the three-dimensional case. As in the two-dimensional case, we have evaluated all the various steps that make up this method, including the most important one which is the domain discretization. As we have already seen, in the three-dimensional case, the elements that constitute the subdivision are mainly tetrahedra of different order. However, given the fact that this method takes many steps and a lot of computational time to solve the problems in the two-dimensional case, in the 3D case, even more so, it involves even slower calculations and a considerable operational difficulty. For this reason, we immediately considered the HiMod method that allows us to obtain the scattering parameters analysis in relation to the deformations evaluation in cylindrical structures by calculating the sound pressure values at the various points. In this chapter, we will therefore start from the evaluation of different three-dimensional structures and we will compare the deformed three-dimensional domain with the deformation-free reference domain and, observing the scattering parameters curves as a function of frequency, we will draw the necessary conclusions. In particular, we will consider geometries that present deformations only along y and those types of geometry whose deformation causes the entire domain to be asymmetrical.

7.1 Three-Dimensional HiMod Numerical Results

As a first example of three-dimensional geometry, we can consider the following structure:
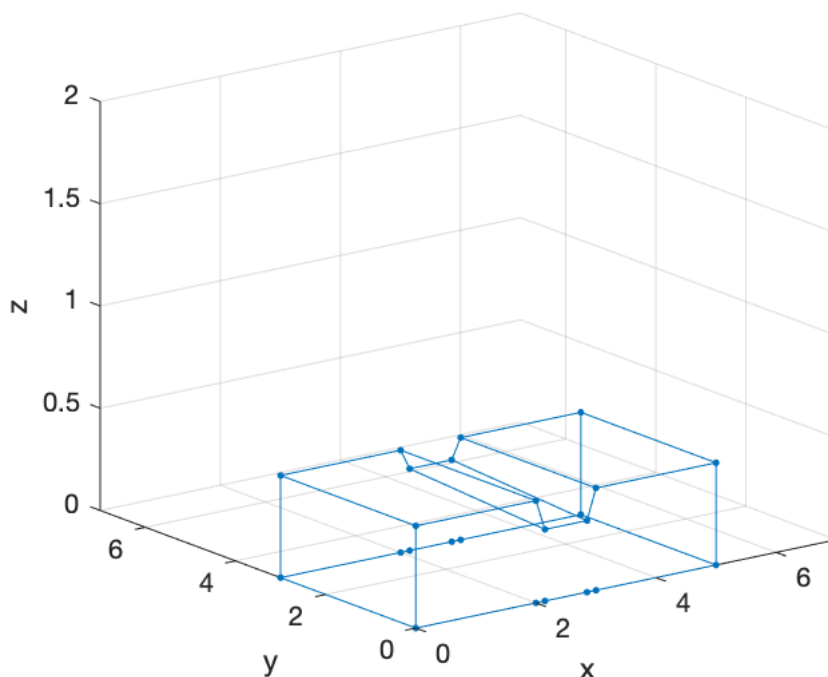

Figure 7.1: Example 1 of 3D deformed geometry

This structure shows a deformation only along the height and appears to be slightly asymmetrical, presenting a smaller deformation on one side than the other. We can also depict 3D geometry after acoustic transformation:

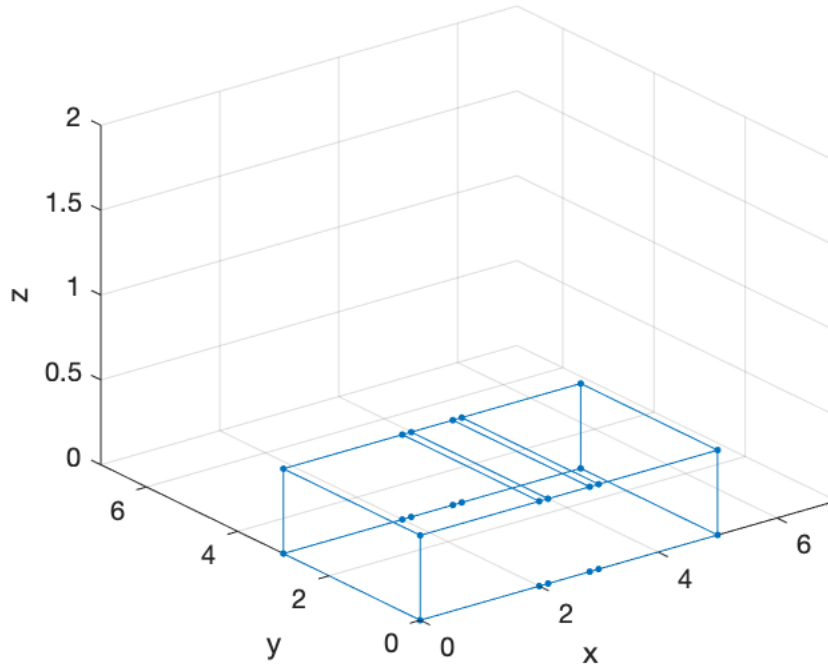Figure 7.2: Three-dimensional reference structure

After having displayed the geometry, we want to observe the comparison between the S_{11} curves. The curve related to the transformation-free structure is obtained through the simulation software Comsol while the Hi-Mod scattering curve is reached with Matlab. By studying a frequency range between 1Hz and 200Hz, we obtain the following graph:
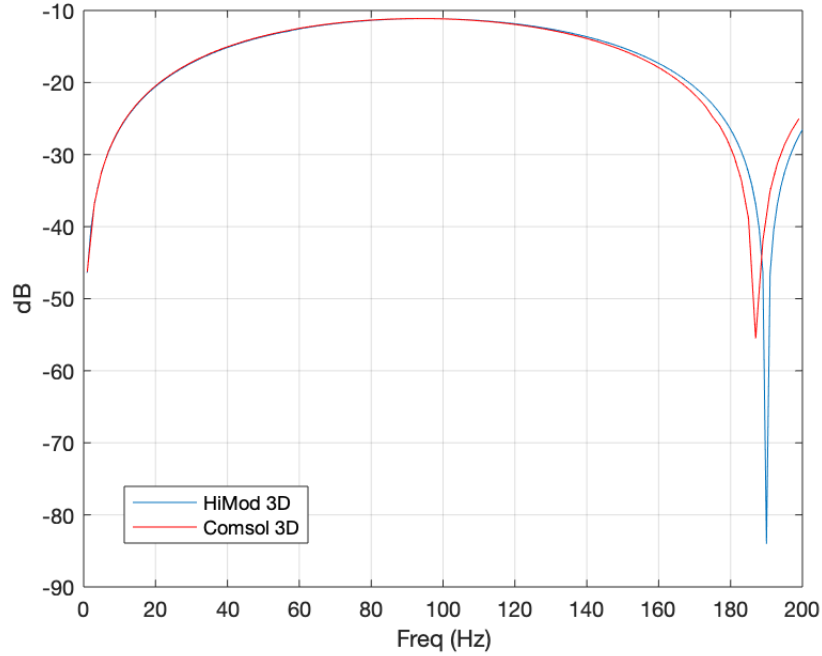
Figure 7.3: S_{11} curve comparison between Comsol 3D FEM and HiMod

We analyze the case of quadratic elements, mesh density equal to 14 and a number of transversal modal functions equal to 25. In figure 7.3 we can see the behavior of the two curves. The overlap is almost perfect except for the frequencies starting from about 120Hz where the curves start to diverge. This divergence is partly due to the fact that Comsol makes a different decomposition of the three-dimensional geometry and therefore analyzes it in a different way compared to Matlab. In this case, although we are considering an asymmetric geometry and therefore more complex to identify than a symmetric domain, we still obtain that the approximation provided by Hi-Mod manages a convergence quite well to the general solution of the problem implemented by FEM.

Now, we can show a structure of this type:
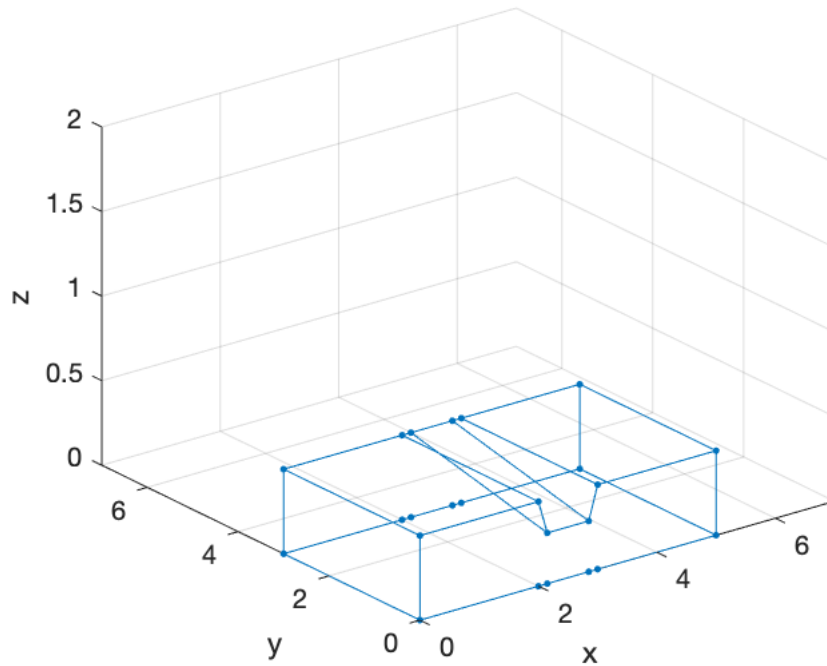
Figure 7.4: Example 2 of 3D deformed geometry

This structure has a fairly considerable deformation on one side while on the other the surface is flat. As in the previous case, we therefore consider an asymmetric surface. The solution to the problem is given by the following graph:
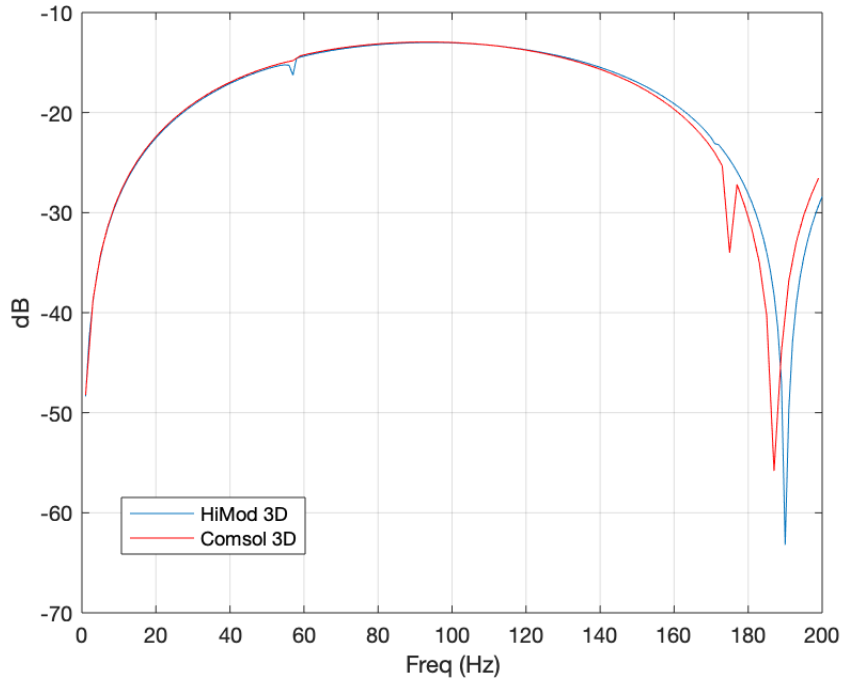
Figure 7.5: S_{11} curve comparison between Comsol 3D FEM and HiMod

In this case, the convergence between HiMod and FEM seems to be less precise than in the previous case and this is given in part by the increase in asymmetricity of the domain. In the previous case, the structure had a slightly deeper deformation on one side and the domain was thus almost symmetrical. Now, the asymmetricity of the figure is visible to the naked eye and this affects the final result. As before, we note that the convergence decreases for frequencies starting from about 120Hz.

Appendix A

Solution Procedures for FEM and HiMod Reduction Method

So far, we have evaluated the two methods that allow us to solve the most varied engineering problems: the Finite Element Method, which boasts many studies behind it, and the newer Hierarchical Model reduction method. After going through the description of the approaches, both as regards the two-dimensional and the three-dimensional case, and having highlighted the advantages of the HiMod method, we can now analyze the different algorithms necessary to find the solution to these problems, and in particular, the algorithms which can be adopted to pick up the sound pressure values in cylindrical structures affected by deformations.

The general final system is given by:

$$Ax = b \tag{A.1}$$

where A is a non-singular square matrix, x is the unknown vector to determine and b is the known vector. Connecting to our problem, the matrix A include the difference $\mathbf{A} - k^2\mathbf{B}$ while the vector b is the known term expressed previously as $\mathbf{C}$ and the unknown x is the pressure.

Having discussed this, the question is now how to extract the values of the system. In this chapter, we will discuss several algorithms which include decomposition methods, frontal and multifrontal methods and conjugate and

biconjugate methods. We will focus mainly on the LU decomposition method which is the one adopted to achieve the pressure results and then report the other techniques only from a general point of view.

A.1   LU Decomposition Method

The methods can be classified into two groups: **direct methods** and **iterative methods** [12]. At the basis of the direct methods lies the Gaussian elimination. Among these procedures we find the **decomposition methods**. The most important is the LU decomposition method. Introduced by Alan Turing in 1948 [34], this method can be used to solve many systems: in an electronic circuit it can be used to derive the value of the current, or it can be applied to extrapolate the sound pressure values in a waveguide as in our case. LU decomposition is a very efficient technique because it requires less computational time than other resolution methods, however, in certain situations, it suffers from a problem known as iteration cycling [35]. In general, LU decomposition is particularly suitable for all those problems that can be represented in matrix form: the approach is in fact designed as the factorization of a matrix in the product of two matrices. In this case, the matrix A defined before represents the matrix to be divided. It turns out:

$$A = LU \tag{A.2}$$

where L is a lower triangular matrix and U is an upper triangular matrix.

The solution can be reached through two steps. First we have to solve:

$$Ly = b \tag{A.3}$$

and then:

$$Ux = y \tag{A.4}$$

A forward substitution procedure is used to find y:

$$y_1 = \frac{b_1}{l_{11}} \tag{A.5}$$

$$y_i = \frac{1}{l_{ii}} \left(b_i - \sum_{j=1}^{i-1} l_{ij} y_j \right) \quad i = 2, 3, ..., n \tag{A.6}$$

A backward substitution procedure is used to find x:

$$x_n = \frac{y_n}{u_{nn}} \tag{A.7}$$

$$x_i = \frac{1}{u_{ii}} \left(y_i - \sum_{j=i+1}^{n} u_{ij} x_j \right) \quad i = n-1, n-2, ..., 1 \tag{A.8}$$

The multiplication between the matrices L and U that leads us to have the matrix A, is illustrated in details as follows:

$$
\begin{bmatrix}
l_{11} & & & & & & \\
l_{21} & l_{22} & & & & & \\
l_{31} & l_{32} & l_{33} & & & & \\
. & . & . & & & & \\
. & . & . & & & & \\
. & . & . & & & & \\
l_{n1} & l_{n2} & l_{n3} & ... & l_{nn}
\end{bmatrix}
\begin{bmatrix}
u_{11} & u_{12} & u_{13} & ... & u_{1n} \\
& u_{22} & u_{23} & ... & u_{2n} \\
& & u_{33} & ... & u_{3n} \\
& & & & . \\
& & & & . \\
& & & & . \\
& & & & u_{nn}
\end{bmatrix}
\tag{A.9}
$$

$$
=
\begin{bmatrix}
a_{11} & a_{12} & a_{13} & ... & a_{1n} \\
a_{21} & a_{22} & a_{23} & ... & a_{2n} \\
a_{31} & a_{32} & a_{33} & ... & a_{3n} \\
. & . & . & & . \\
. & . & . & & . \\
. & . & . & & . \\
a_{n1} & a_{n2} & a_{n3} & ... & a_{nn}
\end{bmatrix}
$$

From this matrix product we obtain the following elements:

$$l_{i1}u_{1j} + l_{i2}u_{2j} + \dots + l_{ij}u_{jj} = a_{ij} \quad i \geq j \tag{A.10}$$

$$l_{i1}u_{1j} + l_{i2}u_{2j} + \dots + l_{ii}u_{ij} = a_{ij} \quad i < j \tag{A.11}$$

For simplicity we consider:

$$u_{ii} = 1 \quad i = 1, 2, \dots, n \tag{A.12}$$

So, in conclusion, this algorithm can be approximated in the following way:

$$u_{ii} = 1 \quad i = 1, 2, \dots, n \tag{A.13}$$

$$l_{ij} = a_{ij} - \sum_{k=1}^{j-1} l_{ik}u_{kj} \quad i \geq j \tag{A.14}$$

$$u_{ij} = \frac{1}{l_{ii}}\left(a_{ij} - \sum_{k=1}^{i-1} l_{ik}u_{kj}\right) \quad i < j \tag{A.15}$$

After obtaining the elements that determine the decomposition, the system can be solved for y and x:

$$y_1 = \frac{b_1}{l_{11}} \tag{A.16}$$

$$y_i = \frac{1}{l_{ii}}\left(b_i - \sum_{j=1}^{i-1} l_{ij}y_j\right) \quad i = 2, 3, \dots, n \tag{A.17}$$

$$x_n = y_n \tag{A.18}$$

$$x_i = y_i - \sum_{j=i+1}^{n} u_{ij}x_j \quad i = n-1, n-2, \dots, 1 \tag{A.19}$$

122

A process similar to LU decomposition is figured out by LDL^T decomposition. The only difference is given by the fact that the matrix A is symmetric. In conclusion, comparing to the complex algorithm to be analyzed, LU decomposition method has a simple computation. It turns out to be very mechanical and the algorithm has a very compact form. LU is particularly effective especially in case of small problems [36] but it is also very good for solving large sparse nonsymmetric linear systems [37].

A.2 Other Methods

Other decomposition methods are represented by the frontal and multifrontal methods. These are procedures suitable for solving large systems with low memory demand [38]. They refer to the assembly of the matrices related to the elements of the domain to obtain the total system matrix and then carry out the Gaussian elimination. In practice, an array consisting of a set of equations, slides along the matrix. The matrix that is generated is called frontal matrix. The advantages of this method concern the low memory usage. However, this method is characterized by a low rate of estimation of the results. The multifrontal method is an improvement of the frontal one that uses several fronts at the same time. This method can be managed only considering the parallel computing. It is mainly used in presence of large-scale problems that require more memory [8]. Of course, large problems will include higher factorization costs. To overcome this obstacle, it is necessary to consider this new method that allows us to evaluate all fronts in parallel. These fronts can be chosen using several algorithms such as minimum degree [39]. During the procedure, the method causes total factorization to be considered as a partial factoring of smaller matrices.

In addition to the direct methods, iterative methods can be employed for the solution of the system. Among these, the most common are the conjugate gradient method and the biconjugate gradient method. The conjugate gradient method was invented by Hestenes and Stiefel around 1951 [40]. Generally, it is implemented for very large systems where it is not practical to solve with a direct method. The method yields an exact solution when the number of iterations is equal to the number of equations that define the system. In theory, it converges to solution in n steps, but due to

numerical round-off errors, can take more than n steps. In some situations, it is however possible to obtain a good approximation for a number of steps $\ll n$. One of the most important features of the conjugate gradient method is that the solution improves at each iteration. Compared to direct methods, the conjugate gradient method is less reliable regarding the data [41]. The biconjugate gradient method is an expansion of the conjugate gradient method that also covers complex symmetric systems. It was developed by Lanczos in 1952 [42]. Unlike the conjugate gradient method, the residual error may also not decrease with each iteration, so the solution may not improve. In particular, the error can grow in some steps and then decrease. This represents the major difference between the conjugate and biconjugate gradient methods. The main advantages of the biconjugate gradient method respect to the simple conjugate gradient method are that the former operates only one matrix-vector product whereas the latter needs two and that the former converges much faster than the latter. In addition, the biconjugate gradient method involves one third the number of iterations that are needed by the conjugate gradient method for the same degree of accuracy. All these considerations make the biconjugate gradient method at least 5 times faster than the simple conjugate gradient method [8].

Conclusions and Future Works

In this thesis work, the aim was to evaluate and monitor deformations in pipelines that can be caused by different external agents. The identification of these deformations was carried out through the development of an acoustic simulator based on the Finite Element Method (FEM). Practically, we defined a coordinate transformation that allowed us to convert the deformed structure into a uniform deformation-free domain. Next, we considered an anisotropic material in such a way that the sound pressure values assessed at each point of the transformed structure were equal to the pressure values of the original structure. We first evaluated a two-dimensional problem where we checked out the comparison between the scattering parameters related to the deformed structure and the same parameters related to the regular structure without deformation. This evaluation was done both for the planar and the radial cases. The latter is based on a system of polar coordinates that make the analysis define a rotary behavior. Through multimodal analysis, the similarities between the two scattering curves were extrapolated and it turned out that the curves overlap almost perfectly. The results show that the accuracy of this overlap is related to the density of the elements that form the domain and to the type of elements considered, which can be linear, quadratic or cubic. The denser the mesh and the higher order the elements, the more correct the results will be, at the expense of an increase in computational time and memory demand.

After evaluating the FEM, we decided to study an alternative method, the Hierarchical Model Reduction (HiMod) that allows us to decrease the calculations and, consequently, to provide us with the same results in much shorter times. This method was implemented for an efficient resolution of the partial differential equations (PDEs) defined in structures that have a dominant direction, therefore it proved to be suitable for our case. Always referring to the two-dimensional case, we considered structures with different deformations for both the planar and the radial cases. As for the latter, we ran into the convergence problems and we could see how the choice of the transversal modal basis is very important and greatly influences the final re-

sult. Dealing with Chebyshev and Zernike polynomials, we have noticed how these functions improve the convergence of the S curves with respect to the simple Bessel functions where the convergence rate is low. Furthermore, for all the cases considered, we noticed a great improvement from the computational point of view. This upgrade is mainly recognized by checking out high levels of mesh density and cubic elements, that is, higher-order elements. In this case, the computational time turns out to be about half of the time taken to obtain the results with the FEM.

The study then extended to three-dimensional structures. After providing a brief description of the FEM for this type of domains, we moved on to determine the pressure values and the convergence between the scattering curves evaluating the HiMod method. In particular, the comparison was made between the s curves related to deformed geometries, with a deformation only along the height, using the software Comsol and the s curves related to 3D transformed geometries according to HiMod method using Matlab. In the evaluation of three-dimensional geometries, we focused on asymmetric structures because they are more difficult to analyze and we obtained that the convergence rate is quite high except for some frequencies and this is due to the fact that Comsol tends to discretize the domain in a totally different way from Matlab. In all the results obtained, it emerged that the computational time using HiMod was significantly reduced, in particular, using Comsol 3D FEM, the time was around 80 s while using HiMod, the simulation was performed in about 8 s, so we got that HiMod is 10 times faster than the standard FEM.

In conclusion, after carrying out these analyzes, it is possible to affirm that the HiMod method allows a great improvement for both two-dimensional and three-dimensional cases and provides the desired results in much shorter times while maintaining a high degree of accuracy ensuring a faster monitoring of the state of the pipes. Despite these great improvements, the road ahead is still long and more investigations are required especially regarding the 3D case. In particular, more complex 3D structures could be inspected, that is, structures that present a greater degree of asymmetricity and the comparison between the s curves could be evaluated to observe the convergence rate. As for the 2D case, however, the problem of convergence linked to the choice of modal functions could be further investigated by trying other types of polynomials different from those considered by us and observing the behavior of the curves.

References

[1] G. Guido Gentili, "Acustica di Trasformazione", Rapporto interno, Politecnico di Milano, 2019.

[2] A. Hrennikoff, "Solution of problems of elasticity by the framework method", *Journal of applied mechanics* 8.4: pp. 169-175, 1941.

[3] R. Courant, "Variational methods for the solution of problems of equilibrium and vibrations", *Bulletin of the American Mathematical Society* 49: pp. 1-23, 1943.

[4] G. Strang, G. Fix, *An Analysis of the Finite Element Method.* Prentice Hall, 1973.

[5] J. N. Reddy, *An Introduction to the Finite Element Method.* 3rd ed. New York: McGraw-Hill, 2005.

[6] G.R. Buchanan, *Schaum's Outline Theory and Problems of Finite Element Analysis.* New York: McGraw-Hill, 1995.

[7] S. S. Rao, *The Finite Element Method in Engineering.* 4th ed. Oxford: Elsevier Inc., 2005.

[8] J. Jin, *The Finite Element Method in Electromagnetics.* 2nd ed. New York: John Wiley & Sons Inc., 2002.

[9] S. G. Mikhlin, *Variational Methods in Mathematical Physics.* New York: Macmillan, 1964.

[10] W. Ritz, "Ueber eine neue Methode zur Lösung gewisser Variationsprobleme der mathematischen Physik", *J. Reine Angew. Math.*, vol. 135, pp. 1-61, 1908.

[11] J. C. Cavendish, H. S. Price, R. S. Varga, "Galerkin methods for the numerical solution of boundary value problems", *Soc. Pet. Eng. J.*, vol. 246, pp. 204-220,1969.

[12] Lance M. Leslie, Bryant J. McAveney, "Comparative Test of Direct and Iterative Methods for Solving Helmholtz-Type Equations", *Monthly Weather Review*, 101, no. 3, pp. 235-239, 1973.

[13] F. Dassi, *Advanced Techniques for the Generation and the Adaptation of Complex Surface Meshes.* Italy: PhD's Thesis, Politecnico di Milano, 2014.

[14] https://pages.jh.edu/~virtlab/ray/acoustic.htm

[15] G. Guido Gentili, C. Riva, *Appunti di onde elettromagnetiche con esercizi.* 5th ed. Maggioli S.p.A., 2007.

[16] https://www.britannica.com/science/Bessel–function

[17] G. Guido Gentili, "Multimode Acoustics", Rapporto interno, Politecnico di Milano, 2019.

[18] https://www.dictionary.com/browse/impedance

[19] Appunti del "Corso di Circuiti attivi a microonde e radiofrequenza", Università degli Studi A. Moro di Bari.

[20] S. Perotto, A. Ern, A. Veneziani, "Hierarchical local model reduction for elliptic problems: a domain decomposition approach", *Multiscale Model Simul.*, 8, no. 4, pp. 1102-1127, 2010.

[21] S. Perotto, A. Ern, A. Veneziani, "Hierarchical model reduction for advection-diffusion-reaction problems", *Technical Report MOX*, Report no. 17, 2008.

[22] M. Aletti, S. Perotto, A. Veneziani, "Educated bases for the HiMod reduction of advection-diffusion-reaction problems with general boundary conditions", *Technical Report MOX*, Report no. 37, 2015.

[23] S. Perotto, A. Veneziani, "Coupled model and grid adaptivity in hierarchical reduction of elliptic problems", *J. Sci. Comput.*, 60, no. 3, pp. 505-536, 2014.

[24] S. Guzzetti, S. Perotto, A. Veneziani, "Hierarchical model reduction for incompressible fluids in pipes", *Int J Numer Eng.*, 114, pp. 469-500, 2018.

[25] Y. A. Brandes Costa Barbosa, S. Perotto, "Hierarchically reduced models for the Stokes problem in patient-specific artery segments", *Technical Report MOX*, Report no. 15, 2019.

[26] S. Perotto, A. Reali, P. Rusconi, A. Veneziani, "HIGAMod: A Hierarchical IsoGeometric Approach for MODel reduction in curved pipes", *Technical Report MOX*, Report no. 60, 2015.

[27] JP Boyd, F. Yu, "Comparing seven spectral methods for interpolation and for solving the Poisson equation in a disk: Zernike polynomials, Logan-Shepp ridge polynomials, Chebyshev-Fourier series, cylindrical Robert functions, Bessel-Fourier expansions, square-to-disk conformal mapping and radial basis functions", *J Comput Phys.*, 230, no. 4, pp. 1408-1438, 2011.

[28] S-H. Kim, "Some properties of Chebyshev polynomials", *Journal of Inequalities and Applications*, 167, 2012.

[29] F. Zernike, "Beugungstheorie des Schneidenverfahrens und Seiner Verbesserten Form der Phasenkontrastmethode", *Physica*, 1, no.8, pp. 689-704, 1934.

[30] http://www.dm.unibo.it/home/citti/html/AnalisiMM/Schwiegerlink-Slides-Zernike.pdf

[31] M. Gellert, R. Harbord, "Moderate degree cubature formulas for 3-D tetrahedral finite-element approximations", *Commun. Appl. Numer. Meth.*, vol. 7, pp. 487-495, 1974.

[32] L. Mansilla Alvarez, P. Blanco, C. Bulant, E. Dari, A. Veneziani, R. Feijóo, "Transversally enriched pipe element method (TEPEM): an effective numerical approach for blood flow modeling", *Int J Numer Methods Biomed Eng.*, 33, no. 4, 2017.

[33] W. Dos Passos, *Numerical Methods, Algorithms and Tools in C #*. Taylor and Francis Group, LLC, 2010.

[34] A. Turing, "Rounding-off errors in matrix processes", *The Quarterly Journal of Mechanics and Applied Mathematics* 1: pp. 287-308, 1948.

[35] A. J. Hoffman, "Cycling in the simplex algorithm", *Sel. Pap.Alan Hoffman with Commentary*, pp. 177-181, 2003.

[36] MZ. Abdulraheem, K. Mohammad, "LU-Decomposition Computerized Method to Solve Linear Programming Problems", *J Appl Computat Math*, vol. 7, 2, 2018.

129

[37] R. C. Mittal, A. Al-Kurdi, "LU-Decomposition and Numerical Structure for Solving Large Sparse Nonsymmetric Linear Systems", *Computers and Mathematics with Applications*, 43, pp. 131-155, 2002.

[38] B. M. Irons, "A frontal method solution program for finite element analysis", *Int. J. Numer. Meth. Eng.*, vol. 2, pp. 5-32, 1970.

[39] J. W. H. Liu, "The multifrontal method for sparse matrix solution: Theory and practice", *SIAM Rev.*, vol. 34, no. 1, pp. 82-109, 1992.

[40] M. R. Hestenes, E. Steifel, "Method of conjugate gradients for solving linear systems", *J. Res. Natl. Bur. Stand.*, vol. 49, pp. 409-436, 1952.

[41] https://stanford.edu/class/ee364b/lectures/conjgradslides.pdf

[42] C. Lanczos, "Solution of systems of linear equations by minimized iterations", *J. Res. Natl. Bur. Stand.*, vol. 49, pp. 33-53, 1952.